Volume 14

Johanna Loevenich

Optimization of itaconic acid production by *U. maydis* through metabolic engineering & adaptive laboratory evolution

The incessant growth of the world population leads to an already gigantic and still increasing demand for food, energy, fuels, and chemicals. With the finiteness of fossil resources as main feedstocks, a change from petroleum-derived to sustainable, economically bio-based production processes is indispensable to accomplish the global needs. One of these processes is the production of itaconic acid. Besides the filamentous fungus *Aspergillus terreus, Ustilago maydis* of the Ustilaginaceae family attracted special attention as production host.

To establish an U. maydis itaconate production host competitive to *A. terreus*, two strategies were chased in this thesis: metabolic engineering and adaptive laboratory evolution. By the reduction of the diverse by-product spectrum of *U. maydis* combined with the upregulation of the itaconate biosynthesis gene cluster regulator, the flow of substrate could be extensively pushed towards itaconate biosynthesis. This lead to an itaconate titer increased by 10.2-fold compared to the wildtype.
In this by-product reduced *U. maydis* strain, further metabolic engineering steps were performed: filamentous growth prevention by *fuz7* deletion and overexpression of *mttA* encoding for the *A. terreus* mitochondrial tricarboxylate transporter. By Δ*fuz7*, the designed strain was able to produce itaconate with improved production parameters. This could even be outplayed by additional P_{ETEF}*mttA* insertion. A clone with three P_{etef}*mttA* copies reached an itaconate titer of 54 g L^{-1} and a maximal yield of 0.64 g_{ITA} g_{glu}^{-1}, which corresponds to 89 % of the theoretical value.

The great itaconate production improvements imply a higher metabolic and osmotic stress level for the cells. Adaptive laboratory evolution was used to generate a strain with increased low pH and product resistance to itaconate. The fitness of *U. maydis* could be significantly improved represented by strains able to grow at pH 4 and in the presents of 40 g L^{-1} itaconate. The consolidation of all major modifications identified in this thesis in one strain, though, resulted in a loss of this tolerance. Especially the deletion of triacylglycerol production, the cells rely on as main energy reserves, seems to destabilize the cells in the long term.

However, the results clearly illustrate that the final engineered strains feature great, far optimized itaconate production parameters close to the theoretical maximum making *U. maydis* an industrial relevant production host for itaconic acid.

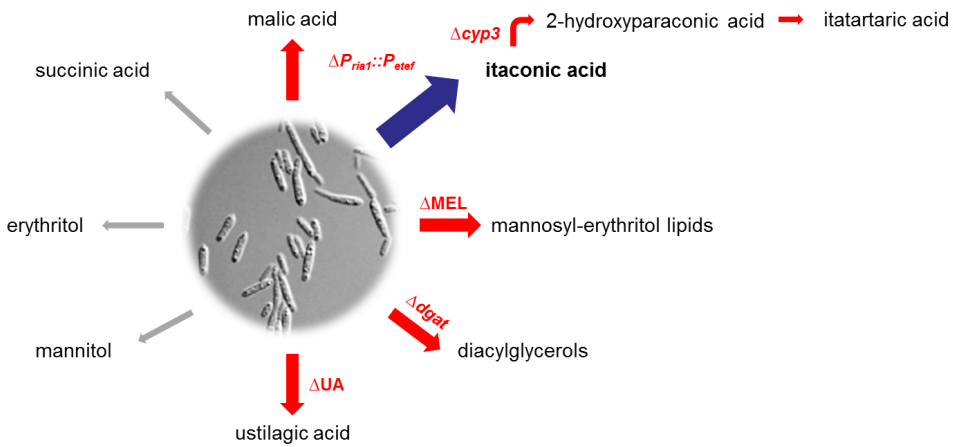

ISBN 978-3-86359-779-5

Optimization of itaconic acid production by *U. maydis* through metabolic engineering & adaptive laboratory evolution

Johanna Loevenich

iAMB Institute of Applied Microbiology | ABBt Aachen Biology and Biotechnology | RWTH AACHEN UNIVERSITY

Edition Wissenschaft Apprimus

Optimization of itaconic acid production by *U. maydis* through metabolic engineering & adaptive laboratory evolution

Von der Fakultät für Mathematik, Informatik und Naturwissenschaften der RWTH Aachen University zur Erlangung des akademischen Grades einer Doktorin der Naturwissenschaften genehmigte Dissertation

vorgelegt von

M. Sc. Molekulare und Angewandte Biotechnologie
Johanna Loevenich

aus
Pinneberg, Schleswig-Holstein, Deutschland

Berichter: Univ.-Prof. Dr.-Ing. Lars M. Blank
Univ.-Prof. Dr. Nick Wierckx

Tag der mündlichen Prüfung: 17.07.2019

Eidesstattliche Erklärung

Ich, Johanna Loevenich,

erkläre hiermit, dass diese Dissertation und die darin dargelegten Inhalte die eigenen sind und selbstständig, als Ergebnis der eigenen originären Forschung, generiert wurden.

Hiermit erkläre ich an Eides statt:

1. Diese Arbeit wurde vollständig oder größtenteils in der Phase als Doktorand dieser Fakultät und Universität angefertigt;

2. Sofern irgendein Bestandteil dieser Dissertation zuvor für einen akademischen Abschluss oder eine andere Qualifikation an dieser oder einer anderen Institution verwendet wurde, wurde dies klar angezeigt;

3. Wenn immer andere eigene- oder Veröffentlichungen Dritter herangezogen wurden, wurden diese klar benannt;

4. Wenn aus anderen eigenen- oder Veröffentlichungen Dritter zitiert wurde, wurde stets die Quelle hierfür angegeben. Diese Dissertation ist vollständig meine eigene Arbeit, mit der Ausnahme solcher Zitate;

5. Alle wesentlichen Quellen von Unterstützung wurden benannt;

6. Wenn immer ein Teil dieser Dissertation auf der Zusammenarbeit mit anderen basiert, wurde von mir klar gekennzeichnet, was von anderen und was von mir selbst erarbeitet wurde;

7. Kein Teil dieser Arbeit wurde vor deren Einreichung veröffentlicht.

05.06.2019

Funding

This work was performed as a part of the TTRAFFIC project, which is funded by the “Bundesministerium für Ernährung und Landwirtschaft” (BMEL) through the project manager “Fachagentur Nachwachsende Rohstoffe e.V.” (FNR) as part of the ERA-IB initiative.

Danksagung

Zuerst möchte ich mich bei Prof. Lars M. Blank bedanken – für die Möglichkeit, am iAMB meine Arbeit durchführen zu dürfen, für die Übernahme der Erstkorrektur und für sämtliche Unterstützung, die ich in all den Jahren von Dir erhalten habe.
Ein ganz großer Dank gilt meinem Zweitgutachter und Betreuer Prof. Nick Wierckx. Indem Du zu jeder Zeit ein offenes Ohr hattest, einen mit zielführenden Ideen und Hilfestellungen versorgt und motiviert hast, hast Du maßgeblich zum Fortschritt und Gelingen dieser Promotion beigetragen. Vielen Dank, dass ich unter Deiner Betreuung diese Arbeit anfertigen durfte.
Vielen Dank auch an alle TRAFFIC-Projektpartner – insbesondere an Marc Gauert, Dirk Ritzmann und Simon Seibert von der BRAIN AG für die Koordination und Durchführung der Lipidanalytik.
Für seine große Hilfe bei der Auswertung der Genom-Sequenzierung möchte ich mich bei Dr. Emad Albarouki bedanken.
Außerdem danke ich meinen Studenten Svenja Meyer, Conrad Müller und Anne Wilbrink für die Zusammenarbeit im Verlauf dieser Arbeit. Mit ihrer Hilfe konnte meine Arbeit entscheidend vorangebracht werden.
Allen Mitarbeitern des iAMB möchte ich meinen größten Dank aussprechen. Ihr habt die letzten Jahre in Aachen zu etwas ganz Besonderem gemacht und dafür gesorgt, dass ich diese Zeit nicht missen möchte. Der Spaßfaktor kam nie zu kurz und hat so manch langen Labortage direkt leichter gemacht. Besonders möchte ich mich bei Wing-Jin Li, Birthe Halmschlag, Isabel Bator und Benedikt Wynands bedanken. Für die richtige Mischung aus konstruktiven, weiterbringenden Diskussionen und privaten Gesprächen bei dem ein oder anderen Kaffee oder Tee – unsere weiterbildenden Maßnahmen zu ausgewählten Sendungen und leckerem Essen an Mittwoch- und Freitagabenden nicht zu vergessen. Ihr wart mir in allen Belangen eine große Stütze und seid mir alle sehr ans Herz gewachsen. Einen weiteren besonderen Dank möchte ich Hamed Tehrani aussprechen – für die tolle Zusammenarbeit, das gegenseitige Unterstützen und immer für Fragen ansprechbar sein, für das Zelebrieren von gutem Essen (vor allem auf Projekttreffen) und einfach dafür, dass Du mein Projektpartner warst.
Meinen Eltern, Christine und Andreas, meinen Großeltern, Anneliese und Winfried, und vor allem meiner Schwester, Theresa, möchte ich von Herzen für ihre bedingungslose Unterstützung und ihren unermüdlichen Zuspruch auf meinem Weg danken. Trotz der Entfernung habe ich immer das Gefühl, Euch an meiner Seite zu haben.
Als letztes möchte ich meinem Mann, Lukas, danken. Du stehst immer hinter mir, weißt mich in den richtigen Situationen mit Deiner Ruhe anzustecken und mit Deinen Worten zu bestärken und zu motivieren. Danke für die unglaubliche gemeinsame Zeit bisher und alles, was noch auf uns wartet.

Summary

The incessant growth of the world population leads to an already gigantic and still increasing demand for food, energy, fuels, and chemicals. With the finiteness of fossil resources as main feedstocks, a change from petroleum-derived to sustainable, economically bio-based production processes is indispensable to accomplish the global needs.

One of these processes is the production of itaconic acid ranked as one of the top 12 value added chemicals from biomass by the DoE. Nowadays, industrial biotechnological production is performed by using the filamentous fungus *Aspergillus terreus*. To circumvent the challenges going along with such a filamentous production host, alternatives are searched. In this context, the Ustilaginaceae family including *Ustilago maydis* attracted special attention.

To establish an industrial itaconate production host competitive to *A. terreus* and to significantly improve the itaconate production performance of *U. maydis*, two strategies were chased in this thesis: metabolic engineering and adaptive laboratory evolution. By the reduction of the diverse by-product spectrum of *U. maydis* MB215 by the deletion of 2-hydroxy paraconate, mannosyl-erythritol lipid, ustilagic acid and triacylglycerol biosynthesis in combination with the upregulation of *ria1*, the itaconate biosynthesis gene cluster regulator, the flow of substrate could be extensively pushed towards itaconate biosynthesis. This lead to an itaconate titer increased by 10.2-fold compared to the wildtype. Due to the upregulation of the *cis*-aconitate/malate antiporter *mtt1* as consequence of *ria1*↑, the production of malate, another by-product, could simultaneously be decreased by 84 %.

In this by-product reduced *U. maydis* strain, further metabolic engineering steps were performed: filamentous growth prevention by *fuz7* deletion and overexpression of *mttA* encoding for the *A. terreus* mitochondrial tricarboxylate transporter. By Δ*fuz7*, the designed strain was able to produce itaconate with improved production parameters, especially with an 25% increased yield from glucose. This could even be outplayed by additional P_{etef}*mttA* insertion. A clone with three P_{etef}*mttA* copies reached an itaconate titer of 54 g L^{-1} and a maximal yield of 0.64 g_{ITA} g_{glu}^{-1}, which corresponds to 89 % of the theoretical value.

The great itaconate production improvements imply a higher metabolic and osmotic stress level for the cells. Adaptive laboratory evolution was therefore used to generate a strain with increased low pH and product resistance to itaconate. The fitness of *U. maydis* could be significantly improved represented by strains able to grow at pH 4 and in the presents of 40 g L^{-1} itaconate. The consolidation of all major modifications identified in this thesis in one strain, though, resulted in a loss of this tolerance. Especially the deletion of triacylglycerol production, the cells rely on as main energy reserves, seems to destabilize the cells in the long term.

However, the results clearly illustrate that the final engineered strains feature great, far optimized itaconate production parameters close to the theoretical maximum making *U. maydis* – besides *A. terreus* – an industrial relevant production host for itaconic acid.

Zusammenfassung

Das stetige Wachstum der Weltbevölkerung führt zu einem bereits jetzt schon gigantischen und immer noch weiter wachsenden Bedarf an Nahrung, Energie, Brennstoffen und Chemikalien. Aufgrund der Endlichkeit fossiler Ressourcen, die überwiegend als Ausgangstoffe verwendet werden, ist ein Wechsel von Erdöl-basierten hin zu nachhaltigen, wirtschaftlich bio-basierten Produktprozessen unabdingbar, um auch in Zukunft die globalen Bedürfnisse decken zu können.
Einen dieser Prozesse stellt die Produktion von Itaconsäure dar, welche als eine der Top 12 aus Biomasse hergestellten Mehrwert-Chemikalien vom DoE eingestuft wurde. Heutzutage erfolgt die biotechnologische Itaconsäure-Produktion im industriellen Maßstab mithilfe des filamentösen Pilzes *Aspergillus terreus*. Um die Probleme zu umgehen, die ein derartig wachsender Produktionswirt mit sich bringt, wird nach Alternativen gesucht. In diesem Zusammenhang gewann die Ustilaginaceae-Familie, einschließlich *U. maydis*, besondere Aufmerksamkeit.
Zwei Strategien wurden nun im Laufe dieser Arbeit mit dem Ziel verfolgt, einen industriell einsetzbaren, gegenüber *A. terreus* konkurrenzfähigen Itaconsäure-Produktionswirt zu etablieren und die Itaconsäure-Produktionsleistung von *U. maydis* wesentlich zu verbessern: Metabolic Engineering und adaptive Laborentwicklung. Die Verkleinerung des vielfältigen Produktionsspektrums von *U. maydis* MB215 durch die Deletion der 2- Hydroxyparaconat-, Mannosylerythritollipid-, Ustilaginsäure- und Triacylglycerol-Biosynthese in Kombination mit der Hochregulierung von *ria1*, dem Regulator des für die Itaconsäure zuständigen Genclusters, führte zu einem erheblich gesteigerten Substratfluss in Richtung Itaconsäure-Biosynthese. Der Itaconsäure-Titer konnte so gegenüber des Wildtyps um das 10,2-fache gesteigert werden. Aufgrund der Hochregulierung des *Cis*-Aconitat/Malat-Antiporters *mtt1* als Folge der *ria1*-Überexpression konnte gleichzeitig die Produktion von Malat, eines weiteren Nebenproduktes, um 84 % reduziert werden.
Weitere Metabolic-Engineering-Strategien wurden in diesem Nebenprodukt-reduzierten *U. maydis* Stamm verfolgt: die Vermeidung filamentösen Wachstums durch die Deletion von *fuz7* und die Überexpression des Gens *mttA*, welches für den mitochondrialen Tricarboxylat-Transporter in *A. terreus* codiert. Der designte Δ*fuz7*-Stamm wies deutlich verbesserte Produktionsparameter auf. Dies zeigte sich vor allem in einer um 25 % erhöhten Ausbeute aus Glucose. Mit der zusätzlichen Insertion von P_{etef}*mttA* konnte dies noch gesteigert werden. Ein Klon mit dreifacher P_{etef}*mttA*-Kopie erreichte einen Itaconsäure-Titer von 54 g L^{-1} und eine maximale Ausbeute von 0.64 g_{ITA} g_{glu}^{-1}, welche 89 % des theoretisch möglichen Wertes entspricht.
Diese großartigen Verbesserungen hinsichtlich der Itaconsäure-Produktion bedeuten aber gleichzeitig ein erhöhtes metabolisches und osmotisches Stresslevel für die Zellen. Um diesem entgegenzuwirken sollte mithilfe von adaptiver Laborentwicklung ein Stamm generiert werden, welcher über eine erhöhte Toleranz gegenüber niedrigen pH-Werten und eine erhöhte Produktresistenz gegenüber Itaconsäure verfügt. Die Fitness von *U. maydis* konnte erheblich verbessert werden, was sich in Stämmen widerspiegelte, die in der Lage waren, auf pH 4 und in der Anwesenheit

von 40 g L^{-1} Itaconsäure zu wachsen. Jedoch führte die Zusammenführung aller wichtigen, in dieser Arbeit identifizierten Modifikationen in einem Stamm zu einem Verlust dieser Toleranz. Vor allem die Deletion der Triacylglycerol-Produktion scheint die Zellen auf lange Sicht erheblich zu destabilisieren – machen diese Lipide doch den Hauptanteil an Energiereserven für die Zellen aus.

Jedoch zeigen die Ergebnisse im Gesamten deutlich, dass die finalen Stämme großartige, weitreichend optimierte Produktionsparameter besitzen, die nah an das theoretische Maximum heranreichen. Diese Entwicklung macht *U. maydis* – neben *A. terreus* – zu einem industriell relevanten Produktionswirt für Itaconsäure.

List of Abbreviations

List of organisms	
A. itaconicus	*Aspergillus itaconicus*
A. nidulans	*Aspergillus nidulans*
A. niger	*Aspergillus niger*
A. terreus	*Aspergillus terreus*
C. albicans	*Candida albicans*
E. coli	*Escherichia coli*
L. lactis	*Lactococcus lactis*
M. ordensis	*Macalpinomyces ordensis*
P. antarctica	*Pseudozyma antarctica*
P. hubeiensis	*Pseudozyma hubeiensis*
P. rugulosa	*Pseudozyma rugulosa*
P. tsukubaensis	*Pseudozyma tsukubaensis*
S. cerevisiae	*Saccharomyces cerevisiae*
S. sorghi	*Sporisorium sorghi*
U. crus-galli	*Ustilago crus-galli*
U. cynodontis	*Ustilago cynodontis*
U. esculenta	*Ustilago esculenta*
U. maydis	*Ustilago maydis*
U. syntherismae	*Ustilago syntherismae*
U. trichophora	*Ustilago trichophora*
List of Enzymes / Proteins / Genes	
Abf	arabinofuranosidase
Adi	aconitate-Δ-isomerase
Ahd	α-hydroxylase
ampR	ampicillin resistance cassette
AOX	alternative oxidase
ARS	autonomously replicating sequence
Atr	ABC transporter
Cad	*cis*-aconitate decarboxylase
Cas	CRISPR associated protein
cbx	carboxin resistance gene
CoA	coenzyme A
ColE1	origin of replication in *E. coli*
Cyp	cytochrome P_{450}
DGAT	diacylglycerol acyltransferase
Emt	erythritol-mannosyl-transferase
ERK	extracellular signal-regulated kinase
Fas	fatty acid synthase
FLP	flippase
FRT	flippase recognition target
Fuz	serine/threonine tyrosine protein kinase
Gab	GABA transporter
hygR	hygromycin resistance cassette
Itp	extracellular itaconate transporter

Mac	mannosylerythritol acyltransferase
MAPK(K)	Mitogen-activated protein kinase (kinase)
Mat	mannosylerythritol acetyltransferase
MEK	MAPK/ERK kinase
Mfs	major facilitator superfamily
Mmf	major facilitator
Mtt	mitochondrial tricarboxylate transporter
NOX	NADH oxidase
P_{450}	pigment 450
PacC	pH-response transcription factor
Pal	phenylalanine ammonia lyase
P_{etef}	etef promoter
Pfk	phosphofructokinase
P_{oma}	oma promoter
Ria	regulator of itaconate biosynthesis
Rim	regulator of “inducer of meiosis 2”
Rua	regulator of ustilagic acid production
Tad	*trans*-aconitate decarboxylase
Uat	acyltransferase
Ugt	UDP-glucose-dependent glycosyltransferase
Uhd	hydroxylase
Ura	orotidine-5’-phosphate decarboxylase (UMAG_04214)
Xln	xylanase
List of Units	
%	percentage
°C	degree Celsius
µL	microliter
µm	micrometer
bn	billion
bp	basepairs
cm	centimeter
d	day
Da	dalton
g	gram
g	gravitational-force
h	hour
kb	kilo basepairs
kg	kilogram
L	liter
M	molar
min	minute
mL	milliliter

mm	millimeter
mM	millimolar
mol	molar
nm	nanometer
nt	nucleotides
Ø	diameter
RIU	refractive index units
rpm	revolutions per minute
v/v	volume per volume
vvm	volume flow per unit of liquid volume per minute
w/v	weight per volume
Δ	heat input
General abbreviations	
ALE	Adaptive Laboratory Evolution
BRAIN AG	Biotechnology Research And Information Network Aktiengesellschaft
cDNA	complementary DNA
CRISPR-Cas9	clustered regulatory interspaced short palindromic repeats – Cas9 nuclease
C_t	threshold cycle number
DNA	deoxyribonucleic acid
DoE	Department of Energy
DSM	Deutsche Sammlung von Mikroorganismen
e.g.	exempli gratia
ER	endoplasmic reticulum
et al.	*et alii* or *et aliae*
FID	flame ionization detection
fwd	forward
G	generation
GC	gas chromatography
GmbH	Gesellschaft mit beschränkter Haftung
HiSeq	high-throughput sequencing
HPLC	high-performance liquid chromatography
HT	Hamed Tehrani
iAMB	Institute of Applied Microbiology
ID	identity
IGV	Integrative Genomics Viewer
InDel	insertion deletion
JB	Johanna Becker
K	clone
log	logarithmic
max	maximum
MTM	modified Tabuchi medium
n	number of samples
NCBI	national center for biotechnology information
NRRL	Northern Regional Research Laboratory

OD	optical density
ORF	open reading frame
PCR	polymerase chain reaction
pH	negative logarithm of the concentration of hydronium ions isoelectric point
pK_a	symbol of the acid dissociation constant at logarithmic scale
qPCR	quantitative PCR
REG	regeneration
rev	reverse
RI	refractive index
RIU	refractive index unit
RNA	ribonucleic acid
r_P	product production rate
rRT	relative retention time
RWTH	Rheinisch-Westfälische Technische Hochschule
S	substrate
sgRNA	single guide RNA
SNP	single nucleotide polymorphism
sp.	species
TCA	tricarboxylic acid
TLC	thin-layer chromatography
TTRAFFIC	Toxicity and TRAnsport For Fungal-based production of Industrial Chemicals
US	United States
US$	United States Dollar
UTR	untranslated region
UK	United Kingdom
UV	ultraviolet
wt	wildtype
YEP	yeast extract peptone
YEPS	yeast extract peptone sucrose
YNB	yeast nitrogen base
$Y_{P/S}$	yield product per substrate consumed
List of chemicals / elements	
ATP	adenosin triphosphate
BDO	Butanediol
C	carbon
Ca	calcium
$CaCl_2$	calcium chloride
$CaCO_3$	calcium carbonate
Cbx	carboxin
CO_2	carbon dioxide
$CoCl_2$	cobalt(II) chloride
$CuSO_4$	copper(II) sulfate
EDTA	ethylenediaminetetraacetic acid
Ery	erythritol
FAMES	fatty acid methyl esters
$FeSO_4$	ferrous sulfate
GDP	guanosine diphosphate

Glu	glucose
GPI	glycophosphatidylinositol
H	hydrogen
H_2O	water
H_2SO_4	sulfuric acid
H_3BO_3	boric acid
HCl	hydrogen chloride
HP	hydroxyparaconate
hyg	hygromycin
ITA	itaconate
K	potassium
KH_2PO_4	potassium dihydrogen phosphate
KI	Potassium iodide
Mal	malate
MEL	mannosylerythritol lipid
MES	2-(N-morpholino) ethanesulfonic acid
$MgSO_4$	magnesium sulfate
$MnCl_2$	manganese(II) chloride
N	nitrogen
Na	sodium
Na_2MoO_4	sodium molybdate
NaCl	sodium chloride
NAD	nicotinamide adenine dinucleotide (reduced)
NADH	nicotinamide adenine dinucleotide (oxidized)
NaOH	sodium hydroxide
NH_4Cl	ammonium chloride
O	oxygen
O_2	molecular oxygen
PEG	polyethyleneglycol
SDS	sodium dodecyl sulfate
TAG	triacylglycerol
TE	Tris-EDTA
THF	tetrahydrofuran
Tris-HCl	tris(hydroxymethyl)amino-methane hydrochloride
UA	ustilagic acid
UDP	uridine diphosphate
$ZnSO_4$	zinc sulfate

List of Figures

List of Tables

Chapter 1

General introduction

1 General Introduction

1.1 Forced replacement of fossil-based compounds by bio-based products from renewable resources

1.1.1 Fossil-based products and their drawbacks

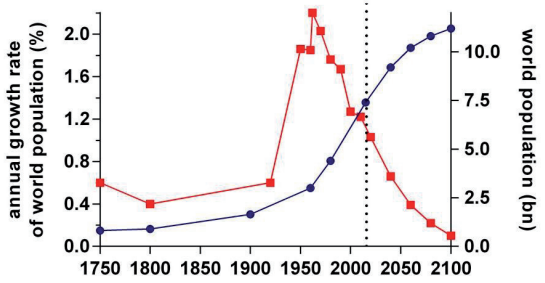

Figure 1: World population growth and its annual growth rate from 1750 to 2010 and projections up to 2100 (modified from [1]).

The world population has increased from 1 billion to over 7 billion humans within the last 200 years [2]. Within only 100 years, from 1900 to 2000 marking the beginning of modernity, a drastic increase in population size from 1.5 to 6.1 billion was registered. Due to lower fertility rates, world population growth decelerates ending up with an estimated annual growth rate of 0.1 % by 2100. Nevertheless, world population will grow by another 3 billion people in the next 80 years [1]. This means a gigantic global demand for food, energy, fuels, and chemicals to maintain and improve human living standards. Agricultural production for instance has to be increased by 70 to reach 100 % until 2050 in order to meet global food demands [3–5]. Depending on the scenario, energy supply is supposed to reach levels in 2040 that are up to 45 % higher than in 2012 [6]. The accomplishment of these needs is mainly based on fossil resources leading to an already huge and still increasing dependency on coal, petroleum, and natural gas [7]. Due to their formation process taking millions of years, these resources are finite and will decrease in availability until completely depleted [8]. This trend will extremely increase prizes and dependency on countries still possessing fossil sources. Additionally, fossil fuel burning negatively affects air quality by increasing pollutant concentrations locally, while contributing to global warming on a larger scale. Increased concentrations of greenhouse gases, such as carbon dioxide, methane, and nitrous oxide, in the troposphere trap solar radiation in form of heat leading to a warming of the earth atmosphere and surface [9,10]. Another issue regarding the consumption of sulfur-containing fossil fuels is the formation of acid rain due to sulfur dioxide and nitrogen oxide emissions [11]. To fight these drawbacks and make alternatives competitive, a replacement of fossil-based by bio-based renewable resources as carbon feedstock is indispensable.

1.1.2 Production of fuels and chemicals from biomass feedstocks

While at the beginning of the 20th century, trees and agricultural crops were used for the production of a variety of industrial materials, a shift towards petroleum occurred in the late 1960s. Despite the energy crisis in the 1970s that accelerated the interest in bio resources-based production, until today most of the worldwide energy market heavily relies on fossil fuels for the generation of thermal energy, fuels in gaseous, liquid, and solid form, and chemicals [12–14]. Depletion of fossil reserves, climate change and dependency on countries exporting fossil materials drives the search for alternative resources [15]. In terms of a short formation period, biomass represents the only renewable CO_2-based source available in abundance. CO_2 has the potential to replace fossil resources applied in the production of chemicals, energy, and fuels, but its use on a commercial scale is still very limited [8,12,16]. Burning biomass indeed causes some pollutants like dust and subsequently acid rain, when no filters are used. But due to comparatively low sulfur contents, wood consumption for example emits 90 % less sulfur than coal. Regarding the greenhouse gas effect, the amount of released carbon dioxide balances with the carbon dioxide absorbed by the plants. Biomass is therefore indicated as carbon dioxide neutral [7].

Biomass is defined as “all non-fossil-based living or dead organisms and organic material that have an intrinsic chemical energy content” [8]. This includes plant material such as algae, animal products, and manure, or agricultural and forestry by-products [8,17]. Biomass classification in terms of its major component differs i.a. between sugars, starch, cellulose, hemicellulose, lignin, oils, and proteins [18]. It is assumed that 146 billion metric tons of biomass are produced worldwide per year, mostly in the form of wild plant growth of which only a fraction of less than 1 % is used. The largest feedstock is cellulose with 49 %, followed by other sugar polymers including starch with 23 %, and proteins with 12 % [18–20]. Regarding biofuel production, biomass is also divided into the categories “first”, “second”, and “third generation feedstock”. “First generation biofuels” directly originate from biomass that is edible including sugar cane, corn, whey, barley, and sugar beets. Ethanol and biodiesel, e.g., are considered as first-generation biofuels, depending on the carbon source and synthesis route. Bioethanol is commonly produced in fermentation processes using C6 sugars (mostly glucose) and yeast strains such as *Saccharomyces cerevisiae*. In order to do so, sugarcane is crushed in warm water to remove sucrose which is then purified for the production of ethanol. Before corn can be used as feedstock for ethanol production, starch has to be hydrolyzed to make the containing sugars accessible. The production process of biodiesel (monoalkyl esters) is quite different. Oils are extracted from the biomass of oily plants and seeds to convert them into biodiesel by a process called transesterification. During this process, glycerol is separated from the bound long chain fatty acids and is replaced by methanol [21,22]. With the use of arable land for biofuel feedstocks, however, the food versus fuel dilemma appeared. Farmland and crops are diverted that are needed to ensure the world’s food supply. The large increase in biofuel production in recent years have resulted in an increase in food prices due to limited feedstocks, needed for both production processes, and restricted farmland [23].

The “food vs. fuel” debate drove the development of second generation or advanced biofuels like cellulosic ethanol and Fischer-Tropsch liquids. These biofuels are

derived from cellulose, hemicellulose, lignin, or pectin (e.g., agricultural and forestry wastes) and therefore from sources not digestible by humans. Before sugar monomers can be fermented to ethanol, the fibrous matrix structure of lignocellulose has to be broken up into hemicellulose, cellulose chains, and lignin and hexose and pentose sugars have to be hydrolyzed from the separation products [24].

Feedstocks formed by aquatic autotrophic organisms (e.g., algae) are termed as "third generation feedstocks" [25]. Due to their high lipid productivity meaning the product of lipid content and biomass productivity, microalgae are an attractive alternative for vegetable oil and therefore biodiesel production [26]. Several algae species produce 50 to 60 % of their dry weight in lipid form making them up to 20 times more efficient per unit area than the best oil-seed crop [27,28]. Species featuring high lipid productivity are, e.g., *Amphora*, *Ankistrodesmus falctaus*, *Chlorella sorokiniana*, and *Tetraselmis suecica*. Other advantages are their rapid growth and their ability to grow in marginal regions, in the ocean, or in brackish water. The latter reduces the conversion of areas that are needed for food supply. But despite these great advantages, biodiesel production from algae is not yet economically profitable [26,29].

Biobased raw material has different application fields. On the one hand, it is used as biofuels, such as biogas, ethanol, methanol, and biodiesel, as an alternative to petroleum fuels. On the other hand, it is applied in bioenergy production instead of petroleum or coal, or as feedstocks for chemical industry by biorefining [30]. A biobased product is characterized by a biomass content of at least 90 % (besides water and other inorganic components) as measured by its volume or weight. Examples for biobased products are paper and paper-like products, wooden composites, paints, lubricants, textiles, wooden furniture, insecticides, and fertilizers, pharmaceuticals, and cosmetics, but also food, drinks, and food supplements [31].

In the biobased process of fuel and chemical production, biomass can be converted in different ways, either by chemical or enzymatic catalysis, or by biological conversion using microorganisms. Each pathway goes along with advantages and disadvantages. High volume throughput, but less molecular structure specificity can be achieved by chemical synthesis. In contrast, biological conversion can result in high specificity, but the production parameters have to be chosen with respect to the microorganisms used [32]. Nevertheless, biological conversion – also called fermentation – has several advantages over the petro chemistry: Each raw material containing carbohydrates can basically be used as substrate. Therefore, besides biomass organic waste or side products from agricultural manufacture such as straw or wood waste can be applied, and more importantly even mixtures of carbon sources. Fermentation processes go along with low pressures and temperatures often resulting in lower initial costs. Most of the by-products are nontoxic. While petroleum and chemical feedstocks mostly have to be imported, raw material for fermentation processes usually has a homemade origin. This improves foreign trade balance and decreases political and economic dependency on countries holding fossil resources. Currently, a main disadvantage of biomass converting factories is the plant capacity which is limited by costs for biomass, transport, and storage [31].

In recent years, the production of valuable chemicals from biomass feedstocks using microorganisms attracted more and more attention and each increase in commodity

prices of the petro chemistry is a further push for the promotion and establishment of biobased processes in the world market, while the low oil price and the low CO_2 certificate price are clearly non supportive.

1.2 Itaconate as a top 12 value-added chemical from biomass

Regarding bio-based chemical production, the U.S. Department of Energy (DoE) evaluated over 300 possible building block chemicals concerning their potential to serve as economic drivers for a biorefinery [32]. Initial screening criteria were raw material and estimated processing costs, estimated selling price, technical complexity associated with the best available processing pathway and market potential. In this first screening, 50 promising building block chemicals were identified. They were organized in groups depending on their carbon content (C1 to C6) and analyzed in terms of direct replacement, novel properties and potential utility as a building block intermediate. Next, chemical functionality and potential use of the candidate groups were assessed followed by the classification of each candidate for its utility to serve as a simple intermediate in traditional chemical processing, as a reagent molecule for adding functionality to hydrocarbons or as by-products from petrochemical synthesis. These evaluation steps ended up with a list of the top 30 building block chemicals all characterized by their multiple functionalities suitable for further conversion as derivatives or molecular families, their possible production from both lignocellulosics and starch and their C1-C6 monomer structure. Additionally, they included no aromatics derived from lignin and they were not already super commodity chemicals. In a last round of screening, the top twelve sugar-derived building block chemicals were identified [32].

Table 1: Top 12 sugar-derived building block chemicals identified by the U.S. Department of Energy [32].

building block chemicals
1,4 succinic, fumaric, and malic acid
2,5 furan dicarboxylic acid
3 hydroxy propionic acid
aspartic acid
glucaric acid
glutamic acid
itaconic acid
levulinic acid
3-hydroxybutyrolactone
glycerol
sorbitol
xylitol / arabinitol

One of these promising candidates is itaconic acid or 2-methylidenebutanedioic acid (CAS 97-65-4), an unsaturated, non-toxic, C5 dicarboxylic organic acid (Figure 2). It is a white crystalline acid in which one carboxyl group is linked to the methylene group and it has a molecular weight of 130.1 g mol^{-1}. Its solubility in water is 83.1 g L^{-1} at 20 °C with a pH of 2. The pK_a values are 3.84 (pK_{a1}) and 5.55 (pK_{a2}) [33,34].

In 1837, itaconic acid was first discovered by Baup as a product of pyrolytic distillation of citric acid [33,35]. In 1932, Kinoshita was the first researcher who isolated itaconic acid from broth of a filamentous fungus naming this *A. itaconicus* as a consequence [36]. Until about 1966, significant steps in the development and

optimization of itaconic acid production were made. 15 years of decreasing interest in this research field followed. But the interest resurged and itaconic acid as a promising platform chemical got into the focus in the following years when attention to sustainability, renewable resources and rising energy costs increased [34].

1.2.1 Application fields of itaconate

Itaconate and its derivatives have a wide application spectrum. Important derivatives are 2-methyl-1,4-butanediamin, itaconic diamide, 3-methylpyrrolidine, 3- and 4-methyl-N-methylpyrrolidinone, 2-methyl-1,4-butanediol, 3-methyl-tetrahydrofuran, and 3- and 4-methyl-γ-butyrolactone (Figure 2) [32].

Itaconate and its methyl, ethyl, or vinyl esters can easily be polymerized using radical polymerization [37]. As co-monomers, they are applied in the industrial production of polymers, surfactants and fibers. The alkali salt or sulfonated form of self-polymerized itaconate, polyitaconate, is applied as a detergent and in shampoos [33]. Itaconate and its derivatives (Figure 2) are also used in the production of resins, as building block for acrylic plastics, acrylate latexes, super-absorbents, and anti-scaling agents, as well as in the synthesis of artificial glass and bioactive compounds in the agricultural, pharmaceutical, and medical sector, especially in the dental, ophthalmic, or drug delivery field [33,38]. Additionally, derivatives such as 3-methyl THF or 2-methyl-1,4-BDO may function as biofuels [39,40]. In their study, Okabe *et al*. give a more detailed survey of the wide range of applications itaconate is used for [33].

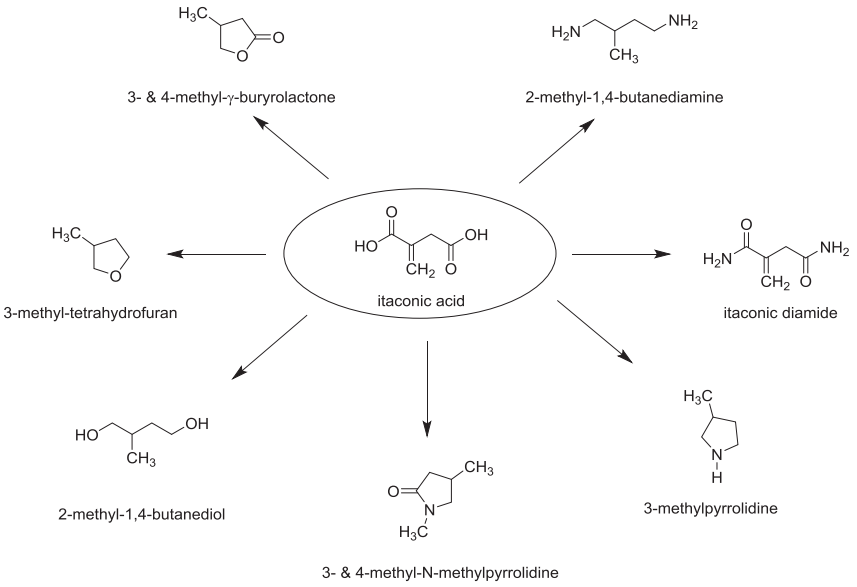

Figure 2: Itaconic acid chemistry of derivatives and the corresponding chemical structures (modified from [32]).

1.2.2 Market potential of itaconate

Due to its potential as renewable resource, the interest in itaconate production increased since the 1990s with an exponential growth in the last 15 years. And it is expected that the constantly growing demand for eco-friendly products will drive the itaconate market to exceed 216 million dollar by 2020 [38,41,42].

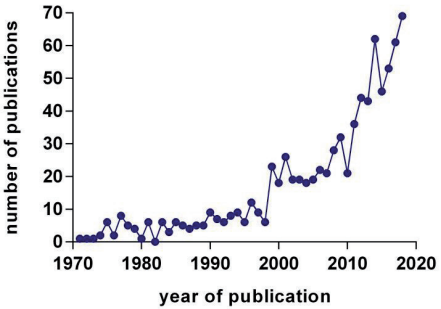

Figure 3: Publication trend in itaconate research. The number of scientific articles was selected from the database Scopus® [43] until the year 2018 by searching for documents containing the key word "itaconic acid" in their title.

Until 1970, the Pfizer Company in the United States was the only commercial producer of itaconate. Later, Japan, China, and Europe followed. Especially China contributes relevantly to the global itaconate supply by maintaining supply and demand of this organic acid. From 1993 to 2000, China started to establish itaconate economy in their own country with the result of 20,000 tons of itaconate produced in 2000. When Cargill and Pfizer Food Science in the USA and the French company Rhodia interrupted their itaconate production, China became the largest producer with companies like Qingdao Langyatai [34,42,44]. Nowadays, the global production is estimated to be around 40,000 tons/year with a capacity of 70 to 80,000 tons/year [45]. The Asia-Pacific region represents the major producer and also consumer for itaconate. It caters over 50 % of the global demand [46]. While years ago, the price of itaconate ranged between US$ 4/kg and US$ 4.3/kg, it is around US$ 1.8-2/kg today depending on supplier and quality. In China, it is even below US$ 1.5/kg [33,47]. It is assumed that the itaconate market will annually grow by 3 to 5 % in the next few years resulting in a production of around 52,000 tons/year in 2025. But if the demand for specialty polymers increases, there is still enormous potential of up to 170,000 tons/year with 260 million dollars in sales (at US$ 1.5/kg) [45]. However, the price range still makes itaconate a valuable product. This and the existence of other substitutes restrict the current itaconate market. To turn itaconate from a niche into a bulk product, production technologies have to be developed respectively improved to let the price fall below US$ 1.5/kg and make itaconate competitive against other monomers [38,42,44].

1.2.3 Industrial production of itaconate

1.2.3.1 Chemical synthesis of itaconate

The first method of producing itaconate was developed by Baup in 1836 [35] (Figure 4). Citric acid monohydrate is placed in a Kjeldahl flask attached to a water-cooled condenser and heated until complete distillation. From the distillate consisting of water and itaconic anhydride, the lower layer of itaconic anhydride is separated and resolved in water. To isolate itaconate, acid crystallization was initiated in an ice bath to allow filtration and drying of the end product [48]. At that time, Baup named the isolated product "citricic acid" [49].

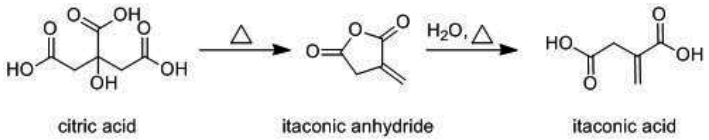

Figure 4: Chemical synthesis of itaconic acid by the pyrolysis of citric acid and the hydrolysis of the resulting anhydride to itaconic acid (modified from [50]).

In 1840, Crasso established the product name "itaconic acid" as an anagram of aconitic acid, another derivative of citric acid. This time, itaconate was generated by the decarboxylation of aconitic acid [34,49]. Other methods were invented, such as oxidation of isoprene or mesityl oxide and subsequent isomerization of the resulting citric acid, carboxylation of acetylene derivatives (e.g., propargyl chloride, butynoates), condensation of succinate or succinin anhydride with formaldehyde to generate citric acid with subsequent isomerization, or oxidation of isoprene [34,44,51,52]. Despite several opportunities to produce itaconate by chemical pathways, none of them can compete with fermentation by fungi in terms of effort, substrate costs, energy input due to high reaction temperatures needed and yields [50,53]. The itaconate yield from citric acid, e.g., is only 0.09 g g^{-1} [48]. Therefore, chemical synthesis is not performed commercially.

1.2.3.2 Biological synthesis of itaconate

In 1931, Kinoshita first reported the production of itaconate by the microbial route. A filamentous fungus isolated from salted plum juice was grown in surface cultures and in the presence of concentrated sugar solutions and high concentrations of chlorides. Yields of up to 0.24 g_{ITA} $g_{substrate}$ were reached. The fungus was called *A. itaconicus* [36,44]. In 1939, several *A. terreus* strains were described as natural itaconate producers able to generate 0.12 g_{ITA} $g_{substrate}$ after 25 days [54]. In 1945, the Northern Regional Research Laboratory (NRRL) of the US Department of Agriculture in Peoria, Illinois, performed a screening of over 300 strains, identified the most published strain *A. terreus* NRRL 1960 (NRRL 1960 = ATCC 10020) which was isolated from a soil sample in Texas [55,56]. Pfizer Co. Inc. reached 28 % of the theoretical yield for producing itaconate with sucrose within 14 days [49] and started to industrially produce itaconate under submerged fermentation conditions and sugar beet as basic feedstock in 1955 [33,57]. In the following years, *A. terreus* NRRL 1960

was mainly used for genetic modifications and process development in subjects like evaluation of substrate or nitrogen source and effect of pH, aeration rate, or fermentation mode [58]. Besides *A. terreus*, other microorganisms have been reported as natural itaconate producers: the basidiomycete *Ustilago maydis* (*Ustilago zeae*) [59], yeasts such as *Candida* sp. [60], *Rhodotorula* sp. [61], or *Pseudozyma antarctica* [62], and also mammalian immune cells, such as macrophages [63]. However, none of these species can compete with *A. terreus* in regard to production parameters like itaconate titer, productivity, and yield (Table 2) which makes this organism still the only used species for commercial itaconate production [34].

Table 2: Selection of itaconate producing microorganisms and the characteristics of the corresponding fermentative processes (modified from [44]).

strain	substrate	working volume, fermentation type	itaconate titer [g L^{-1}]	itaconate yield [g_{ITA} g^{-1}]	time [d]	reference
A. terreus DSM 23081	glucose	1.5 L, submerged fermentation	160	0.46 g_{ITA} g_S	6.8	64
	glucose	15 L, submerged fermentation	86	0.62 g_{ITA} g_S	7	65
	glucose	1.5 L, submerged fermentation	146	0.59 g_{ITA} g_S	12.6	66
A. terreus NRRL 265	sucrose	50 mL, submerged fermentation	49	-	11	55
mutant of *A. terreus* NRRL 265 and 1960	beet and sugarcane molasses	2 L, submerged fermentation	50	-	-	67
A. terreus NRRL 1960	xylose and glucose	14 L, immobilized MO in submerged fermentation	30	0.54 g_{ITA} g_S	4	68
A. terreus NRRL 1960	glucose	6 L, submerged fermentation	130	0.9 g_{ITA} g_S	-	69
A. terreus SKR10 N45	corn starch	100 mL, submerged fermentation	50	0.25 g_{ITA} g_S	6	70
A. terreus TN484-M1	corn sorghum	3 L submerged fermentation	48	0.34 g_{ITA} g_S	6	71
A. terreus CECT 20365	sugar beet press-mud, dry olive residues, glycerol	10 g solid-state fermentation	-	0.44 g_{ITA} kg^{-1}	5	72
mutant of *A. terreus* ATCC 10020	glucose, sucrose, fructose, mannose, starch hydrolysate, molasse	45 mL, semi-solid-state fermentation	-	0.55 g_{ITA} g	5	73
mutant of *Aspergillus niger* ATCC 1015	glucose	100 mL, submerged fermentation	1.2	-	10-13	74
Candida sp.	glucose	25 mL, submerged fermentation	35	-	5	60
mutant of *Escherichia coli*	glucose	1 L, submerged fermentation	32	0.49 g_{ITA} g_S	5	75
Helicobasidium mompa TANAKA	sweet potato	14 mm of the feedstock, solid-state fermentation	0.5	-	-	76
P. antarctica Y-7808	glucose	1 L, submerged fermentation	30	0.38 g_{ITA} g_S	6	62
U. maydis MB215	glucose	2 or 6 L, submerged fermentation	44.5	0.24 g_{ITA} g_S	6	77
mutant of *U. maydis* MB215	glucose	1.3 L, submerged fermentation	63	0.26 g_{ITA} g_S	6.8	78
mutant of *Yarrowia lipolytica*	glucose	1.5 L, submerged fermentation	1.2	0.058 g_{ITA} g_S	7	79

To improve strains regarding their natural of the itaconate production or make other strains synthesize itaconate as a new product by metabolic engineering, adequate knowledge about the underlying biosynthesis pathway is demanded.

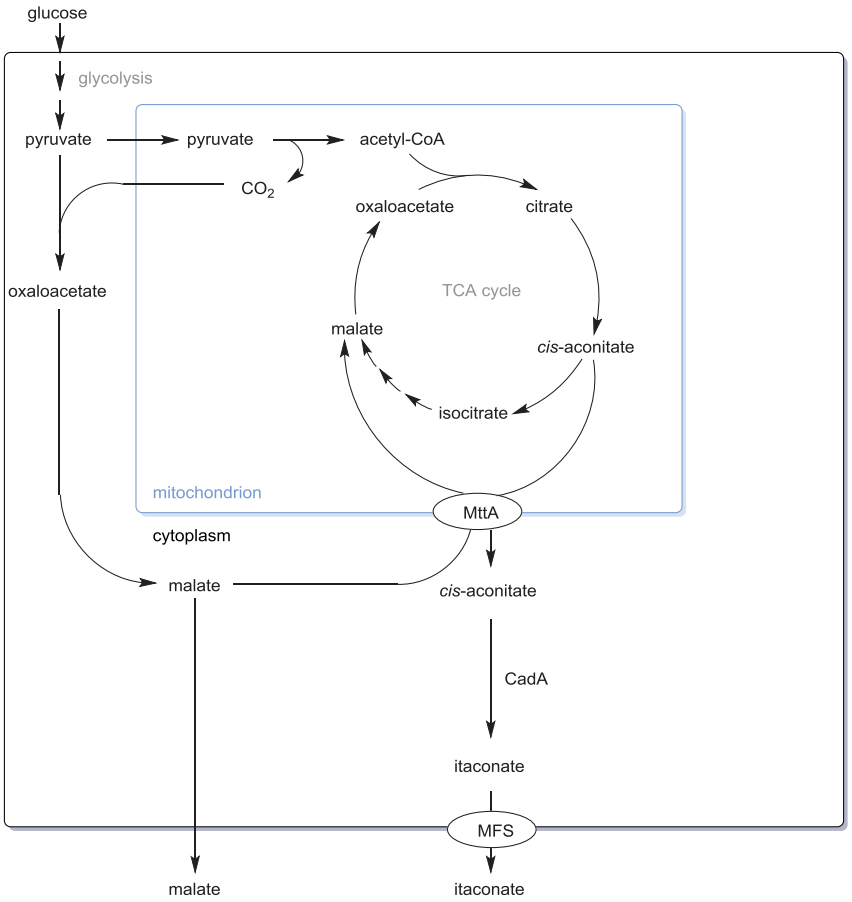

Figure 5: Itaconic acid biosynthesis pathway in *A. terreus*. Pyruvate is generated from glucose through glycolysis taking place in the cytosol and enters the mitochondria. It is converted to acetyl-CoA and forms citrate together with oxaloacetate in the TCA cycle. Citrate is dehydrated to *cis*-aconitate which is transported from the mitochondria into the cytosol via the putative mitochondrial tricarboxylic transporter MttA and converted to itaconate in a *cis*-aconitate decarboxylase (CadA)-mediated reaction. Itaconate is transported out of the cell by a protein of the major facilitator superfamily, MFS (modified from [44]).

Today, after several studies with breakthroughs like analysis of the compartmentalization itaconate pathway in *A. terreus* by fractionized cell extracts [80] or the identification of the itaconate biosynthesis regulating gene cluster by a clone-based transcriptomics approach [81], it is generally accepted that the main pathway proceeds in two compartments starting with the glycolysis in the cytosol followed by the tricarboxylic (TCA) cycle in the mitochondria and aconitate decarboxylation in the cytosol [34,82] (Figure 5). Glucose is taken up by the cell from the extracellular environment into the cytosol and converted into pyruvate via glycolysis. It is either

taken up by the mitochondria or further converted to malate via carboxylation into oxaloacetate. Malate is then transported into the mitochondria by a malate/citrate antiporter where it enters the TCA cycle. The pyruvate directly imported into the mitochondria is dehydrogenated to generate acetyl-coenzyme A (CoA). Acetyl-CoA and oxaloacetate are then catalyzed to citrate within the TCA cycle. From citrate, *cis*-aconitate is formed mediated by an aconitase. Via a mitochondrial tricarboxylic transporter (MttA), *cis*-aconitate is exported into the cytosol where the final step, the decarboxylation of *cis*-aconitate to itaconate with simultaneous release of carbon dioxide, occurs catalyzed by the *cis*-aconitate decarboxylase CadA. Itaconate is then transported into the extracellular space through the putative major facilitator superfamily (MFS) transporter [38,80,81,83].

A. terreus is indeed the best itaconate producing strain able to reach a final titer of 160 g L^{-1} under industrial relevant conditions, but in comparison to a citric acid titer of over 200 g L^{-1} steadily reached in industrial production by fungi itaconate titers are still low [38,64]. Therefore, knowledge of its itaconate biosynthesis pathway was used to perform different approaches of genetic modification events to increase itaconate production in both *A. terreus* and other species. For example, a truncated version of the *A. niger* 6-phosphofructo-1-kinase (*pfkA*) gene, a key component of the glycolysis, was expressed in *A. terreus* and positively influenced its itaconate production [84]. Another approach dealed with the expression of a hemoglobin gene from *Vitreoscilla* in *A. terreus* M8 which reduced the sensitivity to oxygen supply in an otherwise very sensitive-acting organism and simultaneously improved strain regeneration after aeration was interrupted [85]. The *A. terreus cadA* gene encodes for CadA which plays a key function in the itaconate pathway. *CadA* was expressed under the control of a strong constitutive promoter in *A. niger* AB 1.13, a natural citric acid producer with pathways optimized towards organic acids and therefore a promising host for itaconate production. *CadA* expression resulted in 0.7 g L^{-1} itaconate production [81], increased by twofold with the additional expression of *mfsA* and *mttA* in the same strain [86]. This is a titer not comparable with these of *A. terreus*, but a promising finding for further rational improvement of other strains not natively producing itaconate.

The research for other itaconate producing species, such as strains of the genus Ustilaginacea, and the optimization of these is promoted due to some difficulties going along with *A. terreus* fermentations. With US$1.5 - 2 kg^{-1}, production costs are very high and have to be reduced to at least US$0.5 kg^{-1} to be industrially competitive to petrochemical-based products [83,87]. The highest yields are reached using glucose-based feedstocks. But with current prices of US$0.35 – 0.60 kg^{-1}, glucose is too cost-intensive to use as substrate in industrial itaconate production. Raw materials, such as starch, molasses, or hydrolysates of corn syrup [88] or wood [89], might be cheaper alternatives whereof corn starch shows the best properties as carbon source – pure, relatively inexpensive and stable in a mass supply. But due to gelatinization upon heat sterilization, raw corn starch has to be pretreated in a three-step-procedure before it can be used in itaconate production. Disadvantages of other raw materials than pure glucose are a generally lower yield and the presence of harmful components potentially disturbing microbial growth and production [33,42,50,87]. Itaconate production is highly dependent on fermentation medium composition.

Additional and varying concentrations of salts, microelements (e.g., iron, manganese, copper, zinc), phosphate, or nitrogen from the feedstock might change fermentation conditions and therefore affect growth and production. To use alternative feedstocks, additional steps have to be integrated into the production process like biomass pretreatment and verification of the medium composition [34,50].

Another way to lower production costs is further strain optimization to design a highly efficient microorganism and therefore to increase yield, titer, and rate of itaconate production. Volumetric productivity for example has to be increased to at least 2.5 g L^{-1} h^{-1} to be competitive on the world market [90]. Until today, production rates between 0.06 and 1.2 g L^{-1} h^{-1} are reported for *A. terreus* cultivations resulting in long fermentation times of up to 45 days [33,68].

Drawbacks specificially accomponaying with the growth of filamentous fungi are sensitivity to hydro-mechanical stress, laborious handling of spores, increased viscosity of the fermentation broth and interruption of oxygen supply [39,65]. Pausing aeration for 5 min for example damages the mycelia irreversible and itaconate production is completely stopped [91]. Sensitivity is not only reported to shear stress, but also to itaconate concentrations higher than 20 g L^{-1} drastically affecting growth and production rate of *A. terreus* by feedback inhibition [92]. Possibilities to circumvent this inhibition are the use of an itaconate-resistant mutant strain or *in situ* product removal during continuous fermentation [33,93]. Removal methods, such as evaporation-crystallisation, have the disadvantage not to eliminate by-products and substrate. This results in a quality loss of the final product. Another technique is the usage of an organic phase, such as 1-octanol, and tri-*n*-octylamine as reactive compound to extract itaconate from the fermentation broth with a subsequent re-extraction from the organic phase [94]. However, it was verified that 1-octanol is toxic for *A. terreus* in concentrations over 0.1 g L^{-1}. During itaconate extraction based on fermentation broth recycling, this toxicity of the organic phase limits the volume of extracted medium that is permitted to return into the fermentation vessel due to the amount of octanol going along with it. This leads to increasing downstream process costs and separation techniques of the organic phase [83,95].

Additional costs also originate from the fact that *A. terreus* has been classified as a biosafety level 2 organism by several countries including Germany, US, UK, and the Netherlands [96]. It is known that *A. terreus* produces mycotoxins which represent a considerable risk to plants, animals, and humans [97]. This classification demands specific measures relating to the work with *A. terreus* strains [50].

To overcome all these drawbacks and the associated additional costs, new strains have to be generated and optimized with regard to efficient itaconate production to compete with petrol-based compounds on an industrial level. The fungal genus Ustilaginacea is common for its natural production of a wide range of value-added chemicals, including organic acids (malate, succinate, itaconate, 2-hydroxyparaconate, itatartarate), polyols (erythritol, mannitol), oligosaccharides, squalene, enzymes, and biosurfactants (mannosylerythritol lipids (MELs), ustilagic acid (UA)) [93,98–106]. Therefore, species of this genus represent promising candidates for biotechnological applications in itaconate production.

1.3 Ustilaginaceae as alternative production hosts for the secondary metabolite itaconate

The family Ustilaginaceae belongs to the order Ustilaginales, a subordination of the class Ustilaginomycetes (true smut fungi), and includes 17 genera (e.g., *Ustilago*, *Sporisorium*, *Exobasidium*, *Microstroma*, and *Pseudozyma*) and 607 species of smut fungi [107,108]. Ustilaginomycetes represent plant pathogens which damage crops, such as wheat, maize, barley, oats, sorghum, or sugarcane, resulting in serious damages and losses in the agricultural field [109,110]. The corresponding fungi are mostly dimorphic and undergo their life cycle in yeast stages. However, this yeast form is not only characterized by unicellular budding cells, but also by cells that have the potential to build hyphae or divide in other ways than budding. Therefore, these fungi are named “yeasts” or “yeast-like fungi” [108,111–114].

Within the Ustilaginaceae family, the genus *Ustilago* comprises around 200 species including *U. maydis*. *U. maydis* is a well-established model organism for, e.g., investigating fungal mating, DNA recombination, RNA biology, cell signaling and differentiation, and biotrophic interactions between plant and pathogen [115]. It is known as the causative agent of common corn smut disease visible in form of large tumors on its host plant maize (*Zea mays*). These tumors named galls are commercially sold as delicacy in Mexico and cultures around the world under names like “corn truffle” or “maize-mushrooms” [116–118]. Its dimorphic life cycle reflects its pathogenic potential. Growing as haploid yeast in a saprophytic phase and reproducing by budding, *U. maydis* can switch to a filamentous and pathogenic dikaryotic form by the fusion of two sexually compatible cells. The dikaryon is able to initiate plant surface penetration and fungal growth within the maize tissues [110,115,119]. Yield losses caused by *U. maydis* infections are neglectable, but a major problem is represented by the formed galls that might grant toxigenic fungi entry to the plant [120,121]. Toxigenic fungi, such as *Aspergillus* spp. or *Fusarium* spp., might contaminate the whole plant with mycotoxins – a significant issue regarding food safety. However, these interactions are poorly understood until today [122].

To follow the aim of optimizing itaconate production in *U. maydis,* this strain implicates several advantageous aspects. In its haploid form, *U. maydis* shows unicellular growth – a huge advantage over filamentously growing fungi that simplifies handling and fermentations processes and therefore reduces costs [77,123]. With approximately 120 min, it has a relatively short doubling time [124]. It is robust against high product titers, impurities in medium and industrial feedstocks, insensitive to high hydromechanic stress, and osmotolerant [39,83]. Additionally, it can grow on a variety of carbon sources, such as glucose, arabinose, xylose, xylan, cellulose, or biological oils [39,99].

The itaconate biosynthesis pathway in *U. maydis* (Figure 6) and the corresponding genes (Figure 7) are identified and well characterized [78,125]. As in *A. terreus*, *cis*-aconitate is produced in the TCA cycle. By a mitochondrial tricarboxylate *cis*-aconitate/malate antiporter termed Mtt1, *cis*-aconitate is exported into the cytosol where it is converted into itaconate via the intermediate *trans*-aconitate. These two reactions are catalyzed by the *cis*-aconitate isomerase and *trans*-aconitate decarboxylase Adi1 and Tad1, respectively. Itaconate is then directly exported to the

extracellular space via the major facilitator Itp1 or first degraded into (S)-2-hydroxyparaconate (2-HP) via the P450 monooxygenase Cyp3, before 2-HP itself is secreted into the extracellular environment. The whole gene cluster is under the control of the regulator Ria1 [78]. In a previous study, it could be verified that a deletion of *cyp3* and an overexpression of *ria1*, which leads to an up-regulation of the whole gene cluster, drastically increased itaconate production by almost 4-fold compared to the wildtype [78].

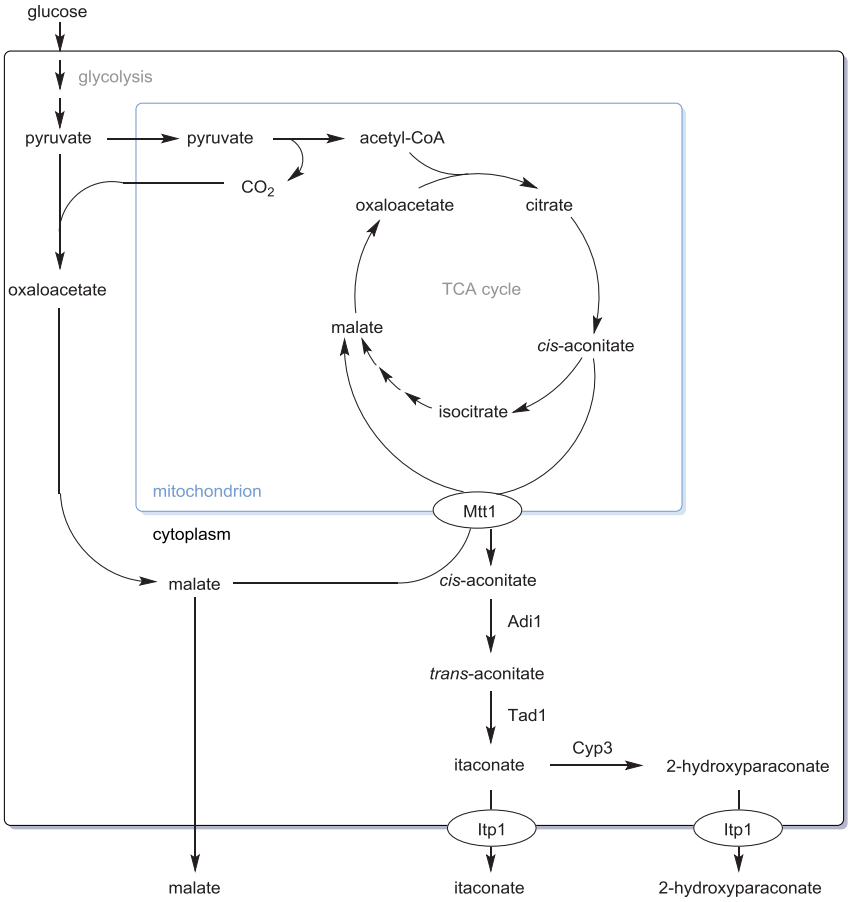

Figure 6: Itaconate biosynthesis pathway in *U. maydis*. Pyruvate is generated from glucose through glycolysis taking place in the cytoplasm. It enters the mitochondria, where it is converted to acetyl-CoA and forms citrate together with oxaloacetate during the TCA cycle. Citrate is dehydrated to *cis*-aconitate which is transported from the mitochondria into the cytosol via the mitochondrial tricarboxylate transporter Mtt1 and converted to *trans*-aconitate by the *cis*-aconitate isomerase Adi1. From *cis*-aconitate, itaconate is generated by the *trans*-aconitate decarboxylase Tad1. Itaconate is either directly transported out of the cell via the major facilitator Itp1 or converted to (S)-2-hydroxyparaconate mediated by the P450 monooxygenase Cyp3, which is than exported via Itp1 (modified from [78]).

Figure 7: Schematic overview of the gene cluster involved in itaconate biosynthesis and transport of *U. maydis* (modified from [125]).

In addition to itaconate, *U. maydis* produces several other metabolites under nitrogen-limiting fermentation conditions [126], including organic acids (malate, succinate, itaconate, itatartarate, (S)-2-hydroxyparaconate), polyols (erythritol, mannitol), extracellular glycolipids (MELs, UA), and intracellular triacylglycerol lipids (TAGs) [99,101,127–129]. Several biochemical pathways and the related genes or gene cluster have been characterized and engineered including those of MELs [130], UA [131] or intracellular TAGs [128,132].

MELs were first detected in 1955 by Haskins *et al*. and described as “extracellular globules of ‘oil’” with a higher density than water [59]. MELs are amphipathic lipids that function as bio surfactants due to their surface activity [133]. It allows adhesion to hydrophobic surfaces and ensures an enhanced availability of hydrophobic nutrients during pathogen-host-interaction [133–135]. The molecular structure of a MEL is characterized by a disaccharide of mannose and erythritol acylated with short- and medium-chain fatty acids at the mannose unit [126,136–138]. Depending on the acetylation degree of the sugar, four groups of MELs are distinguished: fully acetylated MEL A, partially acetylated MEL B and MEL C, and deacetylated MEL D [130,139]. The genes involved in MEL biosynthesis are organized in a gene cluster comprising five open reading frames: *mat1*, *mmf1*, *mac1*, *emt1*, and *mac2* (Figure 9 A). The first step of the hypothetical MEL biosynthesis pathway is mediated by a glycosyltransferase, Emt1 (Figure 8 A). It catalyzes the mannosylation of erythritol to form mannosylerythritol. Mannosylerythritol is acylated by the two putative acyltransferases Mac1 and Mac2, before it is acetylated by the acetyltransferase Mat1. Previous studies verified that the single mutant strains *U. maydis* MB215 Δ*emt1*, Δ*mac1*, and Δ*mac2* completely lost their ability to produce MELs [130,135].

UA was first described in 1950 by Haskins [140] as extracellular substance with antibiotic activity [141]. UAs are visible as needle-like crystals in the medium [140]. The molecular structure is characterized by a cellobiose unit O-glycosidically linked to 15, 16-dihydroxy- or 2,15,16-trihydroxypalmitic acid [142,143]. The cellobiose is single-acetylated and esterified with a short-chain β-hydroxy fatty acid [143]. The enzymes responsible for UA biosynthesis are arranged in a large gene cluster of 12 open reading frames (Figure 9 B) including the regulatory transcription factor *rua1*, a nuclear protein of the C_2H_2 zinc finger family, and two cytochrome P450 monooxygenases named Cyp1 and Cyp2 (Teichmann et al. 2010, 2007). The latter catalyze the first two hydroxylation steps of palmitic acid to 16-hydroxy palmitic acid and further to 15,16-dihydroxy palmitic acid within the UA biosynthesis pathway [143] (Figure 8 B). For c*yp1*-deficient *U. maydis* strains, it could be verified that UA secretion was completely eliminated [135].

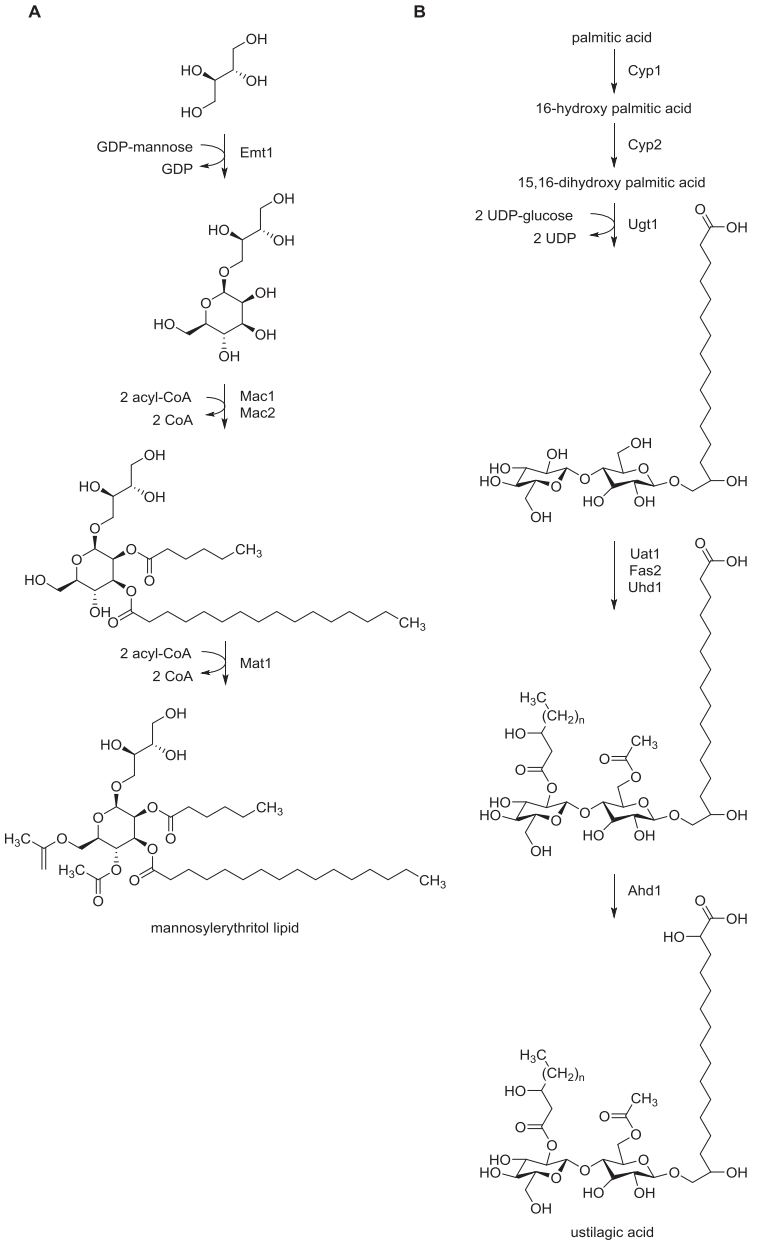

Figure 8: Proposed biosynthetic pathways for MEL (A) and UA production (B). (A) Emt1 – glycosyltransferase, Mac1 – putative acyltransferases, Mac2 – putative acyltransferases; Mat1 – acetyltransferase; (B) Cyp1 – P450 monooxygenase, Cyp2 – P450 monooxygenase, Ugt1 –glycosyltransferase, Uat1 – acyltransferase, Fas2 – single-chain fatty acid synthase, Uhd1 – hydroxylase, Ahd1 – hydroxylase (modified from [130,143]).

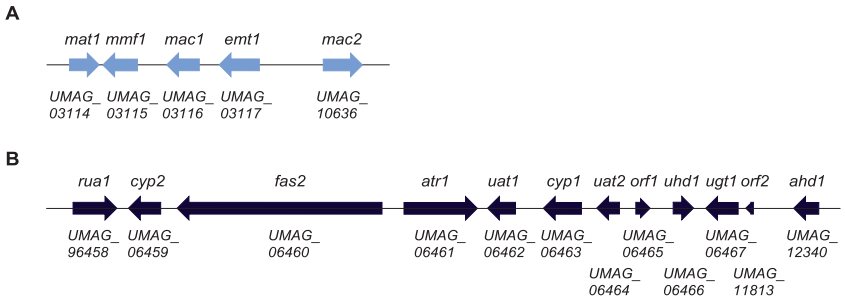

Figure 9: Organization of the gene clusters regulating MEL (A) and UA (B) biosynthesis. *mat1* – acetyltransferase, *mmf1* – major facilitator, *mac1* – putative acyltransferases, *emt1* – glycosyltransferase, *mac2* – putative acyltransferases; (B) *rua1* – regulator of UA gene cluster, *cyp2* – P450 monooxygenase, *fas2* – single-chain fatty acid synthase, *atr1* – potential export protein of ABC-transporter family, *uat1* – acyltransferase, *cyp1* – P450 monooxygenase, *uat2* – acetyltransferase, *orf1* – unknown function, *uhd1* – hydroxylase, *ugt1* – glycosyltransferase, *orf2* – unknown function, *ahd1* – hydroxylase (modified from [130,144]).

Under nitrogen starvation, *U. maydis* also produces large amounts of neutral lipids, mainly TAGs and sterol esters, which are stored as intracellular lipid droplets [128]. Increased TAG synthesis can constitute between 50 and 87 % of the dry weight in some microorganisms including yeast, green algae, or bacteria [145]. The accumulation of lipids as a response to starvation conditions allows the cell to satisfy its energy demands [134,146,147]. De novo fatty acid synthesis significantly contributes to TAG formation. Extracellular fatty acids enter the cell and conjugate with acetyl-CoA to form fatty acyl-CoA. In the ER, glycerolipid-synthesis enzymes mediate the synthesis of diacylglycerol from fatty acyl-CoA. Diacylglycerols are subsequently acylated to TAGs by diacylglycerol acyltransferase (DGAT) enzymes or enter phospholipid-synthesis pathways [128,132]. In *Chlorella minutissima* UTEX 2219, TAG production was increased by 35 % within 14 days in comparison to the wildtype when expressing the genomic sequence of a *dgat* from *Yarrowia lipolytica* P01g, *YALI0E07986p* [148]. Another study confirmed this correspondence between DGAT activity and TAG content. Deleting *dgat1* and *dgat2* in differentiated adipocytes, completely stopped TAG synthesis and lipid droplet formation in this type of mammalian cells [149].

The information about *U. maydis*' secondary metabolites and their biosynthesis show that there is indeed a spectrum of fundamental research discovering underlying pathways and (potentially) evolved genes. In contrast to this basic knowledge, until today little has been done to use it on a biotechnological level.

1.4 Scope and Outline of this thesis

This thesis was written as part of the TTRAFFIC (Toxicity and TRAnsport For Fungal-based production of Industrial Chemicals) project. The overall aim of this thesis was the optimization of itaconate production by *U. maydis* to make it a biocatalyst competitive to *A. terreus*.

Chapter 1 gives a general overview of the need of bio-based fuels and chemicals as alternatives to fossil-based products. In this context, it was focused on the biosynthesis of itaconate which was classified as one of the top 12 value-added chemicals from biomass. Applications and market potential of itaconate as platform chemical are presented, as well as the current industrial production performed by fermentations using the filamentous fungus *A. terreus*. Increasing disadvantages drive the search for alternative production hosts such as the Ustilaginaceae family including *U. maydis*. To improve itaconate production in *U. maydis*, different strategies were pursued:

Section 2.1 deals with the reduction of by-product formation and the resulting effect on itaconate production in terms of the performance parameters titer, yield, and rate. The biosynthesis of the secondary metabolites MELs, UAs, neutral lipids, malate, and 2-HP was reduced respectively blocked by metabolic engineering. Knowledge about the underlying pathways and involved genes was used to manipulate selected genes or complete gene clusters. This way, itaconate production parameters could be significantly enhanced compared to the hyper-producing mutant strain *U. maydis* MB215 Δ*cyp3* P_{etef}*ria1* published by Geiser *et al.* [78].

Based on the results of chapter 2.1, metabolic engineering was further advanced in section 2.2. The production strain described in the previous chapter lost its ability to enter the filamentous growth phase. Additionally, the *mttA* gene of *A. terreus* was overexpressed. While the first mutation had a positive influence on itaconate production, evaluating the expression cassette of integrated *mttA* revealed that the degree of itaconate production improvement is strongly dependent on the copy number.

In section 2.3, another approach than rational strain design was followed. Adaptive laboratory evolution was successfully used to enhance tolerance of *U. maydis* against low pH values and high itaconate concentrations of up to 60 g L^{-1} in the medium. Genome sequencing of selected evolved strains was performed to identify mutations underlying these enhanced tolerances.

In general, this thesis confirms the potential of Ustilaginaceae, especially *U. maydis*, as alternative host for the industrial production of itaconate. Further strain optimization and process development would still enlarge this potential and would make sure that this microorganism significantly contributes to the needed change from petroleum-derived to sustainable, economically bio-based production processes.

Chapter 2

Results

Generation of an *U. maydis* strain optimized for the production of itaconate by the reduction of by-product formation

Contributions:

Marc Gauert, Jörg Mampel, Dirk Ritzmann and Simon Seibert from the BRAIN AG coordinated and performed lipid analysis by FAMES detection. Hamed Hosseinpour Tehrani provided an overexpression construct and a strain engineered by CRISPR/Cas9 technology, which was used as reference for the evaluation of itaconic acid production by HPLC.

2 Results

2.1 Generation of an *U. maydis* strain optimized for the production of itaconate by the reduction of by-product formation

2.1.1 Summary

2.1.2 Introduction

Ustilago maydis, a member of the Ustilaginaceae family, is a well-established model organism for the investigation of fungal mating, DNA recombination, RNA biology, cell signaling, and plant-pathogen interactions [115]. It also represents large biotechnological potential due to features such as natural production of a wide range of value-added molecules, insensitivity to medium impurities and hydromechanic stress, and unicellular growth [39,77,83]. Main metabolites are organic acids (malate, succinate, itaconate, itatartarate, (S)-2-hydroxyparaconate), polyols (erythritol, mannitol), glycolipids (MELs, UA) and intracellular TAGs [99,101,127–129]. Culture conditions influence the composition of the product spectrum. For instance, nitrogen-starvation conditions are an important activator for the synthesis of organic acids and glycolipids [130,135,143]. A decrease in pH however leads to a switch from the production of organic acids to polyols and glycolipids as preferred metabolite classes [150]. Table 3 gives a more detailed overview of *U. maydis* metabolites including molecular structure, associated genes, maximally achieved titers, and application fields.

Especially itaconate is an established bio-based product with high potential as platform chemical. This chemical already has a widespread application spectrum, e.g., in the industrial production of fibers, plastics, rubbers, and surfactants, but also as bioactive compound in agriculture, pharmacy, or medicine sector [33,34] – and the market for itaconic acid is expected to expand in the next years [47]. So far, this chemical is commercially produced in fermentation processes using the filamentous fungus *A. terreus*. Other natural producers like *U. maydis*, *Candida* sp., or *Rhodotorula* sp. are to date not competitive with the production parameters of this microorganism that is able to reach itaconate titers of up to 160 g L^{-1}, yields of 0.63 g_{ITA} g_{glu} and rates of 1.53 g L^{-1} h^{-1} [38,64]. Nevertheless, the efficiency of *A. terreus* in producing itaconate goes along with a high sensitivity to fermentation conditions, such as hydro-mechanical stress, viscosity of fermentation broth or oxygen supply [39,65]. Morphology control is a major challenge which hinders reproducibility of cultivations, even when they are performed with the same strains [34,65].

Table 3: Overview of *U. maydis* metabolites including molecular structure, associated genes, titers achieved by Ustilaginaceae wildtype strains, and application fields.

	metabolite	molecular structure	associated genes/ gene cluster	maximal titers achieved by Ustilaginaceae	application fields
organic acids	2-hydroxy-paraconate (2-HP)	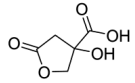	*cyp3* (UMAG_05074) [78,125]	21 g L^{-1} (*U. maydis* MB215 wt) [78] 24 g L^{-1} (*U. maydis* MB215 Δ*Um_mtt1* + P_{etef}*AT_mttA*) [172] 25 g L^{-1} (*U. cynodontis* K320) [175]	
	itaconate (ITA)	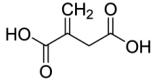	ITA gene cluster (*cyp3* (UMAG_05074), *rdo1* (UMAG_12299), *tad1* (UMAG_05076), *itp1* (UMAG_11777), *adi1* (UMAG_117788), *mtt1* (UMAG_05079), *ria1* (UMAG_05080)) [78,125]	22 g L^{-1} (*U. cynodontis* Δ*fuz7* Δ*cyp3* P_{etef}*mttA* P_{ria1}*ria1*) [238] 28 g L^{-1} (*U. cynodontis* K470) [175] ~ 30 g L^{-1} (*P.antarctica* NRRL Y-7808) [62] 33 g L^{-1} (*U. maydis* MB215 Δ*Um_mtt1* + P_{etef}*AT_mttA*) [172] 45 g L^{-1} (*U. maydis* MB215 wt) [77] 63 g L^{-1} (*U. maydis* MB215 Δ*cyp3* P_{etef} *ria1*) [78] 75 g L^{-1} (*P.tsukubaensis* H488) [239]	production of polymers, resins, plastics, coatings, adhesives [34,38]
	itatartarate (ITT)	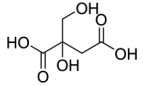	*rdo1* (UMAG_12299) (putatively) [78,101]	~ 15 g L^{-1} (*U. maydis* IFO 6907) [101] 17 g L^{-1} (*U. cynodontis* K320) [175] no standards of itatartarate are commercially available [153]	
	malate (Mal)	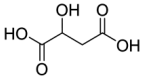	UMAG_00403, UMAG_11161, UMAG_10787	21 g L^{-1} (*U. maydis* 2229 wt) [78] 30 g L^{-1} (*U. maydis* 2162 wt) [150] > 50 g L^{-1} (*U. crus-galli*) [101] 63 g L^{-1} (*Macalpinomyces ordensis* BRIP 26904 a) [93] 134 g L^{-1} (*U. trichophora* TZ1) [240] 195 g L^{-1} (*U. trichophora* TZ1) [164] 196 g L^{-1} (*U. trichophora* TZ1) [163]	acidulant in food, beverage and candy industry; usage in pharmaceuticals, paints, textile finishing [32,240,241]
	succinate (Suc)	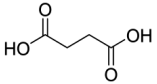	UMAG_00844, UMAG_01172, UMAG_01672, UMAG_11353	5 g L^{-1} (*U. maydis* 2162 wt) [150] 20 g L^{-1} (*U. trichophora* TZ1) [240]	surfactant, detergent and foaming agent, ion chelator in electroplating, pharmaceutical, antibiotics, amino acid and vitamin production [242]

	metabolite	molecular structure	associated genes/ gene cluster	maximal titers achieved by Ustilaginaceae	application fields
polyols	erythritol (Ery)	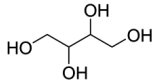	unknown	73 g L^{-1} (*U. maydis* 2162 wt) [243] 100 g L^{-1} (Ustilaginomycetes 618A-01) [244] 243 g L^{-1} (*P. tsukubaensis* KN75) [100]	low calorie sweetener (suitable for diabetics); pharmaceuticals intermediates, fine chemicals, polymers [129,245]
	mannitol (Man)	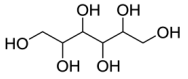	unknown	~ 3 g L^{-1} (*U. esculenta* K500) [101] ~ 6 g L^{-1} (*U. syntherismae* K221) [101] 13 g L^{-1} (*U. cynodontis* K320) [101]	low calorie sweetener (diabetic food), pharmaceutical formulation of chewable tablets and granulated powders [246,247]
glycolipids	mannosyl-erythritol-lipid (MEL)	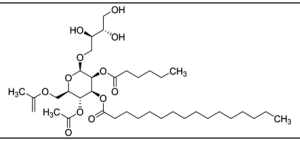	MEL gene cluster (*mat1* (UMAG_03114), *mmf1* (UMAG_03115), *mac1* (UMAG_03116), *emt1* (UMAG_03117), *mac2* (UMAG_10636)) [130]	30 g L^{-1} (*U. maydis*) [248] 32 g L^{-1} (*S. sorghi*) [249] 140 g L^{-1} (*P. antarctica*) [250] 142 g L^{-1} (*P. rugulosa*) [251]	textile, paper, polymer, plastic, cosmetics, pharmaceuticals, food and machinery industry [252]
	ustilagic acid (UA)	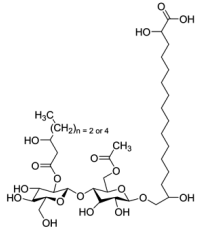	UA gene cluster (*rua1* (UMAG_96458), *cyp2* (UMAG_06459), *fas2* (UMAG_06460), *atr1* (UMAG_06461), *uat1* (UMAG_06462), *cyp1* (UMAG_06463), *uat2* (UMAG_06464), *orf1* (UMAG_06465), *uhd1* (UMAG_06466), *ugt1* (UMAG_06467), *orf2* (UMAG_11813), *ahd1* (UMAG_12340)) [99]	0.6 g L^{-1} (*P. hubeiensis*) [253] 20 g L^{-1} (*U. maydis*) [99,254]	
neutral lipids	triacyl-glycerol (TAG)	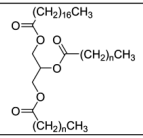	*dgat* (UMAG_03937) [128,132]	16 g L^{-1} (*Pseudozyma* sp.) [255]	biodiesel, biosurfactants in cosmetics, food, bioremediation [256]

Therefore, research increasingly focuses on Ustilaginaceae as alternative unicellular biocatalysts. *U. maydis* represents a promising organism for application in industrial itaconate production. However, the potpourri of metabolites naturally synthesized by *U. maydis* results in sub-optimal specificity, productivity and yield of itaconate as a product. One way to approach this problem is by metabolic engineering. With the fully annotated genome sequence of *U. maydis* strain 521 [151] and whole-genome sequences of nine itaconate-producing Ustilaginaceae [152,153], promoters of the *U. maydis* itaconate cluster enabling heterologous gene expression under nitrogen starvation and therefore during the itaconate production phase [154], the invention of a metabolic redox dynamic monitoring system that is based on the sensor protein Peredox-mCherry to investigate cellular metabolism on the basis of NADH/NAD^+ dynamics [155], there are attractive resources to foster metabolic changes. For efficient gene deletion, gene insertion and promoter exchange, different genetic tools are available, including CRISPR/Cas9 genome editing [156], FLP/FRT system with marker recycling [157], or Golden Gate Cloning [158].

Previous studies already achieved promising results in characterizing and engineering by-product formation pathways. Regarding itaconate production, a combination of deleting *cyp3*, which encodes an itaconate oxidase that converts itaconate into 2-hydroxyparaconate, and overexpressing *ria1*, which encodes the itaconate gene cluster regulator, increased itaconate titers by nearly 4-fold [78]. Simultaneously, overexpressed *ria1* leads to an about 58 % decrease in malate production due to an up-regulation of *mtt1* encoding a *cis*-aconitate/malate antiporter [78]. MEL biosynthesis is mediated by a gene cluster comprising five genes. Single mutant strains *U. maydis* MB215 Δ*emt1*, Δ*mac1* and Δ*mac2* completely lost their ability to produce MELs [130,135]. The gene cluster regulating UA biosynthesis is formed by 12 open reading frames including the cytochrome P450 monooxygenase encoded by *cyp1* [131,143]. It was verified that UA secretion was completely eliminated in c*yp1*-deficient *U. maydis* strains [135]. In view of intracellular TAG formation, it is considered that diacylglycerol acyltransferases (DGAT) represent main contributors in other oleaginous species by mediating the acylation of diacylglycerols to TAGs [128,132].

Based on this detailed knowledge of biosynthetic pathways and the potential application of modern genetic tools, this study used both to reduce the product spectrum of *U. maydis*. Marker-free gene cluster deletion and promoter replacement were combined to focus all carbon flux into itaconate as main product, while simultaneously generating a chassis that is more manageable in a process context.

2.1.3 Results and Discussion

2.1.3.1 Insights into the genomic sequence of the engineered *U. maydis* deletion strain

To generate an *U. maydis* chassis with reduced by-product formation, multiple knockouts were successively performed in one strain. Due to a limited number of selection markers suitable for *U. maydis*, two cloning techniques avoiding this restriction were used: the CRISPR/Cas9 system [156] and a recombination method based on marker insertion by homologous recombination and subsequent FLP-mediated marker-removal [157]. When using the Cas9-based system, repair templates

were used for all knockouts in order to achieve full gene deletions through homologous recombination. These templates consisted of two 1000 bp long fragments corresponding to the flanking regions upstream and downstream of the sequence to be eliminated, and were transformed as linear PCR product along with the circular Cas9 plasmid which included the guide RNA of the target gene.

The conversion of itaconate into (S)-2-hydroxyparaconate was disrupted by the deletion of *cyp3*. To abolish glycolipid production, repair templates were designed to remove the whole gene clusters encoding MEL [130] and UA [143] synthesis pathways. The production of TAGs, which make up the main part of lipid droplets in *U. maydis* [128], was reduced by single gene deletion of UMAG_03937. This gene, subsequently named *dgat*, encodes a putative diacylglycerol acyltransferase. This membrane enzyme is mostly found in the endoplasmic reticulum and catalyzes the final step in TAG biosynthesis. TAGs are essential as energy storage compounds and membrane building and maintaining elements [159,160]. Two diacylglycerol acyltransferase, DGAT1 and DGAT2, were identified amongst others in mammals, fungi, and plants. Sequence alignment of yeast DGAT2 against the *U. maydis* 521 genome revealed a hypothetical *Ustilago* protein product featuring conserved sequence motifs of the DGAT2 family (NCBI accession number XP_760084, UMAG_03937) [161]. Therefore, UMAG_03937 was chosen as target gene for TAG biosynthesis deletion. As last modification, *ria1*, encoding the itaconate cluster regulator, was overexpressed by a promoter exchange to improve itaconate and decrease malate production. This was achieved by the inclusion of the P_{etef} promoter into the repair template, yielding a marker-free insertion (H. Hosseinpour Tehrani, in preparation).

For the generation of Δ*cyp3*, ΔMEL, ΔUA and ΔP_{ria1}::P_{etef}, the CRISPR/Cas9 system was used, while Δ*dgat* was achieved using the FRT/FLP-mediated approach. All modifications were performed consecutively in the order Δ*cyp3*, ΔMEL, ΔUA, Δ*dgat* and ΔP_{ria1}::P_{etef}, ultimately yielding the final chassis strain *U. maydis* MB215 Δ*cyp3* ΔMEL ΔUA Δ*dgat* ΔP_{ria1}::P_{etef} (hence called *U. maydis* MB215 ITA chassis). While Δ*cyp3*, Δ*dgat* and ΔP_{ria1}::P_{etef} were successfully verified by PCR analysis, the confirmation of the deletion of larger genomic fragments (18.5 kb MEL cluster [130], 58 kb UA cluster [143]) could not be conclusively confirmed by PCR analysis. Re-sequencing of the chassis strain genome and comparison to the reference genome of *U. maydis* 521 wildtype [151] illustrated the reasons for such difficulties (Figure 10).

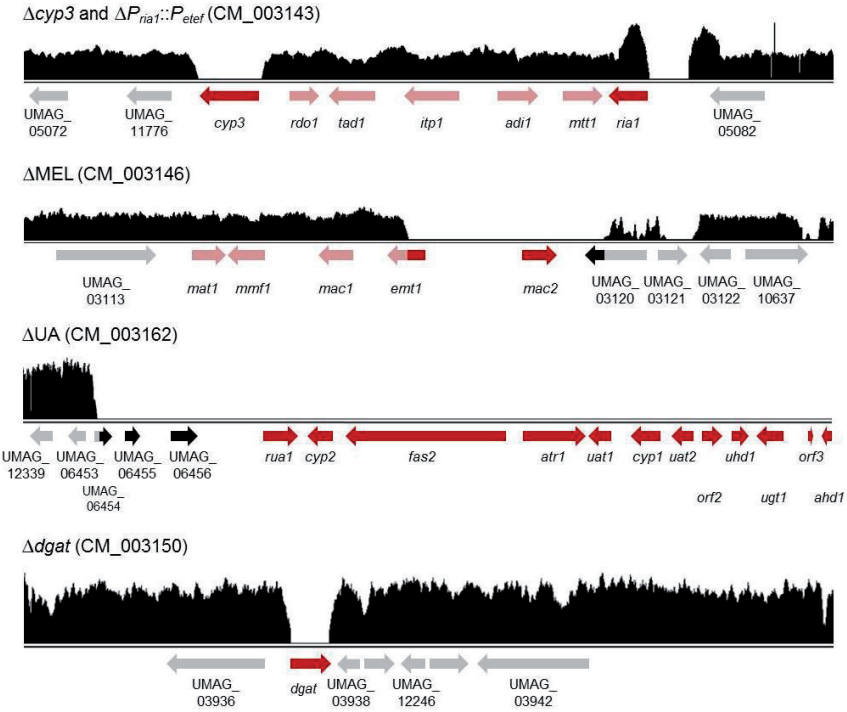

Figure 10: Genome analysis of the final engineered strain *U. maydis* MB215 Δ*cyp3* ΔMEL ΔUA Δ*dgat* ΔP_{ria1}::P_{etef} by whole-genome sequencing. The coverage of Illumina sequencing reads mapped against the *U. maydis* 521 wildtype sequence visualizes the different deletion loci. Target genes are marked in red, verified deletions in dark red and unexpectedly non-performed deletions in light red. Further unexpected gene deletions are marked in black.

This re-sequencing confirms the successful deletion of *cyp3* and *dgat*. However, several unexpected phenomena were encountered with the other modifications. As expected, no reads mapped against the native *ria1* promoter region, indicating successful deletion of the 1334 bp fragment. The coverage of reads mapped against the native P_{tef} promoter was almost twice as high as the baseline (not shown), indicating that the stronger P_{etef} promoter was successfully inserted. However, the coverage of the two 1000 bp regions flanking the promoter, precisely matching the homology arms of the repair template, is approximately twice the mean value. Further single read analysis and PCR verification indicated that the entire pJET1.2-vector carrying the repair template had been integrated into the genome (Figure 11). Thereby, both flanks exist as duplicates, in the native and in the synthetically generated form. This lead to a duplication of P_{etef} *ria1* whereof one *ria1* version existed in a truncated 985 bp form instead of the original 1231 bp. This potentially increases the expression level of *ria1*, partly in truncated form. However, it is unlikely that further overexpression of Ria1 affects itaconate production, given that separate experiments aimed at increasing Ria1 expression through multicopy insertion of a

P$_{etef}$*ria1* construct did not increase production compared to the single copy insertion strain reported by Geiser *et al*. strain [125] (H. Hosseinpour Tehrani, in preparation).

Figure 11: Genomic sequence after exchange of the native *ria1* promoter by the constitutive *etef* promoter.

The targeted deletion of the 18.5 kb MEL gene cluster responsible for the synthesis of MELs identified a disadvantage of the Cas9 system. The system is based on a Cas9 nuclease cleaving within a specific target gene, here *emt1*. The formed double strand break was supposed to be repaired via homologous recombination using the repair template specifically designed for the deletion of the MEL cluster. However, the sequencing shows only the successful deletion of the complete *mac2* gene and of the first 43 % of the *emt1* sequence, while the other cluster genes are still present. Although the full cluster was not deleted as intended, the deletion of *mac2* and the disruption of *emt1* is sufficient to abolish MEL synthesis in *U. maydis* [130,135]. A similar effect occurred with the deletion of the 58 kb cluster encoding the UA biosynthesis pathway. Besides the targeted elimination of all UA cluster genes, additional genes upstream of the cluster were also deleted. UMAG_06454, UMAG _06455 and UMAG _06456 encode hypothetical proteins with unknown function. This event of co-elimination of adjacent sequences also occurred for a part of gene UMAG_03120 flanking the MEL cluster. This gene also encodes an uncharacterized protein. However, no significant sequence similarities between repair template and sequences surrounding the affected regions were identified as hints for the deletions observed. A lack of reads in the end of chromosome 23 where the UA cluster is encoded was also noticeable. However, comparing this coverage to the coverage of the telomeric regions of other chromosomes exhibited an overall downgraded coverage quality in these highly repetitive sequences.
Summarized, all intended genomic modifications were achieved but in three out of four cases where the Cas9 system was used unintended side effects occurred. These unintentional effects indicate that homologous recombination often fails to resolve along the designed repair templates, even with relatively long flanks. In the case of deletion of longer genomic stretches, the unpredictability of the chosen method is exacerbated by the fact that correct deletions are harder to detect by PCR methods due to the lack of a suitable positive control. This highlights the usefulness of genome resequencing, especially in this case of multiple iterative deletions.

2.1.3.2 Investigation of the impact of knockouts of lipid by-products on the *U. maydis* metabolite spectrum by TLC, FAMES detection, and HPLC analysis

To determine the effect of the generated knockouts ΔMEL and ΔUA on the glycolipid production of *U. maydis*, mutant and reference strains were cultivated under nitrogen-limiting conditions and their extracts were analyzed by thin-layer chromatography (TLC). *U. maydis* wt produces both metabolites, MELs and UAs, in large amounts as is evident from the characteristic band patterns for the two

glycolipid classes in TLC. The molecular structure of MELs is characterized by a mannosylerythritol disaccharide acylated with short- and medium-chain fatty acids [126,136–138]. The migration profile of MELs features a pattern of three bands that results from the different acetylation degrees of the lipids. MEL A is fully acetylated and therefore migrates faster than the partially acetylated MEL B and MEL C or the de-acetylated MEL D form [130,139]. In contrast, functioning UA synthesis is visualized by four bands. The molecular structure of UAs is characterized by a cellobiose unit O-glycosidically linked to 15, 16-dihydroxy- or 2, 15, 16-trihydroxypalmitic acid [142]. Two lower bands indicate UA derivatives whose palmitic acid residue holds the third α-hydroxyl group. An upper double band results from derivatives lacking this hydroxyl group.

The deletion of either *mac1*, *mac2*, or *emt1* resulted in a complete loss of MEL synthesis in *U. maydis* [130,135]. Regarding UA biosynthesis, it is known that *ahd1* mediates the last step of the UA biosynthesis pathway, the α-hydroxylation of the palmitic acid moiety. The UA derivatives generated this way are represented by the double band with the slower migration profile. The upper double band is formed by derivatives without such a hydroxyl group. It was proven that a*hd1* deletion strains were not able to produce α-hydroxylated UA derivatives, but only secreted the non-hydroxylated form [143]. In contrast, knocking-out *cyp1* resulted in a complete loss of UA production. It is supposed that Cyp1 functions in the first step and therefore upstream of Adh1 in the UA production pathway [135].

As an initial verification of the expected genotype of the deletion of the MEL and UA clusters, mutant and reference strains were cultivated for 72 h (YNB medium + 5 % glucose, System Duetz®) and their extracts were analyzed by thin-layer chromatography (TLC) (Figure 12).

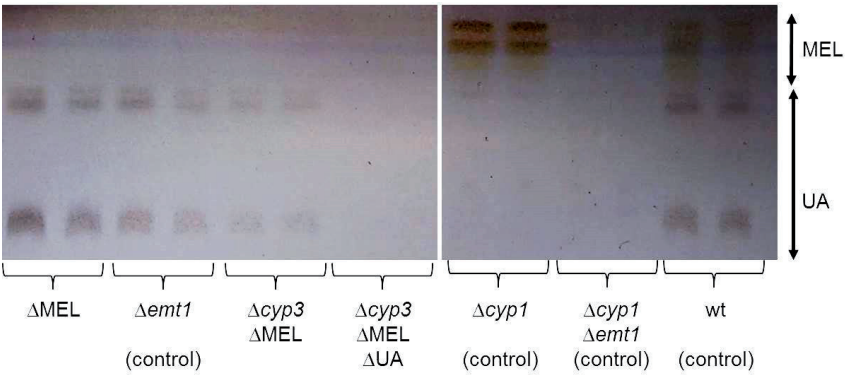

Figure 12: Glycolipid production by *U. maydis* MB215 wildtype and various mutant strains analyzed by separating ethyl acetate extracts in thin-layer chromatography (TLC). *U. maydis* MB215 wildtype produces both glycolipid classes, MELs and UA. MEL-cluster- and *emt1*-deficient strains lack the ability to produce MELs. UA-cluster- and *cyp1*-deletion strains are not able to produce UA.

As controls, *U. maydis* MB215 wildtype and strains with single gene deletions of *cyp1* (UA, provided by E. Geiser) and *emt1* (MEL, generated in this study), as well as the double deletion strain Δ*cyp1* Δ*emt1* (provided by E. Geiser) were used. This

experiment confirms that, although the disruption of the gene clusters did not happen exactly as intended, they did abolish the production of the corresponding glycolipid, as all ΔMEL strains lack the characteristic upper bands in the TLC, while all ΔUA strains lack the lower TLC bands associated with ustilagic acid. As expected, the Δ*cyp3* background did not affect the glycolipid profile. With the Δ*cyp3* ΔMEL ΔUA triple deletion strain, no glycolipid-associated bands could be detected.

Besides TLC, the lipid spectra of the designed deletion strains were analyzed in a more quantitative manner by lipid extraction and fatty acid methyl esters (FAMES) detection. Lipidic extracts were obtained from the whole culture broths after 72 h of cultivation (MTM, 50 g L^{-1} glucose, pH 6.5 buffered with 100 mM MES, System Duetz®) in order to quantify both intra- and extracellular lipids. Lipid composition was analyzed by lipid hydrolysis followed by methylation and flame ionization detection (GC-FID) of the fatty acids. All engineered strains were analyzed along with the wildtype as reference in order to identify the impact of each single mutation.

In the fatty acid profiles, the retentions times correlate with the fatty acid chain lengths. These chain lengths are indicative for the three investigated lipid classes (MELs, UA, and triglycerides), since each have different characteristic chain lengths. MELs are composed of a mannosylerythritol disaccharide esterified with short- (C_1 to C_6) and medium-chain (C_8 to C_{12}) fatty acids [126,136–138,162], while the intracellular lipids consist of a glycerol backbone bound to three mainly long-chain fatty acids, predominantly palmitic (C_{16}), linoleic (C_{18}) and oleic acids (C_{18}) [128]. The molecular structure of cellobiose lipids is characterized by two glucose units forming the cellobiose moiety. This disaccharide is singularly acetylated and esterified with a short-chain fatty acid (C_6 or C_8). Another C_{16}-chain fatty acid, 15,16-dihydroxy- or 2,15,16-trihydroxy-palmitic acid, is O-glycosidically linked [143,144].

As can be expected from the molecular MEL structure, the deletion of this glycolipid class significantly affected the share of detected methylated short- and medium chain fatty acids. Compared to the wildtype spectrum, methylcaproate (C_6) and -laurate (C_{12}) were no longer detectable, while methylmyristate (C_{14}) was decreased to 27 % of the wildtype value (Figure 13, A). The absence, respectively, decrease of C_6- to C_{14}-fatty acids results in a general shift within the fatty acid production spectrum. An upregulation of long-chain fatty acids like methylstearate (C_{18}) by 26 %, -arachidate (C_{20}) 30 %, -behenate (C_{22}) 44 % and -lignocerate (C_{24}) by 116 % is observed indicating that ΔMEL induces an increase in TAG production. Unexpectedly, addition of Δ*cyp3* in *U. maydis* MB215 Δ*cyp3* ΔMEL further stimulates the metabolic flux into the TAG production pathway, illustrated by a 32 % higher amount of methylpalmitate (C_{16}), a 34 % higher amount of methylpalmitoleate ($C_{16:1}$), 25 % more methyloleate ($C_{18:1}$) and 19 % more methylarachidate (C_{20}). The intended product itaconate was also detected by this method as dimethylitaconate, the titer of which was 1.3-fold higher than in the preceding strain *U. maydis* MB215 ΔMEL.

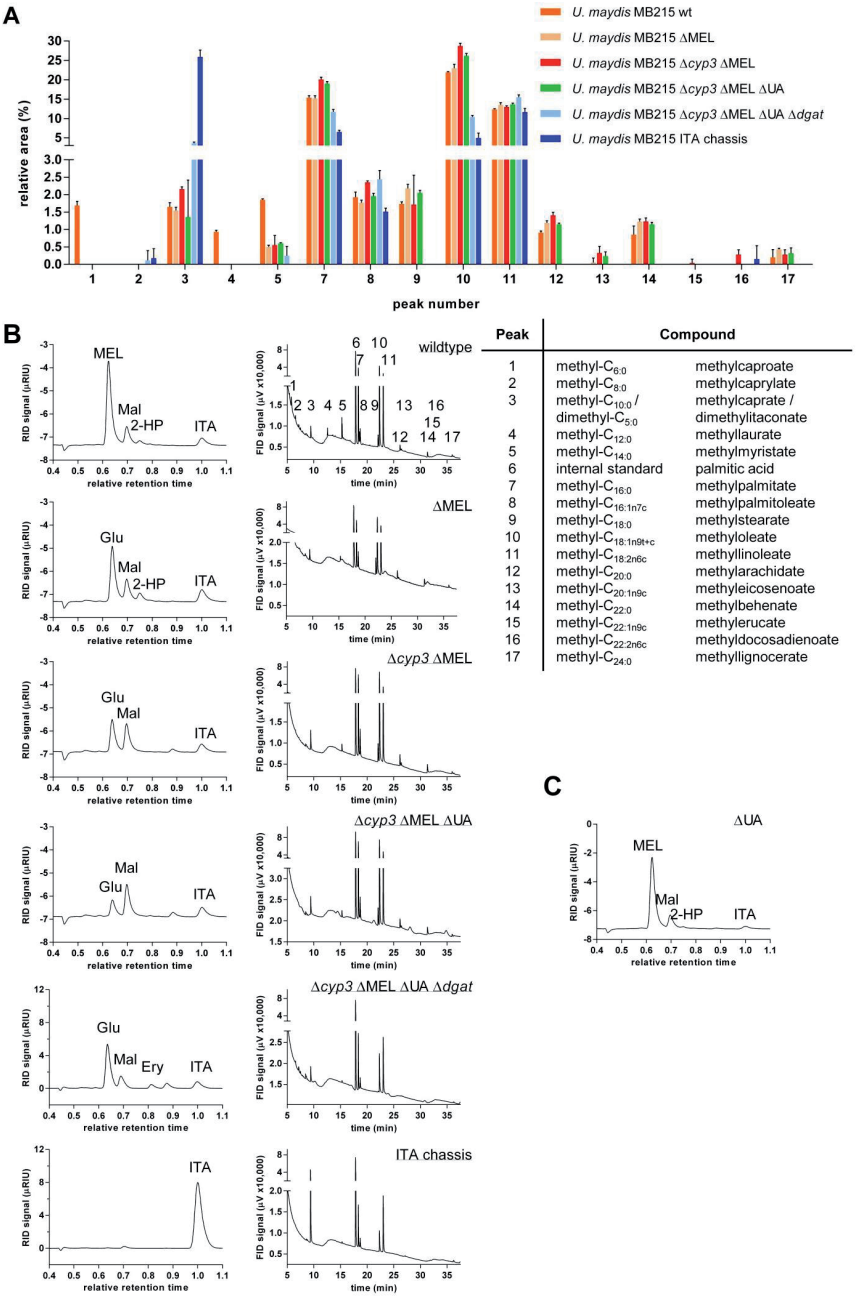

Peak	Compound	
1	methyl-$C_{6:0}$	methylcaproate
2	methyl-$C_{8:0}$	methylcaprylate
3	methyl-$C_{10:0}$ / dimethyl-$C_{5:0}$	methylcaprate / dimethylitaconate
4	methyl-$C_{12:0}$	methyllaurate
5	methyl-$C_{14:0}$	methylmyristate
6	internal standard	palmitic acid
7	methyl-$C_{16:0}$	methylpalmitate
8	methyl-$C_{16:1n7c}$	methylpalmitoleate
9	methyl-$C_{18:0}$	methylstearate
10	methyl-$C_{18:1n9t+c}$	methyloleate
11	methyl-$C_{18:2n6c}$	methyllinoleate
12	methyl-$C_{20:0}$	methylarachidate
13	methyl-$C_{20:1n9c}$	methyleicosenoate
14	methyl-$C_{22:0}$	methylbehenate
15	methyl-$C_{22:1n9c}$	methylerucate
16	methyl-$C_{22:2n6c}$	methyldocosadienoate
17	methyl-$C_{24:0}$	methyllignocerate

Figure 13: (A) Lipid analysis of *U. maydis* MB215 wildtype and various mutant strains by lipid extraction and fatty acid methyl esters (FAMES) detection. For lipid formation, all strains were incubated for 72 h in MTM

with an initial glucose concentration of 50 g L^{-1} and a pH of 6.5 buffered with 100 mM MES using 24-well System Duetz® plates. Error bars indicate the standard deviation from the mean (n = 6). **(B) HPLC and FAMES diagrams of *U. maydis* MB215 wildtype and mutant strains.** For HPLC analysis, supernatants were obtained from culture broths after 96 h (*U. maydis* MB215 wildtype, ΔMEL, Δ*cyp3* ΔMEL, and Δ*cyp3* ΔMEL ΔUA) respectively 124.5 h (*U. maydis* MB215 Δ*cyp3* ΔMEL ΔUA Δ*dgat* and ITA chassis) of cultivation in MTM with 50 g L^{-1} glucose and a pH 6.5 buffered with 100 mM MES using 24-well System Duetz® plates. For FAMES analysis, the strains were cultivated for 72 h in MTM with 50 g L^{-1} glucose and a pH 6.5 buffered with 100 mM MES using 24-well System Duetz® plates. **(C) HPLC diagram of *U. maydis* MB215 ΔUA.** Supernatant was obtained from culture broth after 96 h of cultivation in MTM with 50 g L^{-1} glucose and a pH 6.5 buffered with 100 mM MES using 24-well System Duetz® plates. For all HPLC diagrams, the retention time is specified relative to the retention time of itaconate (Glu: glucose, MEL: mannosyl-erythritol lipids, Mal: malate, 2-HP: (S)-2-hydroxyparaconate, Ery: erythritol, ITA: itaconate).

Interestingly, ΔUA does not show essential differences in the lipid spectrum. This might be due to amounts of UA produced under the given conditions that were too low to generate detectable amounts of the corresponding fatty acid residues. The peaks for the short C_6 or C_8 fatty acid residue appear in the time range which is characterized by a relatively high background signal. Within the first 10 min of detection, this leads to a drop in the baseline curve until it reaches a relatively constant level. C_6 or C_8 peaks below this baseline level would be undetectable. However, the subsequent deletion of *dgat* resulted in a significant reduction or complete loss of longer-chain fatty acids. The presence of C_{14} fatty acids is further decreased by 59 %, while the proportions of methylpalmitate (C_{16}) and -oleate ($C_{18:1}$) are reduced by 38 respectively 60 % in comparison to the triple mutant values. Production of $C_{18:0}$ as well as the whole spectrum of C_{20} to C_{24} fatty acids is completely eliminated. This confirms that the putative *dgat* (UMAG_03937) plays a role in triglyceride production. In the cultures of the Δ*cyp3* ΔMEL ΔUA Δ*dgat* strain, 2.2-fold more dimethylitaconate was detected than in the wildtype samples. With the final overexpression of *ria1*, the resulting *U. maydis* MB215 ITA chassis produced 15.7-fold more dimethylitaconate than the wildtype. This relative increase is confirmed by HPLC measurements of the samples sent for FAMES analysis, which yielded an almost identical factor from the values generated by FAMES analysis. In this strain, the synthesis of C_{16} and $C_{18:1}$ fatty acids is further reduced by 38-52 % compared to its predecessor, corresponding to an overall reduction of 21-77 % compared to the wildtype. This decrease in lipid production likely indicates a decrease in biomass concentration, leading to a lower volumetric production of membrane phospholipids. This might in part be caused by the increased flux towards itaconate, which may impose a “pull” effect on the competing lipid synthesis pathways.

The elimination of lipidic by-product formation is also clearly apparent from the corresponding GC-chromatograms (Figure 13, B). Whereas the wildtype samples have a multitude of small peaks, the chromatogram of the ITA chassis is completely smooth aside from the large dimethylitaconate peak and the C_{16}/C_{18} peaks associated with the membrane lipids from the biomass.

In all, the modifications engineered into the ITA chassis greatly reduced the lipid profile of this strain, and therewith also the associated by-products. The elimination of this by-product formation itself had a significant positive effect on itaconate

production, which was amplified by the overexpression of the itaconate gene cluster regulator encoded by *ria1*.

The deletion of lipid formation turned out to be a major advantage in handling and efficiency of processes such as filtration or centrifugation (Figure 14, B). Within minutes of centrifugation, cells of the ITA chassis strain formed a pellet and the complete supernatant turned transparent. With the wt, this effect was not able to be reached within 60 min. The microscopy images identify strong extracellular lipid production of the wt likely resulting in the formation of a cloudy supernatant of suspended glycolipids during centrifugation (Figure 14, A). It is also expected that TAG formation affects the density of the cells making a subpopulation neutrally buoyant. Both effects are avoided in the ITA chassis strain fostering its centrifugation and filtration efficiency.

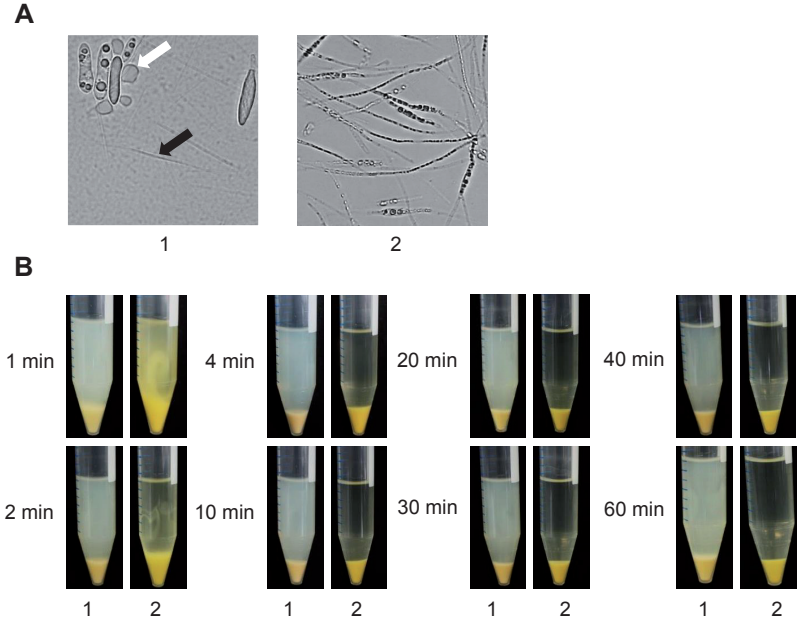

Figure 14: (A) Identification of mannosylerythritol lipid (white arrow) and ustilagic acid (black arrow) production in *U. maydis* MB215 wildtype (1) and *U. maydis* MB215 ITA chassis (2) by microscopy. (B) Impact of knocking out lipid by-products on the centrifugation efficiency at 5,000 rpm using 5 ml culture broth of *U. maydis* MB215 wildtype (1) and *U. maydis* MB215 ITA chassis (2).

Since the GC-FID FAMES analysis is limited to the detection of compounds with a carboxylic acid group that can be methylated, supernatants of the strains mentioned above were additionally analyzed by HPLC-RI. Unlike the FAMES analysis, this HPLC method can detect sugars and polyols, and also enables a more quantitative analysis of the organic acids. For optimal comparison between HPLC samples, all retention times were specified relative to the retention time of itaconate defined as

1.0. With this normalization, small analytical variations are minimized, enabling a more accurate comparison of overlapping peaks in the start of the chromatogram.
In comparison to the wildtype and the final ITA chassis strain, all knockout strains were unable to consume the initial glucose concentration of 50 g L^{-1} in 96 h, respectively 124.5 h resulting in a glucose peak at a relative retention time (rRT) of 0.64, with residual glucose concentrations between 0.90 ± 0.2 g L^{-1} and 7.0 ± 0.4 g L^{-1}. This supports the hypothesis of a metabolic "pull" effect of the secondary metabolite production pathways, since disruption of these pathways decreases the substrate uptake rate, while overexpression of the itaconate production pathway increases it again. Some of the intermediate deletion strains also produce comparatively low amounts of erythritol (Ery) and an unknown compound with a rRT of 0.88, indicating that the disruption of major metabolic outlets "pushes" carbon into alternative pathways. Another peak with a rRT of 0.62 is apparent in the chromatograms of the wildtype and *U. maydis* MB215 ΔUA. This peak is assumed to be caused by MELs, since it is absent in all other strains, which only have the deletion of the MEL cluster in common.
The HPLC analysis confirms that itaconate conversion into (*S*)-2-hydroxyparaconate (rRT of 0.75) is abolished by deletion of *cyp3*. The overexpression of *ria1* combined with all by-product deletions resulted in a 1.1-fold increase compared to *U. maydis* MB215 Δ*cyp3* ΔMEL ΔUA Δ*dgat*, and a considerable 10.2-fold increase of the final itaconate titer compared to the wildtype. The differences in the degree of enhancement between FAMES and HPLC analyses might be due to small experimental deviations of the itaconate production of the wildtype, which can vary strongly based on sampling time, inoculation density and lag phase due to the oxidation of itaconate into 2-hydroxyparaconate.
Simultaneously to the increase in ITA synthesis, the overexpression of *ria1* drastically reduced malate production by 84 %. Malate is considered a precursor of itaconate being exchanged with mitochondrial *cis*-aconitate by the mitochondrial antiporter *mtt1*, which is upregulated by the *ria1* overexpression [78,80]. The resulting increased transport of malate from the cytosol back into mitochondria likely decreases malate secretion [78]. The remaining trace of secreted malate detected in the final ITA chassis can easily be removed by slightly longer incubation since this metabolite is rapidly consumed by *Ustilago* upon depletion of glucose [163,164].
In all, the production of virtually all detectable by-products was abolished in the final ITA chassis strain, while the metabolic flux towards the target product itaconate was drastically increased compared to the wildtype.

2.1.3.3 Evaluation of the engineered strains focusing on itaconate production

To evaluate the effect of the elimination of by-product formation on itaconate production in detail, the performance of the *U. maydis* MB215 ITA chassis (Δ*cyp3* ΔMEL ΔUA Δ*dgat* ΔP_{ria1}::P_{etef}) and its precursor strain *U. maydis* MB215 Δ*cyp3* ΔMEL ΔUA Δ*dgat* was investigated over time by analyzing the culture supernatant via HPLC (Figure 15). *U. maydis* MB215 wildtype and *U. maydis* MB215 Δ*cyp3* ΔP_{ria1}::P_{etef}, a strain equivalent to the already engineered and published itaconate hyper-producing strain *U. maydis* MB215 Δ*cyp3* P_{etef}*ria1* [78], were included as reference strains. The strains were cultivated in 24-well System Duetz® plates in MTM containing an initial

concentration of 50 g L^{-1} glucose as sole carbon source buffered with 100 mM MES at a pH of 6.5.

The strain in which all four by-product-forming genes were deleted without *ria1* overexpression (*U. maydis* MB215 Δ*cyp3* ΔMEL ΔUA Δ*dgat*) produced 2.1 ± 0.4 g L^{-1} itaconate, which is not significantly different from the wildtype. However, *U. maydis* MB215 Δ*cyp3* ΔMEL ΔUA Δ*dgat* consumed 25 % less glucose than the wildtype resulting in a 51 % higher product to substrate yield for itaconate from glucose ($Y_{ITA/glu}$). This confirms the observations described in section 2.1.3.2 which suggest that this strain lacks sufficient metabolic "outlet", thereby reducing its substrate uptake rate. However, with 0.03 and 0.05 g_{ITA} g_{glu}^{-1}, both yields were still low compared to the maximal theoretical yield of 0.72 g_{ITA} g_{glu}^{-1} excluding growth [78]. After 72 h, no further itaconate was produced, likely due to the low pH of the culture as it is known that in wildtype *U. maydis* MB215 itaconate production is inhibited at pH values below 5 [150]. Interestingly, this also further reduced the substrate uptake rate in the Δ*cyp3* ΔMEL ΔUA Δ*dgat* strain. Both strains produced around 3 g L^{-1} malate, which is absent in the two other strains bearing the ΔP_{ria1}::P_{etef} promoter exchange. The wildtype strain additionally produced (S)-2-hydroxyparaconate from itaconate. This pathway is deleted due to Δ*cyp3* in all other strains tested.

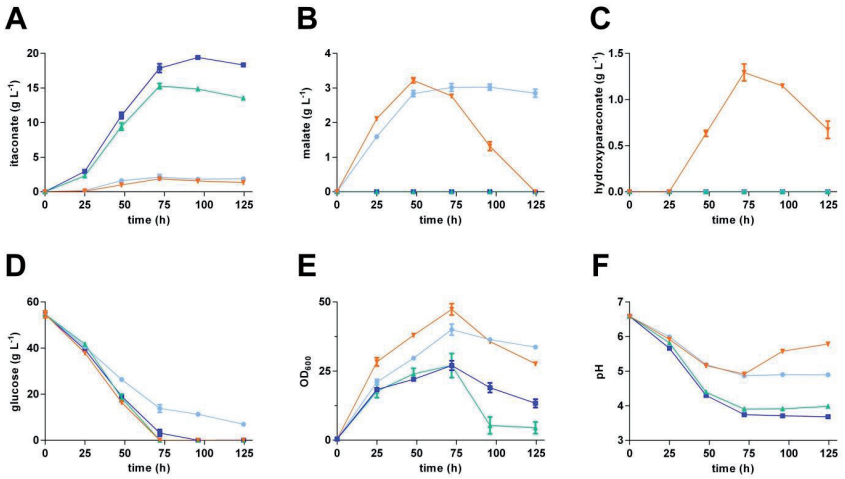

Figure 15: System Duetz® cultivation of various *U. maydis* MB215 strains in MTM. (A) itaconate concentration, (B) malate concentration, (C) (S)-2-hydroxyparaconate concentration, (D) glucose concentration, (E) pH values, and (F) OD_{600} for *U. maydis* MB215 wildtype (orange), *U. maydis* MB215 Δ*cyp3* ΔP_{ria1}::P_{etef} (green), *U. maydis* MB215 Δ*cyp3* ΔMEL ΔUA Δ*dgat* (light blue), and *U. maydis* MB215 Δ*cyp3* ΔMEL ΔUA Δ*dgat* ΔP_{ria1}::P_{etef} (dark blue) measured over time. Screening was performed in MTM containing 50 g L^{-1} glucose and 100 mM MES. Values are the arithmetic mean of three biological replicates. Error bars indicate the standard deviation from the mean.

Table 4: Production parameters of various *U. maydis* MB215 strains resulting from a System Duetz® cultivation in MTM. *U. maydis* MB215 wildtype (orange), *U. maydis* MB215 Δ*cyp3* ΔP_{ria1}::P_{etef} (green), *U. maydis* MB215 Δ*cyp3* ΔMEL ΔUA Δ*dgat* (light blue), and *U. maydis* MB215 Δ*cyp3* ΔMEL ΔUA Δ*dgat* ΔP_{ria1}::P_{etef} (dark blue) were screened for 125 h in MTM containing 50 g L^{-1} glucose and 100 mM MES. Values are the arithmetic mean of three biological replicates. Errors indicate the standard deviation from the mean.

symbol	strain	ITA titer$_{max}$ * (g L^{-1})	r_P ** (g L^{-1} h^{-1})	$r_{P,max}$ *** (g L^{-1} h^{-1})	$Y_{P/S}$ **** (g_{ITA} g_{glu}^{-1})
	U. maydis MB215 wildtype	1.9 ± 0.1	0.03 ± 0.00	0.04 ± 0.00	0.03 ± 0.00
	U. maydis MB215 Δ*cyp3* ΔP_{ria1} ::P_{etef}	15.3 ± 0.4	0.21 ± 0.01	0.31 ± 0.02	0.28 ± 0.01
	U. maydis MB215 Δ*cyp3* ΔMEL ΔUA Δ*dgat*	2.1 ± 0.4	0.02 ± 0.00	0.06 ± 0.00	0.05 ± 0.01
	U. maydis MB215 Δ*cyp3* ΔMEL ΔUA Δ*dgat* ΔP_{ria1} ::P_{etef}	19.4 ± 0.3	0.25 ± 0.01	0.35 ± 0.02	0.36 ± 0.02

* maximum itaconic acid titer ** overall itaconate production rate ([glu] > 3.2 g L^{-1}) *** maximum itaconate production rate
**** yield itaconate per glucose consumed

The previous optimized itaconate producing strain *U. maydis* MB215 Δ*cyp3* ΔP_{ria1}::P_{etef} achieved a maximal titer of 15.3 ± 0.4 g L^{-1} itaconate, which is 8.1-fold higher than that of the wildtype. The final engineered strain *U. maydis* MB215 Δ*cyp3* ΔMEL ΔUA Δ*dgat* ΔP_{ria1}::P_{etef} combines the deletions of the chosen by-products with the overexpression of *ria1*. With this strain, the itaconate titer was further increased to 19.4 ± 0.3 g L^{-1} constituting a 10.2-fold higher titer compared to the wildtype and accordingly a 1.3-fold increase compared to *U. maydis* MB215 Δ*cyp3* ΔP_{ria1}::P_{etef}. The maximal rate$_{ITA}$ ($r_{ITA,max}$) was increased by 13 %, the overall production rate$_{ITA}$ (r_{ITA}) by 19 %, and the $Y_{ITA/glu}$ by 29 %.
These results show that the four deletions reduce the metabolic flux of glucose into these by-product pathways, reflected in a decreased glucose uptake rate. The fact that this alone doesn't lead to a much higher product titer clearly indicates a bottleneck at the level of the itaconate production pathway, which was eliminated by overexpression of *ria1* resulting in an up-regulation of all itaconate cluster genes [125]. The combination of the four knockouts and ΔP_{ria1}::P_{etef} lead to a significant improvement in the itaconate titer and in the corresponding rate and yield parameters.

The production of large amounts of itaconate goes along with a drastic drop of the pH value in the medium. In the previous experiment, the pH decreased from 6.5 to 3.68 for the ITA chassis. In order to eliminate potential pH inhibition as well as glucose limitation, the buffer system was changed from MES to $CaCO_3$ and the substrate concentration was increased. The addition of 66 g L^{-1}, respectively 99 g L^{-1} $CaCO_3$ enables a much higher buffer capacity, which under the chosen conditions keeps the pH constantly between 6 and 7, even with increased initial glucose concentrations of 100 g L^{-1}, respectively 150 g L^{-1} (Figure 16, C). Again, *U. maydis* MB215 Δ*cyp3* ΔP_{ria1}::P_{etef} functioned as reference strain.
From 100 g L^{-1} fully consumed glucose, *U. maydis* MB215 Δ*cyp3* ΔP_{ria1}::P_{etef} maximally synthesized 43.7 ± 4.7 g L^{-1} itaconate within 194 h corresponding to a $Y_{ITA/glu}$ of 0.39 ± 0.05 g_{ITA} g_{glu}^{-1} and a r_{ITA} of 0.22 ± 0.01 g L^{-1} h^{-1} (Figure 16, A; Table 5). In the same time and with comparable glucose consumption behavior, the *U. maydis* MB215 ITA chassis reached a maximal titer of 53.5 ± 5.0 g L^{-1}

accomplishing a $Y_{ITA/glu}$ of 0.47 ± 0.03 g_{ITA} g_{glu}^{-1} and a r_{ITA} of 0.28 ± 0.00 g L^{-1} h^{-1}. These parameters confirm that the three by-product deletions ΔMEL, ΔUA and Δ*dgat* resulted in a more efficient conversion of glucose into itaconate and therefore in a 21 - 27 % improvement of the parameters itaconate titer, r_{ITA}, and $Y_{ITA/glu}$ (Table 5).

The same trend was observed with an initial glucose concentration of 150 g L^{-1} (Figure 16, B), but with slightly lower yields of 0.38 ± 0.01 g_{ITA} g_{glu}^{-1} and 0.41 ± 0.01 g_{ITA} g_{glu}^{-1} (Table 5). Likely, this physiological behavior did not originate from an increased formation of other products, but from an increased CO_2 production due to a higher osmotic stress.

The cultivation with a lower initial glucose concentration also resulted in higher production rates. While *U. maydis* MB215 Δ*cyp3* ΔMEL ΔUA Δ*dgat* ΔP_{ria1}::P_{etef} reached maximal ITA titers within 196 h during the cultivation with 100 g L^{-1} glucose according to a r_{ITA} of 0.28 ± 0.03 g L^{-1} h^{-1}, starting with 150 g L^{-1} glucose yielded maximal itaconate titers after 239 h corresponding to a r_{ITA} of 0.23 ± 0.01 g L^{-1} h^{-1}. The lower production rate might be based on an increased stress level during growth phase as a result of high initial glucose concentrations. This phase is crucial for amongst others biomass production or pathway induction. Therefore, occurring stress negatively influences the following production phase.

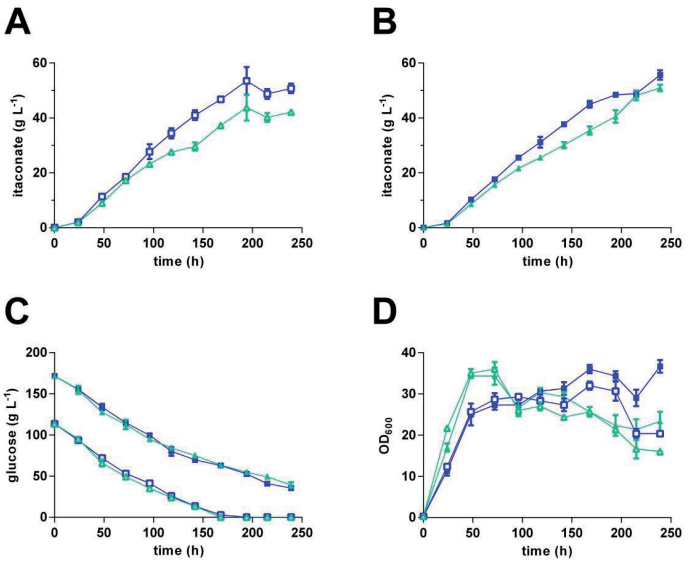

Figure 16: Shake flask cultivation of two *U. maydis* MB215 mutant strains in MTM. (A) itaconate concentration from 100 g L^{-1} glucose, (B) itaconate concentration from 150 g L^{-1} glucose, (C) glucose concentration, (D) OD_{600} measured over time for *U. maydis* MB215 Δ*cyp3* ΔP_{ria1}::P_{etef} (green) and *U. maydis* MB215 Δ*cyp3* ΔMEL ΔUA Δ*dgat* ΔP_{ria1}::P_{etef} (blue) cultivated in MTM containing 100 or 150 g L^{-1} glucose and 66 or 99 g L^{-1} $CaCO_3$ to constantly hold a pH of 6.5. Values are the arithmetic mean of three biological replicates. Error bars indicate the standard deviation from the mean.

Table 5: Production parameters of two *U. maydis* MB215 mutant strains resulting from a shake flask cultivation in MTM. *U. maydis* MB215 Δ*cyp3* ΔP_{ria1}::P_{etef} (green) and *U. maydis* MB215 Δ*cyp3* ΔMEL ΔUA Δ*dgat* ΔP_{ria1}::P_{etef} (blue) were screened for 239 h in MTM containing 100 or 150 g L^{-1} glucose and 66 or 99 g L^{-1} $CaCO_3$ to constantly hold a pH of 6.5. Values are the arithmetic mean of three biological replicates. Errors indicate the standard deviation from the mean.

medium	symbol	strain	ITA titer$_{max}$* (g L^{-1})	r_P** (g L^{-1} h^{-1})	$r_{P,max}$*** (g L^{-1} h^{-1})	$Y_{P/S}$**** (g_{ITA} g_{glu}^{-1})
100 g L^{-1} glu 66 g L^{-1} $CaCO_3$	△	*U. maydis* Δ*cyp3* ΔP_{ria1} ::P_{etef}	43.7 ± 4.7	0.22 ± 0.01	0.35 ± 0.03	0.39 ± 0.05
	□	*U. maydis* Δ*cyp3* ΔMEL ΔUA Δ*dgat* ΔP_{ria1} ::P_{etef}	53.5 ± 5.0	0.28 ± 0.00	0.39 ± 0.01	0.47 ± 0.03
150 g L^{-1} glu 99 g L^{-1} $CaCO_3$	▲	*U. maydis* Δ*cyp3* ΔP_{ria1} ::P_{etef}	50.9 ± 1.2	0.21 ± 0.00	0.30 ± 0.00	0.38 ± 0.01
	■	*U. maydis* Δ*cyp3* ΔMEL ΔUA Δ*dgat* ΔP_{ria1} ::P_{etef}	55.7 ± 1.7	0.23 ± 0.01	0.36 ± 0.02	0.41 ± 0.01

* maximum itaconic acid titer ** overall itaconate production rate ([glu] > 1.2 g L^{-1}) *** maximum itaconate production rate
**** yield itaconate per glucose consumed

Summarized, elimination of by-product formation turned out to be a major advantage not only in process design and efficiency, but also in the optimization of ITA production when combined with the overexpression of *ria1*. The cultivations quantified this enhancement, and laid the basis for further process design, e.g., for pulsed fed-batch fermentations in controlled bioreactors.

Filamentous growth prevention and overexpression of the *A. terreus mttA* in a by-product reduced *U. maydis* strain for optimized itaconate production

Contributions:

Hamed Hosseinpour Tehrani provided an overexpression construct and performed bioreactor cultivations with the help of Svenja Meyer and Katharina Saur using a reference strain generated with the help of Ana Catarina Rodrigues Lóia.

2.2 Filamentous growth prevention and overexpression of the *A. terreus mttA* in a by-product reduced *U. maydis* strain for optimized itaconate production

2.2.1 Summary

2.2.2 Introduction

Itaconate has great potential as bio-based building block in the polymer industry. In 2004, the organic acid was classified as one of the top 12 value-added platform chemicals derived from biomass as a renewable feedstock [32]. Today, itaconate and its derivatives are found in many application fields, such as the production of paper, paints, and fibers, in the medical and pharmaceutical sector, or in waste water treatment [33,34,39], providing a stable market for this bio-based chemical. However, its relatively high production costs prevent an even more expanded usage range [83]. Optimization of promising itaconate production hosts is therefore needed. *A. terreus*, *U. maydis*, *Candida spec.*, or *P. antarctica* are microorganisms naturally producing itaconate [49,60,62,101].

U. maydis produces itaconate as one product from a potpourri of metabolites including organic acids, such as malate, succinate, or (S)-2-hydroxyparaconate, polyols, such as erythritol and mannitol, and different lipid classes [99,101,127–129]. This feature, combined with further benefits like unicellular growth or insensitivity to impurities and hydromechanic stress, makes *U. maydis* an attractive candidate for industrial application [39,77,83]. However, compared to the filamentous ascomycete *A. terreus*, nowadays used for commercial itaconate fermentation production, parameters have to be improved to make *U. maydis* competitive and to profit from its several advantages. In commercial itaconic acid production, yield is the most relevant parameter since for bulk products, such as itaconic acid, the substrate cost is often the most relevant price-determining factor. For itaconate production from glucose, the maximal theoretical yield is 0.72 g_{ITA} g_{glu} assuming zero growth. The yield achieved in practice is affected by different factors such as cell density, morphology, medium composition, pH value, oxygen supply, side product formation, and bottlenecks in the itaconate biosynthesis pathway itself [165].

In nature, *U. maydis* is known for its pathogenicity towards maize (*Zea mays*) causing corn smut disease [151]. To penetrate and invade maize tissue, *U. maydis* switches from a yeast-like, non-pathogenic to a filamentous, pathogenic cell form [166]. Although predominantly growing in its single-cell form in fermentation processes, *U. maydis* can switch to filamentous growth under stress conditions [167–169]. Filamentous growth in cultivation broth leads to problems related to high viscosity, oxygen supply, and cell damage [83]. Fuz7, a component of the Ras/mitogen-activated protein kinase (MAPK) pathway, was identified to play an essential role in regulating pathogenicity [167]. It encodes for a putative serine/threonine tyrosine kinase of the MAP kinase kinase (MAPKK/MEK) family [119]. Deletion of *fuz7* generated mutant strains defective for the filamentous phenotype due to interrupted pheromone signaling [167]. For *Ustilago cynodontis*, H. Hosseinpour Tehrani showed that this

knockout forces the cells in the unicellular morphology also under biotechnologically relevant stresses [170].

To improve the yield for one product, the diverse by-product spectrum of *U. maydis* represents another drawback. One approach to shift the production towards itaconate is the use of metabolic engineering. In chapter 2.1, an itaconate hyper-producing *U. maydis* strain with a reduced by-product spectrum was designed this way producing 10.2-fold more itaconate than the wildtype. It is incapable to synthesize 2-hydroxyparaconate, a downstream oxidation product of itaconate, due to a deletion of *cyp3*, which encodes an itaconate oxidase (Δ*cyp3*). The biosynthesis of three lipid classes was eliminated by deletion of the corresponding gene or gene cluster: MELs (ΔMEL), UA (ΔUA), and TAGs (Δ*dgat*) [128,130–132,135,143]. In addition, the itaconate gene cluster regulator encoding *ria1* was overexpressed ($\Delta P_{ria1}::P_{etef}$). In combination with Δ*cyp3,* this led to a 84 % decrease in malate production due to an up-regulation of the *cis*-aconitate/malate antiporter *mtt1*.

In this work, the reduced by-product spectrum was combined with a *fuz7* deletion to prevent filamentous growth and secondly with the overexpression of the mitochondrial tricarboxylate transporter from *A. terreus*, *At_mttA* [171]. The first step of the itaconate biosynthesis pathway in *U. maydis* is the transport of *cis*-aconitate from the mitochondria to the cytosol mediated by Mtt1. However, this initial step is rate-limiting during itaconate production [78,125], and Tehrani *et al*. demonstrated that an *At_mttA* overexpressing *U. maydis* strain has an increased itaconate titer and yield compared to an equivalent *mtt1* overexpression [172]. This way, an *U. maydis* strains was designed to produce itaconate with improved production parameters especially with an increased yield from glucose.

2.2.3 Results and Discussion

2.2.3.1 Prevention of filamentous growth by *fuz7* deletion and its influence on itaconate production

Although wildtype *U. maydis* grows unicellularly in axenic cultures, certain stresses imposed by enhanced itaconate production can induce filamentous growth [170]. Thus, in order to ensure a stable yeast-like morphology, the signal cascade inducing the filamentous phenotype was disrupted by the deletion of *fuz7* (UMAG_01514) in the *U. maydis* MB215 ITA chassis generated in chapter 2.1. The influence of this knockout was assessed in System Duetz® cultivations in MTM containing 50 g L^{-1} glucose and 100 mM MES. The reference strain with intact *fuz7*, *U. maydis* MB215 Δ*cyp3* ΔMEL ΔUA Δ*dgat* ΔP_{ria1}::P_{etef}, achieved a maximal itaconate titer of 19.4 ± 0.3 g L^{-1}, while the strain with Δ*fuz7* produced 24.4 ± 0.5 g L^{-1} corresponding to a 1.3-fold increase (Figure 17 A, Table 6). Full consumption of glucose by both strains resulted in a 25 % improved yield from 0.36 ± 0.02 g_{ITA} g_{glu} to 0.45 ± 0.01 g_{ITA} g_{glu} for the engineered Δ*fuz7* strain. Reaching the final titers within the same time increased the overall production rate by 12 % and the maximal rate by even 26 % (Table 6).

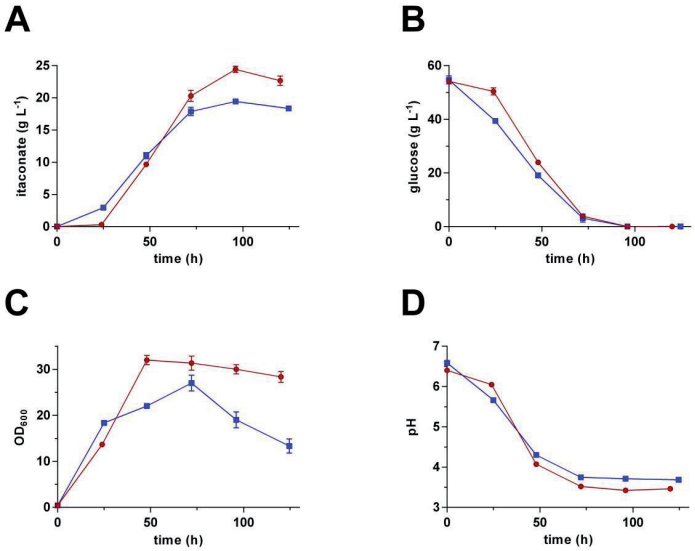

Figure 17: System Duetz® cultivation of an *U. maydis* MB215 Δ*fuz7* mutant in MTM containing 50 g L^{-1} glucose and 100 mM MES. (A) itaconate concentration, (B) glucose concentration, (C) OD_{600}, and (D) pH values measured over time for the control strain *U. maydis* MB215 Δ*cyp3* ΔMEL ΔUA Δ*dgat* ΔP_{ria1}::P_{etef} (blue) and the *fuz7* knockout *U. maydis* MB215 Δ*cyp3* ΔMEL ΔUA Δ*dgat* ΔP_{ria1}::P_{etef} Δ*fuz7* (red). Values are the arithmetic mean of three biological replicates. Error bars indicate deviation from the mean.

Table 6: Comparison of titer, (maximum) rate, and yield for itaconate production of two *U. maydis* MB215 mutant strains after ~120 h of System Duetz® cultivation in MTM containing 50 g L-1 glucose and 100 mM MES. Values are the arithmetic mean of three biological replicates. ± values indicate deviation from the mean.

symbol	strain	ITA titer$_{max}$* (g L^{-1})	r_P** (g L^{-1} h^{-1})	$r_{P,max}$*** (g L^{-1} h^{-1})	$Y_{P/S}$**** (g_{ita} g_{glu}^{-1})
■	*U. maydis* MB215 Δ*cyp3* ΔMEL ΔUA Δ*dgat* ΔP_{ria1}::P_{etef}	19.4 ± 0.3	0.25 ± 0.01	0.35 ± 0.02	0.36 ± 0.02
●	*U. maydis* MB215 Δ*cyp3* ΔMEL ΔUA Δ*dgat* ΔP_{ria1}::P_{etef} Δ*fuz7*	24.4 ± 0.5	0.28 ± 0.01	0.44 ± 0.03	0.45 ± 0.01

* maximum itaconic acid titer ** overall itaconate production rate ([glu] > 3.9 g L^{-1}) *** maximum itaconate production rate
**** yield itaconate per glucose consumed

The results clearly illustrate the benefit of preventing filamentous growth. Normally, *U. maydis* cells start to adhere to the walls of the culture plates during the production phase, when low pH stress and increasing product concentrations occur. This results in irregular or even interrupted oxygen and nutrient supply and exclusion from the buffer effect in the medium for the affected cells. This cell accumulation on the walls was reflected in decreasing optical density values after 72 h (Figure 17, C) and a drastically reduced itaconate productivity (Figure 17, A). This is in contrast to the *fuz7* mutant, which showed a constant itaconate production rate in the production phase, until glucose was depleted (Figure 17, B).

2.2.3.2 Integration and overexpression of the mitochondrial transporter *mttA* from *A. terreus* and its impact on itaconate production

In order to compensate the rate-limiting step in the itaconate production pathway of *U. maydis*, the transport of *cis*-aconitate from the mitochondria to the cytosol mediated by Mtt1, [78,125] an *At_mttA* overexpressing *U. maydis* strain was designed by integrating a P_{etef}*mttA* construct into the *ip*-locus on the genome of the novel Δ*fuz7* mutant strain from section 2.2.3.1. The MttA shuttle enzyme has the great advantage of a higher metabolic flux of itaconic acid precursor molecules than its *U. maydis* analog Mtt1 leading to an increase in itaconate titer and yield [172].

From previous experiments, the potential of multicopy integration events into both, the *ip*-locus and random genomic sites, is known. Therefore, several clones were screened to identify differences and pick the best itaconate producer. Insertion of at least one *mttA* copy was verified by PCR for five clones (K3, K8, K9, K10, and K14) resulting in the strains listed in Table 7. Regarding itaconate production (Figure 18 A), glucose consumption (Figure 18 B), and growth behavior (Figure 18 C), the strains significantly differed from each other.

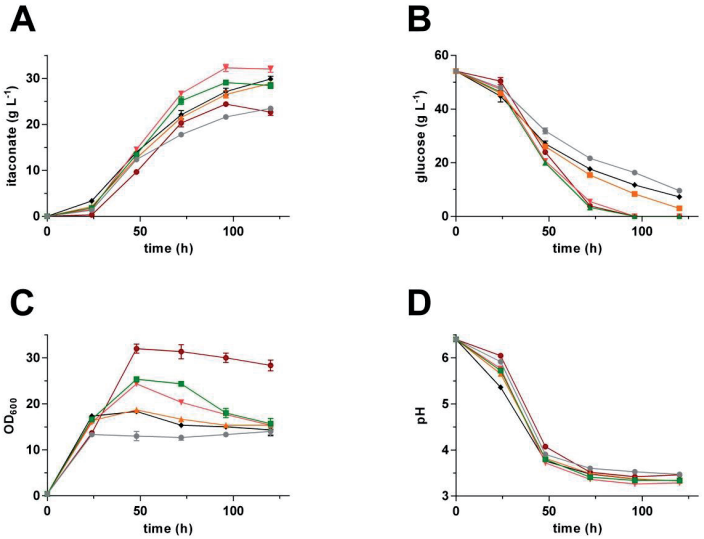

Figure 18: System Duetz® cultivation of five *U. maydis* MB215 ::P_{etef}*mttA* mutants in MTM containing 50 g L^{-1} glucose and 100 mM MES. (A) itaconate concentration, (B) glucose concentration, (C) OD_{600}, and (D) pH values measured over time for the control strain *U. maydis* MB215 Δ*cyp3* ΔMEL ΔUA Δ*dgat* ΔP_{ria1}::P_{etef} Δ*fuz7* (red) and the ::P_{etef}*mttA* transformants *U. maydis* MB215 Δ*cyp3* ΔMEL ΔUA Δ*dgat* ΔP_{ria1}::P_{etef} Δ*fuz7* ::P_{etef}*mttA,* K3 (grey), K8 (green), K9 (orange), K10 (pink), and K14 (black). Values are the arithmetic mean of three biological replicates. Error bars indicate deviation from the mean.

Table 7: Overview of titer, (maximum) rate, and yield regarding itaconate production of *U. maydis* MB215 mutant Δ*cyp3* ΔMEL ΔUA Δ*dgat* ΔP_{ria1}::P_{etef} Δ*fuz7* and five clones of *U. maydis* MB215 Δ*cyp3* ΔMEL ΔUA Δ*dgat* ΔP_{ria1}::P_{etef} Δ*fuz7* ::P_{etef}*mttA*, after 120 h of System Duetz® cultivation in MTM containing 50 g L^{-1} glucose and 100 mM MES. Values are the arithmetic mean of three biological replicates. ± values indicate deviation from the mean.

symbol	strain	ITA titer$_{max}$* (g L^{-1})	r_P** (g L^{-1} h^{-1})	$r_{P,max}$*** (g L^{-1} h^{-1})	$Y_{P/S}$**** (g_{ita} g_{glu}^{-1})
●	*U. maydis* MB215 Δ*cyp3* ΔMEL ΔUA Δ*dgat* ΔP_{ria1} ::P_{etef} Δ*fuz7*	24.4 ± 0.5	0.28 ± 0.01	0.44 ± 0.03	0.45 ± 0.01
●	*U. maydis* MB215 Δ*cyp3* Δ*M*EL ΔUA Δ*dgat* ΔP_{ria1} ::P_{etef} Δ*fuz7* ::P_{etef} *mttA*_K3	23.5 ± 0.6	0.20 ± 0.00	0.46 ± 0.02	0.53 ± 0.01
■	*U. maydis* MB215 Δ*cyp3* ΔMEL ΔUA Δ*dgat* ΔP_{ria1} ::P_{etef} Δ*fuz7* ::P_{etef} *mttA*_K8	29.1 ± 0.1	0.35 ± 0.01	0.49 ± 0.03	0.54 ± 0.01
▲	*U. maydis* MB215 Δ*cyp3* ΔMEL ΔUA Δ*dgat* ΔP_{ria1} ::P_{etef} Δ*fuz7* ::P_{etef} *mttA*_K9	28.9 ± 0.3	0.24 ± 0.00	0.44 ± 0.01	0.57 ± 0.01
▼	*U. maydis* MB215 Δ*cyp3* ΔMEL ΔUA Δ*dgat* ΔP_{ria1} ::P_{etef} Δ*fuz7* ::P_{etef} *mttA*_K10	32.3 ± 0.8	0.37 ± 0.00	0.54 ± 0.01	0.60 ± 0.02
◆	*U. maydis* MB215 Δ*cyp3* ΔMEL ΔUA Δ*dgat* ΔP_{ria1} ::P_{etef} Δ*fuz7* ::P_{etef} *mttA*_K14	29.9 ± 0.7	0.25 ± 0.00	0.44 ± 0.01	0.64 ± 0.03

* maximum itaconic acid titer ** overall itaconate production rate ([glu] > 5.5 g L^{-1}) *** maximum itaconate production rate **** yield itaconate per glucose consumed

Under low pH conditions and from an initial glucose concentration of 50 g L^{-1}, the reference strain without *mttA*, *U. maydis* MB215 Δ*cyp3* ΔMEL ΔUA Δ*dgat* ΔP_{ria1}::P_{etef} Δ*fuz7*, reached a maximal itaconate titer of 24.4 ± 0.5 g L^{-1}. With the exception of K3,

all *mttA* transformants outperformed the reference strain with titers between 28.9 ± 0.3 g L^{-1} and 32.3 ± 0.8 g L^{-1} corresponding to a 18 – 32 % improvement (Figure 18 A, Table 7). K3, K9, and K14 did not consume the full amount of glucose during 120 h of cultivation (Figure 18 B). Strains K8 and K10 had the highest rates, which were 25 and 32 % higher, respectively, compared to the reference. Concerning the overall yield, all *mttA* transformants performed better than the reference, with K14 reaching 88 % of the theoretical maximum (Table 7), corresponding to an increase of 42 % compared to the control strain. Regarding the yields achieved during the production phase (24 – 72 h), all *mttA* transformants also outperformed the reference strain extensively with yields between 0.64 ± 0.02 and 0.82 ± 0.04 g_{ITA} g_{glu} compared to a yield of 0.44 ± 0.01 g_{ITA} g_{glu} for the reference strains. *MttA* integration also had a deep impact on the growth represented by the OD_{600} values after 24 h (Figure 18 C). While *U. maydis* MB215 Δ*cyp3* ΔMEL ΔUA Δ*dgat* ΔP_{ria1}::P_{etef} Δ*fuz7* reached OD_{600} values above 30, all *mttA* transformants remained below this value. Concerning growth, rate, and yield, the *mttA* transformants can be graded into three groups depicting similar trends. K3 had the lowest OD_{600}, rate, and yield values. K9 and K14 showed values in the medium range for the OD_{600} and rate, while K8 and K10 achieved the highest OD_{600} values combined with the highest rates. Concerning the yield, K8, K9, K10, and K14 achieved values in a similar high range with K14 reaching the highest yield of all *mttA* transformants. These trends indicate the presence of a diverse *mttA* copy number in the tested transformants. Hosseinpour Tehrani *et al.* (2019) verified that in *mttA* overexpressing strains biomass growth and glucose consumption were strongly decreased [172]. It is assumed that the growth phase-related production of MttA, which is under the control of the constitutive P_{etef} promoter, forces the *cis*-aconitate export from the mitochondria that in turn leads to the observed growth defects in comparison to the control strain without a copy of *mttA*.

The trends regarding OD_{600} and rate values were reproducible under screening conditions where pH stress was excluded of by the use of $CaCO_3$ as buffer system (Figure 19). However, the titers achieved were higher than the ones from the MES-buffered cultivation due to the higher buffer capacity of $CaCO_3$ and substrate concentration (Figure 19, A). With 54.4 ± 0.2 g L^{-1}, K14 produced the highest titer.

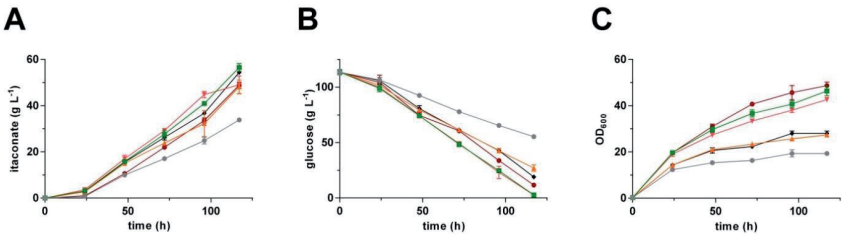

Figure 19: System Duetz® cultivation of six *U. maydis* MB215 mutants in MTM containing 100 g L^{-1} glucose and 66 g L^{-1} $CaCO_3$ to constantly hold a pH of 6.5. (A) itaconate concentration, (B) glucose concentration, and (C) OD_{600} measured over time for *U. maydis* MB215 Δ*cyp3* ΔMEL ΔUA Δ*dgat* ΔP_{ria1}::P_{etef} Δ*fuz7* (red) and five clones of *U. maydis* MB215 Δ*cyp3* ΔMEL ΔUA Δ*dgat* ΔP_{ria1}::P_{etef} Δ*fuz7* ::P_{etef}*mttA,* K3 (grey), K8 (green), K9 (orange), K10 (pink), and K14 (black). Values are the arithmetic mean of three biological replicates. For some data points, outliers were omitted. Error bars indicate deviation from the mean.

Table 8: Overview of titer, (maximum) rate, and yield regarding itaconate production of two *U. maydis* MB215 mutant strains, *U. maydis* MB215 Δ*cyp3* ΔMEL ΔUA Δ*dgat* ΔP_{ria1}::P_{etef} Δ*fuz7* and five clones of *U. maydis* MB215 Δ*cyp3* ΔMEL ΔUA Δ*dgat* ΔP_{ria1}::P_{etef} Δ*fuz7* ::P_{etef}*mttA*, after 117 h of System Duetz® cultivation in MTM containing 100 g L^{-1} glucose and 66 g L^{-1} $CaCO_3$. Values are the arithmetic mean of three biological replicates. For some data points, outliers were omitted. ± values indicate deviation from the mean.

symbol	strain	ITA $titer_{max}$ * (g L^{-1})	r_P ** (g L^{-1} h^{-1})	$r_{P,max}$ *** (g L^{-1} h^{-1})	$Y_{P/S}$ **** (g_{ita} g_{glu}^{-1})
	*U. maydis* MB215 Δ*cyp3* ΔMEL ΔUA Δ*dgat* ΔP_{ria1} ::P_{etef} Δ*fuz7*	48.8 ± 1.3	0.42 ± 0.01	0.70 ± 0.07	0.47 ± 0.01
	*U. maydis* MB215 Δ*cyp3* ΔMEL ΔUA Δ*dgat* ΔP_{ria1} ::P_{etef} Δ*fuz7* ::P_{etef} *mttA*_K3	33.8 ± 0.5	0.29 ± 0.00	0.43 ± 0.06	0.58 ± 0.04
	*U. maydis* MB215 Δ*cyp3* ΔMEL ΔUA Δ*dgat* ΔP_{ria1} ::P_{etef} Δ*fuz7* ::P_{etef} *mttA*_K8	56.5 ± 1.7	0.48 ± 0.01	0.74 ± 0.09	0.51 ± 0.02
	*U. maydis* MB215 Δ*cyp3* ΔMEL ΔUA Δ*dgat* ΔP_{ria1} ::P_{etef} Δ*fuz7* ::P_{etef} *mttA*_K9	48.1 ± 2.9	0.41 ± 0.02	0.52 ± 0.02	0.56 ± 0.03
	U. maydis MB215 Δ*cyp3* ΔMEL ΔUA Δ*dgat* ΔP_{ria1} ::P_{etef} Δ*fuz7* ::P_{etef} *mttA*_K10	49.0 ± 3.8	0.42 ± 0.03	0.64 ± 0.07	0.44 ± 0.03
	*U. maydis* MB215 Δ*cyp3* ΔMEL ΔUA Δ*dgat* ΔP_{ria1} ::P_{etef} Δ*fuz7* ::P_{etef} *mttA*_K14	54.4 ± 0.2	0.46 ± 0.00	0.82 ± 0.01	0.57 ± 0.00

* maximum itaconic acid titer ** overall itaconate production rate *** maximum itaconate production rate
**** yield itaconate per glucose consumed

2.2.3.3 Correlation between copy number of P_{etef}*mttA* and impact on itaconate production

In order to test whether these significant differences in production parameters and growth behavior are a result of differences in the copy number of P_{etef}*mttA*, this copy number was determined by quantitative PCR and application of the ΔC_t-method according to Pfaffl [173]. Primer efficiencies and C_t values of *mttA* and two reference genes, UMAG_02595 and UMAG_03726, were evaluated. Ratios between *mttA* and each reference gene were calculated independently using the Pfaffl-method and the resulting mean of both ratios was rounded to a single-digit value (Table 9).

Table 9: Determination of P_{etef}*mttA* copy number in five *U. maydis* MB215 Δ*cyp3* ΔMEL ΔUA Δ*dgat* ΔP_{ria1}::P_{etef} Δ*fuz7* ::P_{etef}*mttA* clones via quantitative PCR and ΔC_t-method according to Pfaffl [173]. *U. maydis* MB215 Δ*05079* ::P_{etef}*mttA* containing a single copy of *mttA* was used as positive, *U. maydis* MB215 wildtype as negative control. Efficiencies of primer pairs used: 2.014 for JB-126/JB-127 (R^2 = 0.999), 1.994 for JB-128/JB-129 (R^2 = 0.999) and 1.976 for JB-132/JB-133 (R^2 = 1.0). C_t values are the arithmetic mean of three technical replicates. ± values indicate deviation from the mean.

strain	C_t value UMAG_02595 (JB-126/ JB-127)	C_t value UMAG_03726 (JB-128/ JB-129)	C_t value *mttA* (JB-132/ JB-133)	ratio of *mttA* to UMAG_ 02595	ratio of *mttA* to UMAG_ 03726	rounded mean
***U. maydis* MB215 Δ*cyp3* ΔMEL ΔUA Δ*dgat* ΔP_{ria1}::P_{etef} Δ*fuz7* ::P_{etef}*mttA*_K3**	28.3 ± 0.12	28.4 ± 0.31	26.7 ± 0.36	3.2	3.1	3
***U. maydis* MB215 Δ*cyp3* ΔMEL ΔUA Δ*dgat* ΔP_{ria1}::P_{etef} Δ*fuz7* ::P_{etef}*mttA*_K8**	27.8 ± 0.10	27.9 ± 0.11	28.5 ± 0.21	0.7	0.6	1
***U. maydis* MB215 Δ*cyp3* ΔMEL ΔUA Δ*dgat* ΔP_{ria1}::P_{etef} Δ*fuz7* ::P_{etef}*mttA*_K9**	28.2 ± 0.27	28.5 ± 0.16	26.4 ± 0.18	3.7	3.9	4
***U. maydis* MB215 Δ*cyp3* ΔMEL ΔUA Δ*dgat* ΔP_{ria1}::P_{etef} Δ*fuz7* ::P_{etef}*mttA*_K10**	26.8 ± 0.17	26.6 ± 0.35	26.6 ± 0.10	1.2	0.9	1
***U. maydis* MB215 Δ*cyp3* ΔMEL ΔUA Δ*dgat* ΔP_{ria1}::P_{etef} Δ*fuz7* ::P_{etef}*mttA*_K14**	26.6 ± 0.03	27.0 ± 0.13	25.2 ± 0.13	2.8	3.3	3
***U. maydis* MB215 Δ*05079* ::P_{etef}*mttA* (single copy of P_{etef}*mttA*)**	25.7 ± 0.14	25.8 ± 0.24	25.7 ± 0.32	1.0	1.0	1
***U. maydis* MB215 wildtype**	27.6 ± 0.10	27.9 ± 0.29	35.9 ± 1.20	0.0	0.0	0

As positive control, *U. maydis* MB215 ΔUMAG_05079::P_{etef}*mttA* was used. This strain was previously proven to be a single-copy *mttA* transformant by Southern blot [172]. Indeed, the qPCR methods yielded a value of 1 for this strain. For the *U. maydis* MB215 Δ*cyp3* ΔMEL ΔUA Δ*dgat* ΔP_{ria1}::P_{etef} Δ*fuz7* ::P_{etef}*mttA* transformants, copy numbers between 1 and 4 were determined (Table 9).

Combining these results with the previous physiological analysis, a correlation between *mttA* copy number and several growth and itaconate production aspects becomes apparent illustrated in Figure 20. Cells with a single *mttA* copy reached the highest OD_{600}, glucose consumption, and itaconate production rate values. The transformants with multiple copies showed the lowest OD_{600} combined with higher yields. One transformant, K3, represents an outlier regarding these trends, clearly visible in the direct comparison to K14 having the same copy number of 3. This might be a hint for *mttA* insertion into a different locus than the *ip*-locus of K3 leading to defects in growth and consequently itaconate production.

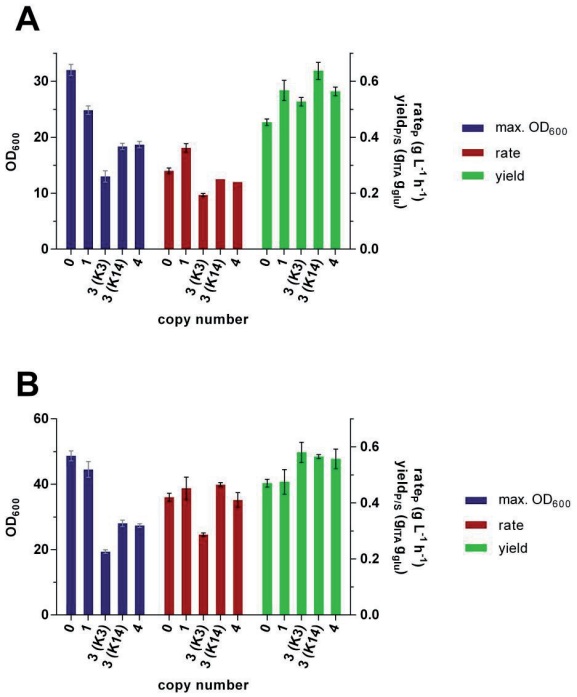

Figure 20: Comparison of maximal OD_{600} (blue), itaconate production rate (red), and itaconate from glucose yield (green) values achieved by the reference *U. maydis* MB215 Δ*cyp3* ΔMEL ΔUA Δ*dgat* ΔP_{ria1}::P_{etef} Δ*fuz7* without a *mttA* copy (0) and five *U. maydis* MB215 Δ*cyp3* ΔMEL ΔUA Δ*dgat* ΔP_{ria1}::P_{etef} Δ*fuz7* ::P_{etef}*mttA* clones possessing 1 (K8 & K10), 3 (K3 & K14), or 4 copies (K9) of *mttA* during cultivation in MTM containing 50 g L^{-1} glucose and 100 mM MES (A) or 100 g L^{-1} glucose and 66 g L^{-1} $CaCO_3$ (B).

2.2.3.4 Up-scaling of the itaconate production of the novel engineered strain in a 1.5 L bioreactor

To find a clone with a convincing overall production performance for up-scaling application, the different features have to be balanced against each other (Figure 20). In both media tested, K14 showed the best yields of 0.64 ± 0.03 g_{ITA} g_{glu} and 0.57 ± 0.00 g_{ITA} g_{glu}, which is close to the theoretical maximum.

To investigate the itaconate production of this strain in a more industrially relevant setup, the culture was scaled up to a 1.5 L bioreactor with pulsed glucose feed. When using 50 g L^{-1} glucose as initial carbon and 0.8 g L^{-1} NH_4Cl as nitrogen source and controlling the pH by NaOH-titration, 59.6 ± 5.9 g L^{-1} itaconate was produced by *U. maydis* MB215 Δ*cyp3* ΔMEL ΔUA Δ*dgat* ΔP_{ria1}::P_{etef} Δ*fuz7* ::P_{etef}*mttA*_K14 within 285 h with an overall productivity of 0.21 ± 0.02 g L^{-1} h^{-1} and a yield of 0.42 ± 0.02 g_{ITA} g_{glu} (Figure 21 A + B, data from H. Hosseinpour Tehrani [170]). When using 200 g L^{-1} glucose as initial carbon and 4 g L^{-1} NH_4Cl as nitrogen source and controlling the pH by $CaCO_3$, 205.6 ± 1.1 g L^{-1} itaconate were achieved within 481 h with an overall productivity of 0.43 ± 0.00 g L^{-1} h^{-1} and a yield of 0.32 ± 0.00 g_{ITA} g_{glu} (Figure 22 A + B, data from H. Hosseinpour Tehrani [170]).

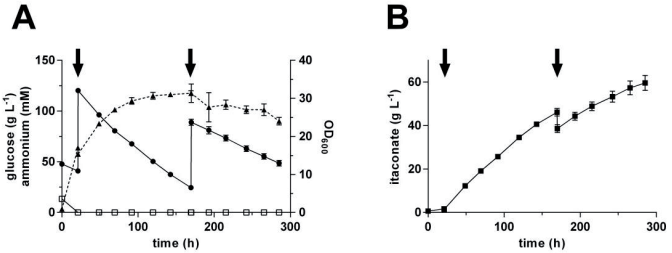

Figure 21: pH-controlled pulsed fed-batch fermentation of *U. maydis* MB215 Δ*cyp3* ΔMEL ΔUA Δ*dgat* ΔP_{ria1}::P_{etef} Δ*fuz7* ::P_{etef}*mttA*_K14. (A) concentration of glucose (●) and ammonium (□), OD_{600} (▲) and (B) concentration of itaconate (▲) during fermentation in a bioreactor containing batch medium (50 g L^{-1} glucose, 0.8 g L^{-1} NH_4Cl, 30 °C, 1000 vvm, and pH 6.5 kept constant by automatic titration of NaOH). Arrows indicate the addition of 80 g glucose. Values are the arithmetic mean of three biological replicates. Error bars indicate deviation from the mean (data provided by H. Hosseinpour Tehrani).

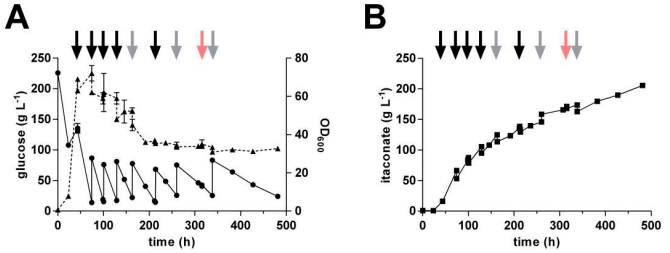

Figure 22: High-density pulsed fed-batch fermentation of *U. maydis* MB215 Δ*cyp3* ΔMEL ΔUA Δ*dgat* ΔP_{ria1}::P_{etef} Δ*fuz7* ::P_{etef}*mttA*_K14. (A) concentration of glucose (●) and ammonium (□), OD_{600} (▲) and (B) concentration of itaconate (▲) during fermentation in a bioreactor containing batch medium (200 g L^{-1} glucose, 4 g L^{-1} NH_4Cl, $CaCO_3$ as buffering agent, 30 °C, 1000 vvm (top pitched blade impeller, bottom Rushton impeller). Arrows indicate the addition of 80 g glucose + 50 g $CaCO_3$ (black arrow), 80 g glucose (grey arrow), or 50 g $CaCO_3$ (rose arrow). Values are the arithmetic mean of two technical replicates taken from the top and bottom of the bioreactor. Error bars indicate deviation from the mean (data provided by H. Hosseinpour Tehrani).

To evaluate these results, the performance of another engineered strain, *U. maydis* MB215 Δ*cyp3* Δ*fuz7* ΔP_{ria1}::P_{etef} ::P_{etef}*mttA*_K14, was investigated under equal fermentation conditions. In shake flask experiments, *U. maydis* MB215 Δ*cyp3* ΔMEL ΔUA Δ*dgat* ΔP_{ria1}::P_{etef} Δ*fuz7* ::P_{etef}*mttA*_K14 significantly outperformed this strain with a 64 % higher titer and a yield improved by even 68 % (data from H. Hosseinpour Tehrani [170], data not shown). Now, under titration conditions, *U. maydis* MB215 Δ*cyp3* Δ*fuz7* ΔP_{ria1}::P_{etef} ::P_{etef}*mttA*_K14 achieved a maximal ITA titer of 35.9 ± 1.5 g L^{-1} corresponding to an overall productivity of 0.12 ± 0.00 g L^{-1} h^{-1} and a yield of 0.20 ± 0.01 g_{ITA} g_{glu}, whereas with $CaCO_3$ buffer, 220.3 g L^{-1} itaconate were produced with an overall productivity of 0.46 g L^{-1} h^{-1} and a yield of 0.33 g_{ITA} g_{glu} (Table 10, data from H. Hosseinpour Tehrani [170]).

Table 10: Production parameters of two engineered *U. maydis* MB215 strains in two different types of fed-batch fermentations (data from H. Hosseinpour Tehrani [170]).

fermentation conditions	strain	fermentation time (h)	ITA $titer_{max}$* (g L^{-1})	r_P** (g L^{-1} h^{-1})	$Y_{P/S}$*** (g_{ita} g_{glu}^{-1})
50 g L^{-1} glucose 0.8 g L^{-1} NH_4Cl NaOH	*U. maydis* MB215 Δ*cyp3* ΔMEL ΔUA Δ*dgat* ΔP_{ria1} ::P_{etef} Δ*fuz7* ::P_{etef} *mttA*_K14	285	59.6 ± 5.9	0.21 ± 0.02	0.42 ± 0.02
	U. maydis MB215 Δ*cyp3* Δ*fuz7* ΔP_{ria1} ::P_{etef} ::P_{etef} *mttA*_K14	291	35.9 ± 1.5	0.12 ± 0.00	0.20 ± 0.01
200 g L^{-1} glucose 4 g L^{-1} NH_4Cl $CaCO_3$	*U. maydis* MB215 Δ*cyp3* ΔMEL ΔUA Δ*dgat* ΔP_{ria1} ::P_{etef} Δ*fuz7* ::P_{etef} *mttA*_K14	481	205.6 ± 1.1	0.43 ± 0.00	0.32 ± 0.00
	U. maydis MB215 Δ*cyp3* Δ*fuz7* ΔP_{ria1} ::P_{etef} ::P_{etef} *mttA*_K14	480	220.3	0.46	0.33

* maximum itaconic acid titer ** overall itaconate production rate *** yield itaconate per glucose consumed

The results show that the novel engineered mutant strain clearly outperformed the control strain lacking the lipid knockouts ΔMEL ΔUA and Δ*dgat*. Under titration conditions, the titer was increased by 66 %, while overall productivity was improved by 75 % and the yield was actually doubled. This strain comparison illustrates the increasing impact of a reduced lipid spectrum on itaconate production performance. Together with the upregulation of the itaconate gene cluster, the flux of substrate is "pushed" into the direction of itaconate. However, under higher stress conditions of the fed-batch fermentation, both the control and the final mutant strain underperformed compared to the published strain *U. maydis* MB215 Δ*cyp3* P_{etef}*ria1* [78]. It is assumed that the *mttA* insertion likely has a negative effect on the strain performance in the presents of an increased stress level. This might be due to an increased sensitivity to osmotic stress. In this case, a continuous or higher controlled fed-batch fermentation mode with lower baseline glucose levels would be beneficial.
Though, the combination of all modifications designed an itaconate producing *U. maydis* host strain with optimized performance and production parameters promising for following strain and process optimization.

Improvement of pH / itaconate tolerance of *U. maydis* MB215 by Adaptive Laboratory Evolution

Contributions:

Emad Albarouki assisted in genome data analysis, Conrad Müller in cloning and physiological strain characterization.

2.3 Improvement of pH / itaconate tolerance of *U. maydis* MB215 by Adaptive Laboratory Evolution

2.3.1 Summary

2.3.2 Introduction

The fungus *Ustilago maydis*, a member of the Ustilaginaceae family and causative agent of the corn smut disease, is a natural producer of the organic acid itaconate which was rated as one of the top 12 value-added chemicals from biomass [32,151]. Using *U. maydis* as itaconate production host offers several advantages, amongst others unicellular growth, insensitivity to high hydromechanic stress, and robustness against impurities in medium and industrial feedstocks [39,83]. In terms of the itaconate production parameters yield and titer, great improvements have been made by strain and process engineering (chapter 2.1 and 2.2), leading to “tolerance” as a new potential bottleneck. Improved itaconate productivity goes along with a higher stress level for the cells, both at the metabolic level, but also due to increasing product titers and consequently a higher osmotic pressure and possibly lower pH [92]. These effects result in a switch of the morphology from a yeast-like to a mycelial form [174] and a deceleration in the synthesis of additional acidic metabolites with a simultaneous increase in polyol accumulation [175]. Titrating base to hold the pH at a neutral level results in higher osmotic stress for the cells and does not avoid product inhibition by itaconate itself [39,77]. The required titrating base influences waste and costs, and consequently the end product price [77,150]. Therefore, robust *U. maydis* strains with high itaconate-, pH-, and osmotolerance are indispensable for industrially relevant, high performance itaconate production processes.

As a response to varying external pH and to adapt to the new environment, drastic changes occur in the fungal transcriptome by up- and down-regulating a multitude of genes encoding for different product categories, such as secreted enzymes (proteases, phosphatases), permeases, and enzymes involved in the synthesis of exported metabolites [176–178]. Thus e.g. regulating alterations in the lipid, protein, and polysaccharide composition of cell wall and plasma membrane [179]. But to date, most of the mechanisms involved are still unknown for Basidiomycota species, such as *U. maydis* [180]. The Pal/Rim pathway, including the zinc finger transcription factor PacC/Rim101, is one of the best characterized mechanisms especially in *A. nidulans* as model organism. It represents a main contributor to signal transduction and adaption as a response to changes in environmental pH [181]. But in contrast to alkaline and neutral ambient pH conditions, at acidic pH signal transduction does not take place via the Pal/Rim pathway due to PacC/Rim101 being inactive. As consequence, the transcription of genes induced at alkaline pH is repressed, while genes induced at acid pH are activated [181]. In *A. nidulans*, null mutations in one of its seven Pal/Rim pathway genes, *pacC*, *palA*, *palB*, *palC*, *palF*, *palH*, and *palI*, lead to an enhanced expression of those genes primarily expressed under acidic conditions in the wildtype [177,182]. However, *U. maydis* has to possess other stress response signaling pathways than Pal/Rim due to the fact that especially the expression of genes related to secondary metabolite production are altered which are not under the

control of the Pal/Rim pathway [176]. To identify potential genes positively influencing itaconate-, pH- or osmotolerance, different strategies can be applied. Metabolic engineering, the application of rational DNA technology approaches, plays a major role in the development of highly efficient microbial production strains [183,184]. However, detailed knowledge about metabolic networks and genetic regulations is necessary to rationally design strains, which represents a main drawback, when attempting to engineer a complex and multi-factorial phenotype like stress tolerance. Therefore, novel techniques such as *in vitro* screening methods, directed evolution and subsequent genomic analysis are of rising interest for industrial biocatalysis [183,185].

In this context, adaptive laboratory evolution (ALE) was applied to *U. maydis* MB215 in this study to improve target parameters like low pH tolerance and product resistance to itaconate. To identify novel genes that play a potential role in these characteristics, the genome of three evolved clones able to grow at pH 4 in the presence of high itaconate concentrations between 40 and 60 g L^{-1} was sequenced and screened for mutations foundational to the tolerant phenotype.

2.3.3 Results and Discussion

2.3.3.1 Evolution and selection of an *U. maydis* MB215 strain with enhanced pH and itaconate tolerance using ALE

Adaptive laboratory evolution (ALE) is a method for strain development based on random variations over many generations to obtain a desired phenotype [183]. In this study, ALE was performed in a two-step selection process to increase pH and itaconate resistance of *U. maydis* MB215. For the first 12 rounds of adaption, gradient plates were used consisting of MTM buffered at a pH of 3.5 with 20 mM potassium hydrogen phthalate, containing 50 g L^{-1} glucose, and possessing an itaconate gradient ranging from 0 to 100 g L^{-1} (Figure 23, A). In each round, the top 10 % of the cells, able to grow towards higher itaconate concentrations, were selected and plated on a new gradient plate. This way, cells were obtained able to grow at pH 3.5 and in the presence of ~ 80 g L^{-1} itaconate on solid agar plates. However, transferring these evolved strains to liquid medium with the same conditions did not show any improved tolerance compared to the wt. Therefore, the evolutionary selection was performed directly in shake flasks (Figure 23, B) to increase the adaption pressure on each single cell and to further adapt the cells picked from the 12th round of gradient plate evolution. In sequential batch shake flasks, the pH of the MTM was buffered to 4 using 100 mM potassium hydrogen phthalate, the itaconate concentration was gradually increased from 0 g L^{-1} to 40, 50, or 60 g L^{-1} by re-inoculation every 2 to 4 days for 90 days in total, while 50 g L^{-1} glucose were used as substrate. This way, four populations were evolved in parallel ending up with four adapted cultures named *U. maydis* MB215 G1.1, G1.2, G1.3, and G1.4. Analyzing growth behavior of the final evolved cultures in four different medium conditions verified successful adaption to low pH and high itaconate concentrations (Figure 23, C – F). In Growth Profiler cultures in MTM buffered at pH 4 with 100 mM potassium hydrogen phthalate and containing 50 g L^{-1} glucose, the itaconate concentration was adjusted to 10 (Figure 23, C), 20 (Figure 23, D), 30 (Figure 23, E), or 40 g L^{-1} (Figure 23, F). Regarding the growth parameters final optical density, growth rate and lag phase, all four evolved cultures significantly out-performed the wt strain in all conditions. However, although maximum growth rates of the evolved cultures were similar, among the evolved cultures there were major differences in growth. In all conditions, *U. maydis* MB215 G1.1 reached the highest final cell density. *U. maydis* MB215 G1.2 and G1.3 reached similar, significantly lower final densities with a longer lag phase of G1.2. *U. maydis* MB215 G1.4 reached the lowest final cell density, but with a shorter lag phase of 7 to 12 h in all scenarios.

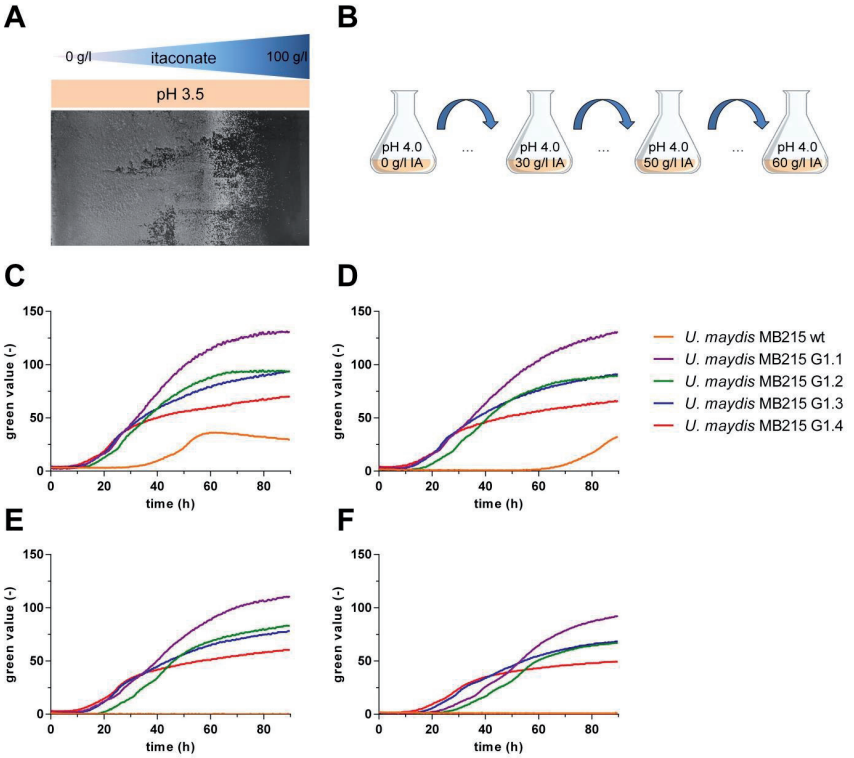

Figure 23: ALE and screening of *U. maydis* MB215 wildtype for enhanced tolerance concerning low pH values and high itaconate concentrations. (A) ALE using gradient plates (solid MTM buffered at a pH of 3.5 with 20 mM potassium hydrogen phthalate, containing 50 g L^{-1} glucose and an itaconate gradient ranging from 0 to 100 g L^{-1}) resulted in the evolved culture *U. maydis* MB215 G1. (B) Following ALE of *U. maydis* MB215 G1 using shake flasks with MTM buffered at pH 4 with 100 mM potassium hydrogen phthalate, containing 50 g L^{-1} glucose, and gradually increased itaconate concentration with final concentrations of 40 – 60 g L^{-1}. Separate evolution resulted in four evolved cultures named *U. maydis* MB215 G1.1, G1.2, G1.3, and G1.4. (C-F) Screening of *U. maydis* MB215 G1.1, G1.2, G1.3, and G1.4 over 89 h for growth using a Growth Profiler machine and MTM buffered to pH 4 with 100 mM potassium hydrogen phthalate and containing 10 g L^{-1} (C), 20 g L^{-1} (D), 30 g L^{-1} (E), or 40 g L^{-1} itaconate (F). Green values were measured of single cultures. *U. maydis* MB215 wildtype was used as reference strain.

From each final evolved culture, 24 single colonies were isolated. Screening in MTM buffered at pH 4 with 100 mM potassium hydrogen phthalate and containing 50 g L^{-1} glucose and 40 g L^{-1} itaconate led to the selection of five promising candidates characterized by at least one of the following criteria compared to the other clones: high final green value, short lag phase, and high growth rate (Figure 24). The trends observed above for the evolved populations were reproduced in these selected clones, with some achieving a much higher green value, while others had a shorter lag phase.

These data illustrate the success of the ALE process. Compared to the wildtype, which only tolerated up to 20 g L^{-1} itaconate with a drastic reduction in growth, the evolved strains grew readily in up to 40 g L^{-1} itaconate.

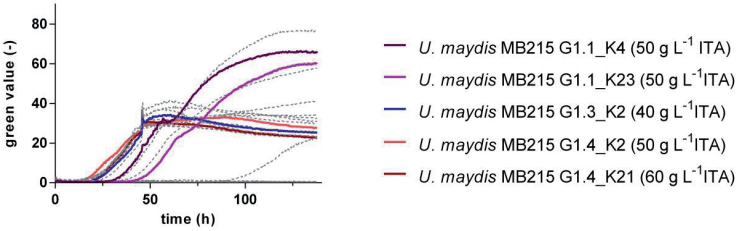

Figure 24: Screening of 24 single colonies isolated from each of the evolved cultures *U. maydis* MB215 G1.1, G1.2, G1.3, and G1.4 for growth in MTM buffered with 100 mM potassium hydrogen phthalate at pH 4 and containing 50 g L^{-1} glucose and 40 g L^{-1} itaconate using a Growth Profiler machine. Five clones with outstanding final density, short lag phase, and/or growth rate are highlighted in colors.). Green values were measured of single cultures. The single values of the dataset of each culture were normalized to 0 on the lowest value in each dataset.

2.3.3.2 Metabolic engineering of evolved strains to optimize itaconate production

With these candidates, metabolic engineering was performed to combine enhanced resistance with an increased itaconate production. Deletion of *cyp3*, which blocks itaconate degradation into (S)-2-hydroxyparaconate, together with the overexpression of *ria1*, regulator of the itaconate biosynthesis gene cluster, significantly increases itaconate production by 8-fold compared to the wt (section 2.1.3.3). Both genetic modifications were integrated into the genome of the evolved clones and the impact on their itaconate production was investigated in several different culture conditions (Figure 25 – Figure 27).

Using 50 g L^{-1} glucose and 100 mM MES buffer at pH 6.5 (Figure 25) revealed that *U. maydis* MB215 G1.4_K21 Δ*cyp3* $\Delta P_{ria1}::P_{etef}$ had completely lost its ability to produce itaconate (Figure 25, A), but rather exhibited a 13-fold increased malate production (Figure 25, B). The loss of itaconate production after prolonged ALE on glycerol was also observed by Zambanini *et al.* [93]. Under the chosen, stressful ALE conditions, a low pH combined with a high itaconate concentration, it is likely beneficial for the cells to keep the level of stress as low as possible by stopping itaconate production to maintain their fitness. Itaconate production is switched on after nitrogen depletion [39]. A loss of this function might be avoided by re-inoculating before nitrogen is fully consumed or by testing the ability of producing itaconate after each round of re-inoculation.

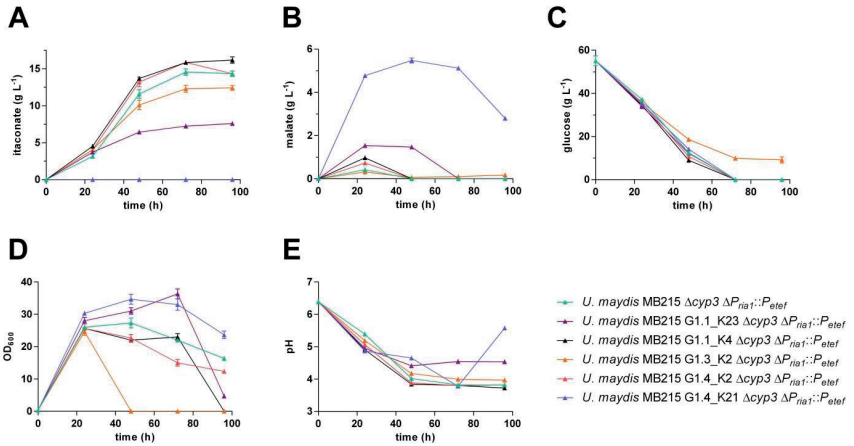

Figure 25: Itaconate production of five evolved *U. maydis* MB215 Δ*cyp3* ΔP_{ria1}::P_{etef} clones using the non-evolved *U. maydis* MB215 Δ*cyp3* ΔP_{ria1}::P_{etef} strain as reference. Cultivation was performed in System Duetz® plates and MTM containing 50 g L^{-1} glucose buffered with 100 mM MES at pH 6.5. (A) itaconate concentration, (B) malate concentration, (C) glucose concentration, (D) OD_{600}, and (E) pH values measured over time. Values are the arithmetic mean of three biological replicates. Error bars indicate deviation from the mean (n = 3).

Table 11: Production parameters of various *U. maydis* MB215 strains resulting from a System Duetz® cultivation in MTM. *U. maydis* MB215 Δ*cyp3* ΔP_{ria1}::P_{etef} (green), *U. maydis* MB215 G1.1_K4 Δ*cyp3* ΔP_{ria1}::P_{etef} (black), and *U. maydis* MB215 G1.4_K2 Δ*cyp3* ΔP_{ria1}::P_{etef} (salmon) were screened for 96 h in MTM containing 50 g L^{-1} glucose and buffered at pH 6.5 with 100 mM MES. Values are the arithmetic mean of three biological replicates. Errors indicate the standard deviation from the mean.

	symbol	strain	ITA titer$_{max}$* (g L^{-1})	r_P** (g L^{-1} h^{-1})	$r_{P,max}$*** (g L^{-1} h^{-1})	$Y_{P/S}$**** (g_{ITA} g_{glu}^{-1})
50 g L^{-1} glu 100 mM MES	▲	*U. maydis* MB215 Δ*cyp3* ΔP_{ria1}::P_{etef}	14.6 ± 0.4	0.20 ± 0.01	0.35 ± 0.03	0.26 ± 0.01
	▲	*U. maydis* MB215 G1.1_K4 Δ*cyp3* ΔP_{ria1}::P_{etef}	16.2 ± 0.4	0.22 ± 0.00	0.38 ± 0.01	0.29 ± 0.01
	▲	*U. maydis* MB215 G1.4_K2 Δ*cyp3* ΔP_{ria1}::P_{etef}	15.9 ± 0.3	0.22 ± 0.00	0.38 ± 0.03	0.29 ± 0.01

* maximum itaconic acid titer ** overall itaconate production rate *** maximum itaconate production rate
**** yield itaconate per glucose consumed

Also *U. maydis* MB215 G1.1_K23 Δ*cyp3* ΔP_{ria1}::P_{etef} and *U. maydis* MB215 G1.3_K2 Δ*cyp3* ΔP_{ria1}::P_{etef} were not able to compete with itaconate production parameters achieved by the non-evolved reference strain *U. maydis* MB215 Δ*cyp3* ΔP_{ria1}::P_{etef}. Similar to *U. maydis* MB215 G1.4_K21 Δ*cyp3* ΔP_{ria1}::P_{etef}, *U. maydis* MB215 G1.1_K23 Δ*cyp3* ΔP_{ria1}::P_{etef} partially shifted its acid production towards malate and achieved a 3.7-fold increased malate titer. Besides a lower itaconate titer, the maximal malate titer of *U. maydis* MB215 G1.3_K2 Δ*cyp3* ΔP_{ria1}::P_{etef} was also under 1 g L^{-1}. The reduced acid production was also reflected in incomplete substrate utilization (Figure 25, C). However, two clones, *U. maydis* MB215 G1.1_K4 Δ*cyp3* ΔP_{ria1}::P_{etef} and *U. maydis* MB215 G1.4_K2 Δ*cyp3* ΔP_{ria1}::P_{etef}, showed an 1.1-fold improved itaconate production performance regarding maximal titer, rate, and yield. A detailed overview of the production parameters achieved is found in Table 12.

Providing 100 g L^{-1} glucose in MTM (buffered at pH 6.5 with 100 mM MES) excluded substrate limitation and revealed ITA titers that can be achieved under low pH conditions due to the limited buffer capacity (Figure 26, A – H). Besides a 1.1- to 1.3-fold increased $r_{ITA,\ max}$ for the evolved *U. maydis* MB215 Δ*cyp3* ΔP_{ria1}::P_{etef} strains (Figure 26, A), none of the evolved strains showed any significant improvement in other itaconate production parameters. However, the evolved strains showed higher optical densities (Figure 26, C) when stress due to a decreasing pH occurred (Figure 26, D). This was also reflected in higher glucose uptake rates for these strains (Figure 26, B). In contrast, in the first 50 h, characterized by a lack of low pH stress, the non-evolved reference strain, *U. maydis* MB215 Δ*cyp3* ΔP_{ria1}::P_{etef}, showed the fastest growth.

In a further attempt to increase itaconate production, genes or gene clusters responsible for the production of a majority of lipidous by-products were deleted, and filamentous growth was avoided by *fuz7* deletion. Concerning lipid production, the synthesis of two glycolipid classes, MELs and UA, and of TAGs was deleted. These modifications, combined with the previously inserted deletion of *cyp3* and overexpression of *ria1*, represent the consolidation of all major modifications identified in this thesis. The introduction of these modifications in the evolved strains improved the maximal itaconate titer by 1.1-fold compared to the non-evolved chassis. The G1.1 strain also achieved a 1.2-fold increased $r_{ITA,\ max}$ (Figure 26, E), but other major differences due to the evolution process were missing. Interestingly, the final reference strain, *U. maydis* MB215 Δ*cyp3* ΔP_{ria1}::P_{etef} Δ*dgat* ΔMEL ΔUA Δ*fuz7*, showed the highest optical densities (Figure 26, G) with a comparably low glucose uptake rate (Figure 26, F). For MES-buffered cultivations, the pH dropped to a minimal pH of 3.27. It was expected that especially under these conditions the evolved strains would have a crucial advantage. The lack of this effect led to a switch from MES to $CaCO_3$ as buffer system to verify the transferability of the titer and rate improvements to conditions where the ALE would not have a major effect (Figure 27, A – H). Regarding the two evolved precursor strains, only the G1.1 strain was able to compete with the Δ*cyp3* ΔP_{ria1}::P_{etef} reference strain regarding the production parameters titer and yield (Figure 27, A + B). Concerning the rate, this strain significantly outperformed the reference strain. It produced itaconate with a 1.2-fold higher r_{ITA} and a 1.3-fold higher $r_{ITA,\ max}$. Again, both evolved Δ*cyp3* ΔP_{ria1}::P_{etef} strains reached higher optical densities going along with a faster glucose uptake than the corresponding reference strain (Figure 27, C). These observations couldn't be confirmed for the final chassis strains whereof the non-evolved strain performed similar or even better than the evolved ones concerning growth and itaconate production (Figure 27, E – H). A detailed overview of the production parameters achieved is found in Table 12.

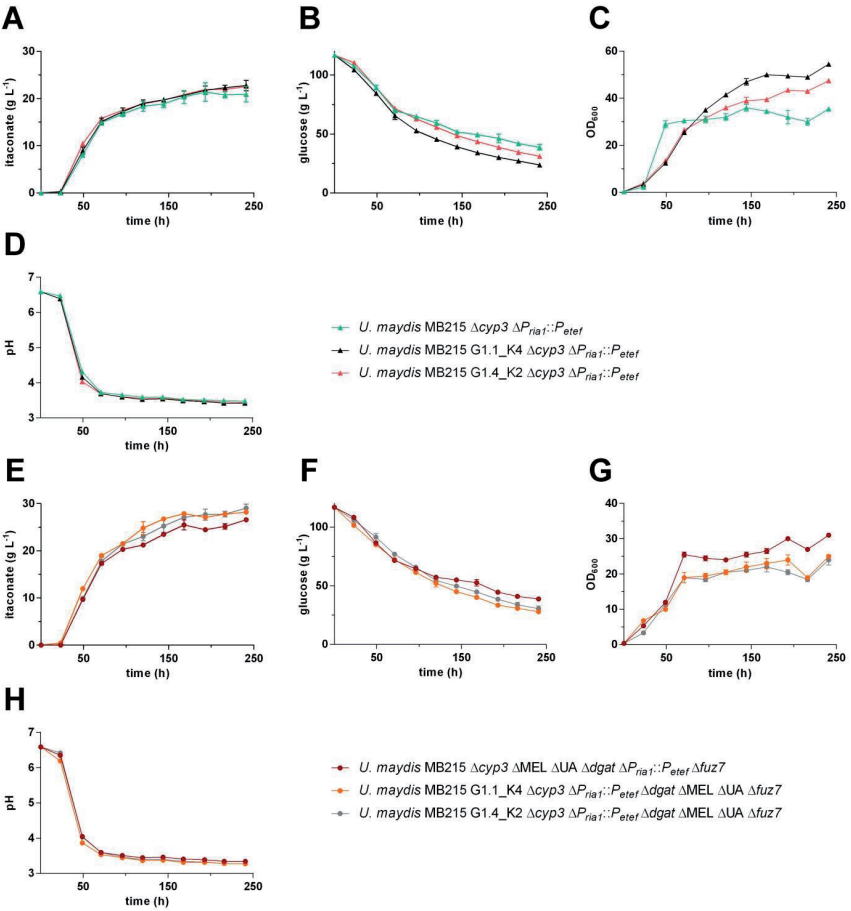

Figure 26: 500 mL shake flask cultivation of two evolved *U. maydis* MB215 Δ*cyp3* ΔP_{ria1}::P_{etef} and two evolved *U. maydis* MB215 Δ*cyp3* ΔP_{ria1}::P_{etef} Δ*dgat* ΔMEL ΔUA Δ*fuz7* clones using the non-evolved strains *U. maydis* MB215 Δ*cyp3* ΔP_{ria1}::P_{etef} and *U. maydis* MB215 Δ*cyp3* ΔMEL ΔUA Δ*dgat* ΔP_{ria1}::P_{etef} Δ*fuz7* as reference. Cultivation was performed in MTM containing 100 g L^{-1} glucose buffered with 100 mM MES at pH 6.5. (A + E) itaconate concentration, (B + F) glucose concentration, (C + G) OD_{600}, and (D + H) pH values measured over time. Values are the arithmetic mean of two biological replicates. Error bars indicate deviation from the mean (n = 2).

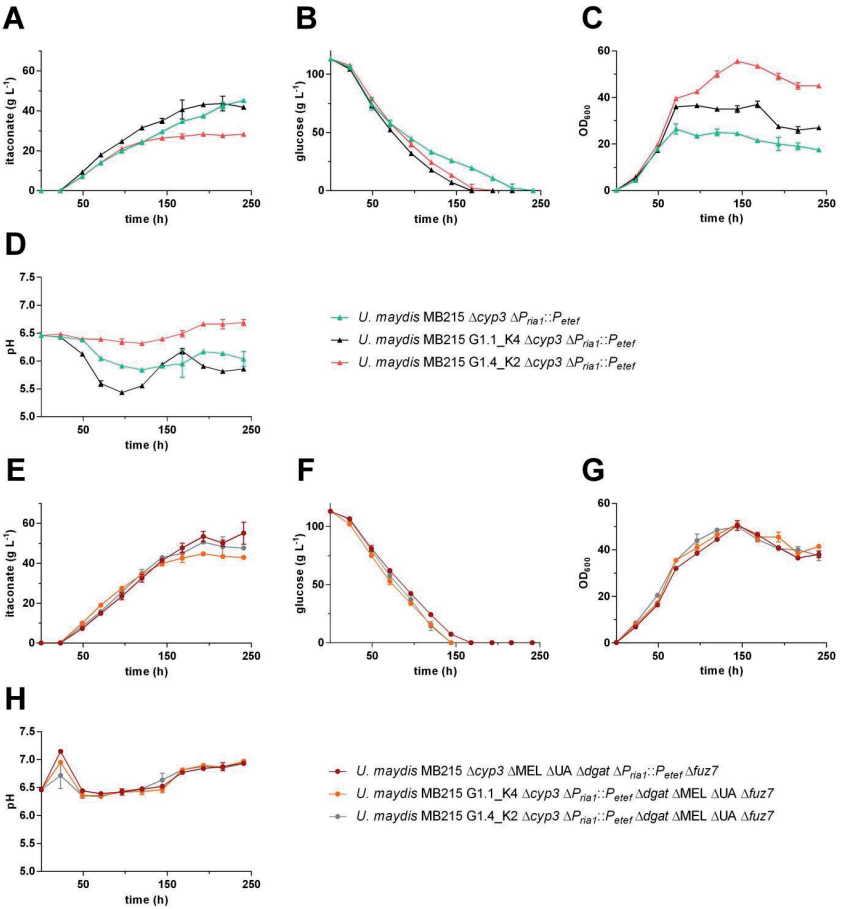

Figure 27: 500 mL shake flask cultivation of two evolved *U. maydis* MB215 clones genetically modified afterwards with Δ*cyp3* ΔP_{ria1}::P_{etef} and Δ*cyp3* ΔP_{ria1}::P_{etef} Δ*dgat* ΔMEL ΔUA Δ*fuz7*, and the corresponding non-evolved reference strains *U. maydis* MB215 Δ*cyp3* ΔP_{ria1}::P_{etef} and *U. maydis* MB215 Δ*cyp3* ΔMEL ΔUA Δ*dgat* ΔP_{ria1}::P_{etef} Δ*fuz7*. Cultivation was performed in MTM containing 100 g L^{-1} glucose buffered with 66 g L^{-1} $CaCO_3$ at pH 6.5. (A + E) itaconate concentration, (B + F) glucose concentration, (C + G) OD_{600}, and (D + H) pH values measured over time. Values are the arithmetic mean of two biological replicates. Error bars indicate deviation from the mean (n = 2).

Table 12: Production parameters of various *U. maydis* MB215 strains resulting from a shake flask cultivation in MTM. *U. maydis* MB215 Δ*cyp3* ΔP_{ria1}::P_{etef} (green), *U. maydis* MB215 G1.1_K4 Δ*cyp3* ΔP_{ria1}::P_{etef} (black), *U. maydis* MB215 G1.4_K2 Δ*cyp3* ΔP_{ria1}::P_{etef} (salmon), *U. maydis* MB215 Δ*cyp3* ΔP_{ria1}::P_{etef} Δ*dgat* ΔMEL ΔUA Δ*fuz7* (red), *U. maydis* MB215 G1.1_K4 Δ*cyp3* ΔP_{ria1}::P_{etef} Δ*dgat* ΔMEL ΔUA Δ*fuz7* (orange), and *U. maydis* MB215 G1.4_K2 Δ*cyp3* ΔP_{ria1}::P_{etef} Δ*dgat* ΔMEL ΔUA Δ*fuz7* (grey) were screened for 241 h in MTM containing 50 g L^{-1} glucose and 100 mM MES buffer at pH 6.5. Values are the arithmetic mean of two biological replicates. Errors indicate the standard deviation from the mean (n = 2).

	symbol	strain	ITA titer$_{max}$* (g L^{-1})	r_P** (g L^{-1} h^{-1})	$r_{P,max}$*** (g L^{-1} h^{-1})	$Y_{P/S}$**** (g_{ITA} g_{glu}^{-1})
100 g L^{-1} glu 100 mM MES		*U. maydis* MB215 Δ*cyp3* ΔP_{ria1} ::P_{etef}	21.4 ± 2.0	0.09 ± 0.01	0.31 ± 0.00	0.30 ± 0.04
		U. maydis MB215 G1.1_K4 Δ*cyp3* ΔP_{ria1} ::P_{etef}	22.8 ± 1.1	0.09 ± 0.00	0.34 ± 0.03	0.24 ± 0.01
		U. maydis MB215 G1.4_K2 Δ*cyp3* ΔP_{ria1} ::P_{etef}	22.5 ± 0.3	0.11 ± 0.01	0.39 ± 0.00	0.26 ± 0.01
		U. maydis MB215 Δ*cyp3* ΔMEL ΔUA Δ*dgat* ΔP_{ria1} ::P_{etef} Δ*fuz7*	26.6 ± 0.3	0.11 ± 0.00	0.37 ± 0.00	0.34 ± 0.01
		U. maydis MB215 G1.1_K4 Δ*cyp3* ΔP_{ria1} ::P_{etef} Δ*dgat* ΔMEL ΔUA Δ*fuz7*	28.2 ± 0.3	0.12 ± 0.00	0.44 ± 0.00	0.32 ± 0.01
		U. maydis MB215 G1.4_K2 Δ*cyp3* ΔP_{ria1} ::P_{etef} Δ*dgat* ΔMEL ΔUA Δ*fuz7*	29.0 ± 0.9	0.12 ± 0.00	0.38 ± 0.01	0.34 ± 0.00
100 g L^{-1} glu 66 g L^{-1} $CaCO_3$		*U. maydis* MB215 Δ*cyp3* ΔP_{ria1} ::P_{etef}	45.2 ± 1.1	0.20 ± 0.01	0.31 ± 0.03	0.40 ± 0.01
		U. maydis MB215 G1.1_K4 Δ*cyp3* ΔP_{ria1} ::P_{etef}	43.2 ± 0.1	0.24 ± 0.03	0.40 ± 0.01	0.38 ± 0.00
		U. maydis MB215 G1.4_K2 Δ*cyp3* ΔP_{ria1} ::P_{etef}	28.2 ± 0.2	0.16 ± 0.01	0.32 ± 0.03	0.25 ± 0.00
		U. maydis MB215 Δ*cyp3* ΔMEL ΔUA Δ*dgat* ΔP_{ria1} ::P_{etef} Δ*fuz7*	55.1 ± 5.5	0.28 ± 0.01	0.38 ± 0.01	0.49 ± 0.05
		U. maydis MB215 G1.1_K4 Δ*cyp3* ΔP_{ria1} ::P_{etef} Δ*dgat* ΔMEL ΔUA Δ*fuz7*	44.7 ± 0.7	0.28 ± 0.01	0.41 ± 0.01	0.40 ± 0.01
		U. maydis MB215 G1.4_K2 Δ*cyp3* ΔP_{ria1} ::P_{etef} Δ*dgat* ΔMEL ΔUA Δ*fuz7*	50.6 ± 1.0	0.30 ± 0.01	0.39 ± 0.02	0.45 ± 0.01

* maximum itaconic acid titer ** overall itaconate production rate ([glu] > 2.3 g L^{-1}) *** maximum itaconate production rate
**** yield itaconate per glucose consumed

2.3.3.3 Investigating the itaconate production performance of two evolved and engineered G1.1 strain in larger-scale cultivation

Itaconate production of *U. maydis* MB215 G1.1_K4 Δ*cyp3* ΔP_{ria1}::P_{etef} and *U. maydis* MB215 G1.1_K4 Δ*cyp3* ΔP_{ria1}::P_{etef} Δ*dgat* ΔMEL ΔUA, which showed the better performance of the two evolved strains in previous experiments, was investigated in a pH-controlled high-density pulsed fed-batch fermentation with 4 g L^{-1} NH_4Cl and an initial concentration of 221 ± 3.8 g L^{-1} glucose. As a control, *U. maydis* MB215 Δ*cyp3* ΔP_{ria1}::P_{etef} was also cultivated (Figure 28).

With a maximal itaconate titer of 77.6 ± 0.3 g L^{-1}, *U. maydis* MB215 G1.1_K4 Δ*cyp3* ΔP_{ria1}::P_{etef} was not able to compete with the Δ*cyp3* ΔP_{ria1}::*Petef* reference strain, which reached a titer of 90.8 ± 2.2 g L^{-1} (Figure 28, C; Table 13). *U. maydis* MB215 G1.1_K4 Δ*cyp3* ΔP_{ria1}::P_{etef} Δ*dgat* ΔMEL ΔUA reached a titer in the same range (90.7 ± 1.0 g L^{-1}) indicating a boost in itaconate production compared to *U. maydis* MB215 G1.1 Δ*cyp3* ΔP_{ria1}::P_{etef} due to the lipid knockouts, confirming the results of section 2.1.3.3 in a more industrially relevant setup. This stimulating effect based on the lipid knockouts was also reflected in another production parameter, $r_{ITA, max}$ (Table 13). Within the $r_{ITA, max}$ time slot, all three strains achieved itaconate titers in the range of 50 g L^{-1} (Figure 28, C). However, in comparison to both Δ*cyp3* ΔP_{ria1}::P_{etef} strains reaching this titer within ~ 83 h, *U. maydis* MB215 G1.1_K4 Δ*cyp3* ΔP_{ria1}::P_{etef} Δ*dgat* ΔMEL ΔUA reached the same value ~ 24 h earlier, after ~ 68 h, represented in the

highest $r_{P,max}$ value (Table 13). Due to quite similar glucose consumption (Figure 28, D), this went along with the best yield value of 0.27 g_{ITA} g_{glu}^{-1} achieved by *U. maydis* MB215 G1.1_K4 Δ*cyp3* ΔP_{ria1}::P_{etef} Δ*dgat* ΔMEL ΔUA in comparison to 0.23 g_{ITA} g_{glu}^{-1} for the control strain and 0.21 g_{ITA} g_{glu}^{-1} for *U. maydis* MB215 G1.1_K4 Δ*cyp3* ΔP_{ria1}::P_{etef}.

Unexpectedly, *U. maydis* MB215 G1.1_K4 Δ*cyp3* ΔP_{ria1}::P_{etef} reached a 3-fold higher malate titer of 24.9 ± 1.7 g L^{-1} (Figure 28, C). The maximal titers of itaconate and malate differed between the strains, but regarding the total amount of these acids all strains produced the same quantity of around 100 g L^{-1}.

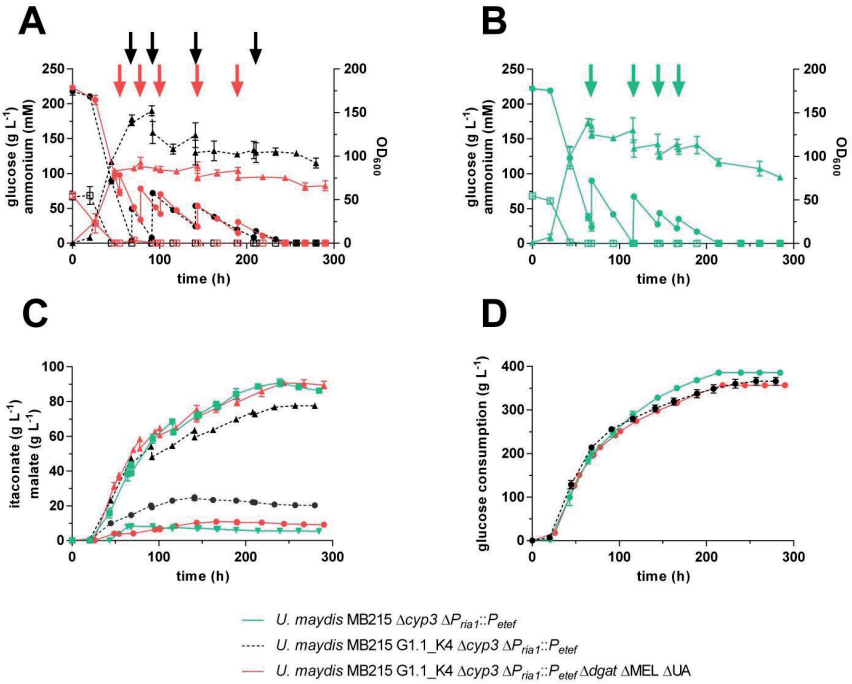

Figure 28: Controlled high-density pulsed fed-batch fermentation of three engineered *U. maydis* MB215 strains, *U. maydis* MB215 G1.1_K4 Δ*cyp3* ΔP_{ria1}::P_{etef} (black dots lines), *U. maydis* MB215 G1.1_K4 Δ*cyp3* ΔP_{ria1}::P_{etef} Δ*dgat* ΔMEL ΔUA (red solid lines) and *U. maydis* MB215 Δ*cyp3* ΔP_{ria1}::P_{etef} (green solid lines) as reference. (A + B) concentration of glucose (●) and ammonium (□), OD_{600} (▲), (C) concentration of itaconate (▲) and malate (●), and (D) glucose consumption during fermentation in a bioreactor with batch medium (200 g L^{-1} glucose, 4 g L^{-1} NH_4Cl, pH 6.5 kept constant by automatic titration of NaOH, 30 °C, 1000 vvm). Arrows indicate glucose feeding times. Values are the arithmetic mean of two biological replicates. Error bars indicate deviation from the mean.

Table 13: Overview of itaconate titer, (maximum) rate, and yield achieved by three engineered *U. maydis* MB215 strains in pH-controlled high-density pulsed fed-batch fermentation with 4 g L^{-1} NH_4Cl and a starting concentration of 200 g L^{-1} glucose. Values are the arithmetic mean of two biological replicates. ± values indicate deviation from the mean.

symbol	strain	ITA $titer_{max}$* (g L^{-1})	r_P** (g L^{-1} h^{-1})	$r_{P,max}$*** (g L^{-1} h^{-1})	$Y_{P/S}$**** (g_{ITA} g_{glu}^{-1})	Mal $titer_{max}$* (g L^{-1})	acid $titer_{max}$* (g L^{-1})
	U. maydis MB215 Δ*cyp3* ΔP_{ria1}::P_{etef}	90.8 ± 2.2	0.41 ± 0.00	1.10 ± 0.05	0.24 ± 0.00	8.3 ± 0.9	99.0 ± 3.1
- - - - -	*U. maydis* MB215 G1.1_K4 Δ*cyp3* ΔP_{ria1}::P_{etef}	77.6 ± 0.3	0.33 ± 0.00	0.92 ± 0.02	0.21 ± 0.01	24.9 ± 1.7	102.5 ± 1.3
	U. maydis MB215 G1.1_K4 Δ*cyp3* ΔP_{ria1}::P_{etef} Δ*dgat* ΔMEL ΔUA	90.7 ± 1.0	0.39 ± 0.01	1.34 ± 0.07	0.25 ± 0.00	10.8 ± 0.4	101.5 ± 0.6

* maximum itaconic acid titer ** overall itaconate production rate ([glu] > 10.4 g L^{-1}) *** maximum itaconate production rate
**** yield itaconate per glucose consumed

The results demonstrate that the evolution process and the following consolidation of all major modifications determined in this thesis did not have the intended significant influence on the itaconate production itself. It was assumed that ALE in medium characterized by a high itaconate concentration and a low pH generated strains with high tolerance towards these features. Under itaconate producing conditions, this increased tolerance might be reflected in higher maximal itaconate titers. Interestingly, these expectations have not been fulfilled. Indeed, pH tolerance could apparently be enhanced. The fitness of the cells was extensively improved at low pH which was reflected in high glucose uptake rates and optical density values. However, this effect disappeared, when including lipid knockouts in these strains. The deletion of lipid, especially TAG production drastically affects the availability of readily metabolizable energy reserves and membrane building and maintaining elements for the cells [159,160]. Naturally evolved to rely on TAGs as main energy reserve under starvation conditions, the stability of the cells might be affected in the long term – a very relevant aspect in processes that run under growth-limiting and stressful conditions for a long time.

The ALE process concentrated on the growth phase of *U. maydis* characterized by no or marginal itaconate production. This phase was chosen to avoid a potential loss of the ability to produce itaconate – like it happened for *U. maydis* MB215 G1.4_K21 Δ*cyp3* ΔP_{ria1}::P_{etef}. This means that key players of global effects taking place in the growth phase were evolved, such as transporters and H^+-ATPases, e.g. resulting in an increased glucose uptake rate. But obviously, this evolution did not positively affect the dynamic effects running in the production phase and therefore at low pH, where no further growth takes place and the cells just have to keep their maintenance metabolism sustainable.

The hypothesis that the balance between itaconate import and export is the important factor for the reachable itaconate titer might be another reason for the missing direct influence of an increased pH tolerance on itaconate production [172]. Also overproducing *U. maydis* strains reach a low final pH in weakly buffered medium. This shows that a low pH *per se* does not have a limiting effect on itaconate production. It is supposed that the equilibrium between itaconate import and export determines its maximally achievable titer. This balance strongly depends on the ambient pH. An increased internal itaconate production rate in overproducing strains boosts itaconate secretion and a drop of the external pH. At a pH below 5.5, secreted itaconate is mostly available in its fully protonated form which is able to cross the cytoplasmic membrane by diffusion and therefore re-enter the cell [78]. The lower the

pH, the higher is the proportion of protonated itaconate and thus the higher its uptake rate. For the equilibrium of uptake and secretion rate, this means a decrease of the net production which at some point will go to zero – visible as a stop in itaconate production in the graphs. Itaconate re-entering the cell results in an increase in the intracellular itaconate concentration which in turns lead to an inhibition of its own production and a vast effort for the cell to keep the internal pH constant.
But with a view to all these arguments, it should be considered that for the final engineered strains, it is concerned with already far optimized ones able to achieve production parameters close to the theoretical maximum. Further optimization is indeed desirable, though they won't yield large increases than achieved with primary modifications.

2.3.3.4 Whole genome sequencing of the evolved strains

To gain a detailed insight into the impact of ALE on the genome and especially on single genes, whole genome sequencing was performed by the Eurofins Genomics Company GATC Biotech AG with three of the evolved strains, *U. maydis* MB215 G1.1_K4, *U. maydis* MB215 G1.3_K2, and *U. maydis* MB215 G1.4_K2, and the reference *U. maydis* MB215 wt. As additional reference to identify mutations originating from the working strains but not from the ALE itself, the simultaneously sequenced *U. maydis* MB215 Δ*cyp3* ΔMEL ΔUA Δ*dgat* $\Delta P_{ria1}::P_{etef}$ strain (section 2.1.3.1) was consulted. GATC Biotech used the annotated genome of *U. maydis* 521 as reference database. With this procedure, an enormous amount of variants was found in each strain (Table 14). With the help of Dr. Albarouki (iAMB, RWTH Aachen University) the results were mapped against the wt strain the sequenced strains directly originated from, *U. maydis* MB215 wt. A drastically reduced number of SNPs and InDels (raw SNPs and InDels in Table 14), further decreased by the exclusion of low-quality-variants (filtered SNPs and InDels in Table 14) was the result. In the following analysis steps, mutation sites were analyzed using the *U. maydis* MB215 wt genome as reference.

Table 14: Whole genome sequencing of five *U. maydis* MB215 strains performed by the Eurofins Genomics Company GATC Biotech AG using Illumina technology and *U. maydis* 521 as reference to detect SNP and InDel variants. Subsequent analysis of the assembly results by direct comparison to the original wt strain, *U. maydis* MB215, of the evolved or engineered strains.

	GATC Biotech analysis			iAMB analysis			
strain	SNPs	InDels	variants in total	raw SNPs	filtered SNPs	raw InDels	filtered InDels
U. maydis MB215 G1.1_K4	38,752	6,756	45,508	1,078	358	1,643	1,611
U. maydis MB215 G1.3_K2	38,951	6,756	45,707	1,800	309	1,914	1,835
U. maydis MB215 G1.4_K2	39,192	7,168	46,360	1,830	302	1,904	1,834
U. maydis MB215 Δ*cyp3* ΔMEL ΔUA Δ*dgat* $\Delta P_{ria1}::P_{etef}$	38,905	7,127	46,032	1,871	270	1955	1,867
U. maydis MB215 wt	38,300	6,823	45,123				

With this approach, five mutations were found in all three evolved strains, while they were absent in the reference sequence of MB215, but also in the ITA chassis strain

(section 2.1.3.1). This can be a hint for pH-tolerance mediating genes, but it can't be excluded that for these mutations it concerns mutational hotspots, where the risk for genetic mutations is significantly elevated, or bioinformatics artefacts.

Four of the mutations found were within gene sequences (Table 15). Looking into the resulting changes in the translation and amino acid code revealed the integration of a stop codon into two genes, UMAG_02068 and UMAG_03806, making it highly likely to affect gene function, and thus potential targets for further investigation. To evaluate if these genes play a role in the improved fitness of the cells under stress conditions, they were deleted in *U. maydis* MB215 wildtype and *U. maydis* MB215 G1.4_K2 and growth was analyzed using a Growth Profiler (Figure 29).

Table 15: Whole genome sequencing of three evolved strains, *U. maydis* MB215 G1.1_K4, *U. maydis* MB215 G1.3_K2, and *U. maydis* MB215 G1.4_K2, revealed four mutations occurring in all three strains.

gene ID	gene function	mutation	position	change in translation code	change in amino acid
UMAG_10016	hypothetical protein	T → C	2,579 / 3,486 bp	ATG → ACG	methionine → threonine
UMAG_02068	hypothetical protein	C → T	370 / 1,476 bp	CAA → TAA	glutamine → stop codon
UMAG_03806	hypothetical protein	C → T	762 / 1,011 bp	CGA → TGA	arginine → stop codon
UMAG_05275	hypothetical protein	T → C	599 / 1,422 bp	CTG → CCG	leucine → proline

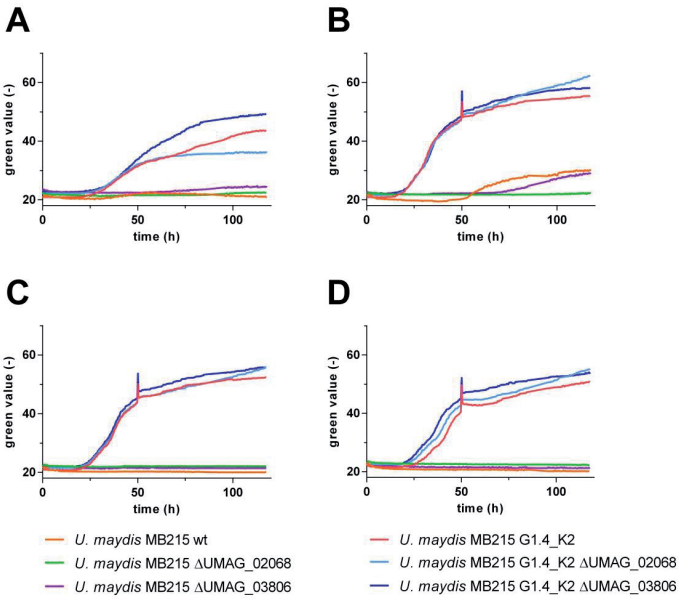

Figure 29: Effect of UMAG_02068 and UMAG_03806 deletion on growth of *U. maydis* MB215 wildtype and the evolved strain *U. maydis* MB215 G1.4_K2. Cultivation was performed in MTM buffered with 100 mM potassium hydrogen phthalate at pH 4 and containing 50 g L^{-1} glucose and (A) 0 g L^{-1}, (B) 10 g L^{-1}, (C) 20 g L^{-1}, and (D) 30 g L^{-1} itaconate. Green values were measured in biological triplicates using a Growth Profiler.

In all conditions tested, pH 4 in combination with 0 (Figure 29, A), 10 (Figure 29, B), 20 (Figure 29, C), and 30 g L^{-1} itaconate (Figure 29, D), neither the deletion of UMAG_02068 nor of UMAG_03806 affected the growth of the mutants compared to the controls. This is the case for both the wildtype control and the *U. maydis* MB215 G1.4_K2 as reference.

2.3.3.5 Investigation of potential genes playing crucial roles in the adaption process to acidic environmental pH

Due to the most likely targets not yielding any success in a reverse engineering approach (Figure 29) and the very high number of detected mutations making a wider screening impractical, literature was consulted in a next step to reveal genes that play crucial roles in the regulation of acid/pH tolerance in other fungi and therefore representing promising targets to investigate in *U. maydis*. *A. nidulans*, for example, growing under acidic conditions shows an upregulation of genes encoding for GABA transporters and acid phosphatases and a downregulation of alkaline phosphatase encoding genes [177,178]. Such studies can indeed give hints towards genes important for low pH tolerance, but simultaneously the up- and downregulation processes will also result in a lot of secondary effects not (directly) related to pH tolerance. It is known that genes such as the GABA transporter *gabA* [186–188], the acid phosphatase *pacA* [187,189], the xylanase *xlnB* [190,191], acid phosphodiesterases [187,192], the ketoreductase *stcU* catalyzing the reduction of versicolorin A within the sterigmatocystin/aflatoxin biosynthesis pathway in *Aspergillus* species [193], or the α-L-arabinofuranosidase *abfB* [194] are preferentially expressed under acidic growth conditions [177]. In addition, it is expected that H^+-transporting ATPases play crucial roles in low pH regulation processes by exporting H^+ out of the cell to maintain pH homeostasis, especially for long-term acid stress [195]. An increased activity of H^+ ATPases was observed for several acid-tolerant organisms, such as bacteria or plants, as a response to the cultivation under acidic medium conditions to regulate the cytoplasmic pH [196–199]. Despite the assumption of playing a predominant role in alkaline pH regulation, the Pal/Rim pathway components were also considered as potentially relevant target genes. Therefore, *U. maydis* homologs of the *A. nidulans*, the Pal/Rim pathway, and H^+ ATPase genes were investigated in the evolved *U. maydis* MB215 strains. However, the results of Table 16 – Table 18 depict that neither the respective genes nor potential promoter sequences featured mutations.

Table 16: Analysis of *U. maydis* 521 homologs of selected *A. nidulans* genes upregulated under acidic conditions and potential corresponding promoter sequences with regard to mutations caused by SNPs or InDels in the three evolved and sequenced *U. maydis* MB215 strains.

A. nidulans gene ID	function in *A. nidulans*	gene ID of (potential) *U. maydis* 521 homologs	function in *U. maydis* 521	score	query cover	ident	SNPs / InDels in evolved strains (within gene or potential promoter sequence)
gabA (AJ131668.1)	GABA transporter	UMAG_02791 UMAG_02146	hypothetical protein hypothetical protein	306 / 517 282 / 517	91 % 99 %	37 % 34 %	no / no no / no
pacA (Z79750.1)	phosphate-repressible acid phosphatase	UMAG_10068	hypothetical protein	180 / 618	81 %	30 %	no / no
xlnB (AN9365.2)	endo-1,4-β-xylanase	UMAG_06350	putative endo-1,4-beta-xylanase A (UMAG_06350)	131 / 221	71 %	48 %	no / no
	acid phospho-diesterases	UMAG_02531 (Agarwal, Schultz, and Perlin 2010) UMAG_10895 (Agarwal, Schultz, and Perlin 2010)	phosphodiesterase/ nucleotide pyrophosphatase phosphodiesterase				no / no no / no
stcU (AN7806.2)	ketoreductase	UMAG_00108 UMAG_11693 UMAG_10038	hypothetical protein hypothetical protein multifunctional beta-oxidation protein	114 / 264 110 / 264 97.4 / 264	96 % 96 % 98 %	30 % 34 % 32 %	no / no no / no no / no
abfB (AN1571.2)	α-L-arabino-furanosidase	no similarities found					

Table 17: Analysis of pH responsive Pal/Rim pathway genes identified in *U. maydis* and potential corresponding promoter sequences with regard to mutations caused by SNPs or InDels in the three evolved and sequenced *U. maydis* MB215 strains.

pal/rim gene	conserved *U. maydis* homologue	reference	SNPs / InDels in evolved strains (within gene or potential promoter sequence)
pacC / *rim101*	UMAG_10426	[181]	no / no
palA / *rim20*	UMAG_11510	[200]	no / no
palB / *rim13*	UMAG_02075	[200]	no / no
palC / *rim23*	UMAG_04392	[200]	no / no
palF / *rim8*	not trackable	[200]	
palH / *rim21*	not trackable	[200]	
palI / *rim9*	UMAG_00581	[200]	no / no

Table 18: Analysis of *U. maydis* H^+-transporting ATPase genes and potential corresponding promoter sequences with regard to mutations caused by SNPs or InDels in the three evolved and sequenced *U. maydis* MB215 strains.

U. maydis gene ID	function	SNPs / InDels in evolved strains (within gene or potential promoter sequence)
UMAG_00508	V-type H+-transporting ATPase 16kDa proteolipid subunit	no / no
UMAG_00630	V-type H+-transporting ATPase subunit a	no / no
UMAG_10926	V-type H+-transporting ATPase subunit A	no / no
UMAG_00975	F-type H+-transporting ATPase subunit g	no / no
UMAG_01103	F-type H+-transporting ATPase subunit delta	no / no
UMAG_01205	H+-transporting ATPase	no / no
UMAG_11698	V-type H+-transporting ATPase subunit B	no / no
UMAG_05090	F-type H+-transporting ATPase subunit gamma	no / no
UMAG_06324	F-type H+-transporting ATPase subunit O	no / no
UMAG_10180	F-type H+-transporting ATPase subunit f	no / no
UMAG_02064	V-type H+-transporting ATPase subunit F	no / no
UMAG_02360	F-type H+-transporting ATPase subunit h	no / no
UMAG_02581	H+-transporting ATPase	no / no
UMAG_02782	V-type H+-transporting ATPase subunit d	no / no
UMAG_10280	V-type H+-transporting ATPase subunit e	no / no
UMAG_10397	F-type H+-transporting ATPase subunit beta	no / no
UMAG_10479	F-type H+-transporting ATPase subunit k	no / no
UMAG_11520	V-type H+-transporting ATPase subunit E	no / no
UMAG_04167	V-type H+-transporting ATPase subunit D	no / no
UMAG_04345	V-type H+-transporting ATPase subunit G	no / no
UMAG_04716	V-type H+-transporting ATPase subunit C	no / no
UMAG_05503	V-type H+-transporting ATPase subunit H	no / no
UMAG_10754	F-type H+-transporting ATPase subunit epsilon	no / no
UMAG_11576	F-type H+-transporting ATPase subunit j	no / no
UMAG_10213	F-type H+-transporting ATPase subunit alpha	no / no
UMAG_10548	F-type H+-transporting ATPase subunit b	no / no
UMAG_11802	V-type H+-transporting ATPase 21kDa proteolipid subunit	no / no
UMAG_12050	F-type H+-transporting ATPase subunit d	no / no

In 2013, Cervantes-Montelongo *et al.* did an extensive transcriptome study about up- and downregulation of genes in *U. maydis* FB2 under acidic and alkaline conditions [176]. When transferring *U. maydis* FB2 from neutrality to pH 3, 301 differentially expressed genes, of which 162 were up-, and 139 were down-regulated, were identified representing 4.4 % of the whole genome. Most of these genes belonged to the categories of unclassified proteins (116) and metabolism (62). The metabolism genes mainly belonged to three sub-groups: metabolism of carbohydrates and carbon compounds, metabolism of N, amino acids, and ammonia, and metabolism of fatty acids, lipids, and isoprenoids. Due to the high numbers of genes down-regulated at acidic and alkaline conditions, it is assumed that *U. maydis* turns off several functions that are not directly necessary for survival, when adapting to the stressful environment. The three most highly down-regulated genes (UMAG_01432, UMAG_01433, UMAG_11339) belong to a 9-gene-cluster essential for iron transport. It is suggested that this system is not needed under acidic conditions due to a higher solubility of iron ions at acidic pH [201]. Nitrate and nitrite reductase and nitrate transport-related genes (UMAG_03847, UMAG_11104, UMAG_11105) were down-regulated at low pH. It is assumed that at alkaline pH metabolic energy has to be spent to reduce nitrate to ammonium ions for nitrogen assimilation [176,202]. UMAG_02804 with seven transmembrane domains and UMAG_06335 with nine TM domains represent promising candidates for possible pH signal receptors due to their

G protein-coupled receptor features [176,203]. But also in the sequences of these genes, no mutations occurred in the evolved *U. maydis* MB215 strains (Table 19).

Table 19: Transcriptome analysis of *U. maydis* FB2 wildtype strain revealed a number of highly up- and down-regulated genes at pH 3 ([176,204–206]). The three most highly up- and down-regulated genes are marked with the equivalent number of stars (*). For the evolved and sequenced *U. maydis* MB215 strains, the appropriate genes and potential corresponding promoter sequences were investigated for mutations caused by SNPs or InDels.

U. maydis gene ID	function	regulation under acidic pH	SNPs / InDels in evolved strains
UMAG_00204	hypothetical protein, related to Ca^{2+}-transporting ATPase	down	no / no
UMAG_01431	hypothetical protein, related to ATP-binding cassette transporter protein	down*	no / no
UMAG_01432	hypothetical protein, related to N6-hydroxylysine acetyl transferase	down**	no / no
UMAG_01433	hypothetical protein, related to Enoyl-CoA hydratase	down	no / no
UMAG_02379	hypothetical protein	up**	no / no
UMAG_02581	putative H^+-transporting P-type ATPase	down	no / no
UMAG_02763	hypothetical protein	down	no / no
UMAG_02803	hypothetical protein, related to beta-1,3-glucan binding protein	up	no / no
UMAG_02804	hypothetical protein, 7 TM domains	up	no / no
UMAG_03049	hypothetical protein, related to neutral amino acid permease	up***	no / no
UMAG_03284	hypothetical protein, probable CipC homolog needed for synthesis of hyphal cell wall	up	no / no
UMAG_03524	hypothetical protein, related to peroxisomal amine oxidase (copper-containing)	down	no / no
UMAG_04474	guanine nucleotide-binding protein alpha-3 subunit → involved in transmission of pheromone signaling and pathogenic development	up	no / no
UMAG_04779	hypothetical protein, related to SEC59 - Dolichol kinase	down	no / no
UMAG_05122	hypothetical protein, related to carboxylic acid transport protein JEN1	up	no / no
UMAG_05227	hypothetical protein	up	no / no
UMAG_05704	hypothetical protein	up	no / no
UMAG_06335	hypothetical protein, 9 TM domains	up*	no / no
UMAG_10119	putative ser/thr protein kinase	up	no / no
UMAG_10426	transcription factor pacC	down	no / no
UMAG_10663	putative Rho family GTPase	up	no / no
UMAG_11057	oligopeptide transporter 2	up	no / no
UMAG_11338	hypothetical protein, related to AIF1 - mitochondrial cell death effector	down	no / no
UMAG_11339	hypothetical protein, related to a siderophore iron transporter 3	down***	no / no
UMAG_11922	hypothetical protein, related to Chitin deacetylase precursor	up	no / no

Recently, Matsushika *et al*. identified a novel pH-regulated system in the multiple-stress-tolerant yeast *Issatchenkia orientalis* [207]. IoGAS1 is about 60 % identical to the *S. cerevisiae gas1* and to *Candida albicans phr1* and *phr2* gene encoding for glycoproteins localized to the plasma membrane through a GPI anchor and involved in cell wall biosynthesis. IoGAS1 was obtained to play a critical role in the adaption process to varying pH with the exhibition of β-1,3-glucanosyltransferase activity and two glutamate residues having a special task. For the *C. albicans* homologs, the expression increases with decreasing pH of the medium. The amino acid sequence of IoGAS1 transpired to be 40 % identical to the hypothetical *U. maydis* protein UMAG_01640. However, Cervantes-Montelongo *et al*. identified a down-regulation of UMAG_01640 at pH 3 [176].

In 2017, a low-pH-inducible promoter of *gas* gene encoding 1,3-β-glucanosyltransferase, *Pgas*, was reported in *A. niger*. Functioning highly efficiently at a pH of 2.0, it was used to express the *A. terreus cis*-aconitate decarboxylase (*cad*) gene in *A. niger* H915-1 resulting in a 5.3-fold higher itaconate titer in comparison to the *cad* gene under the control of *PgpdA*, a strong constitutive promoter used for the engineering of *A. niger* [208]. This promoter might be used for the expression of specific genes able to stimulate pH / itaconate tolerance such as genes encoding H^+ ATPases. When the pH drops during itaconate production, genes under the control of *Pgas* would be expressed and antagonize or at least decelerate further pH decrease to minimize the amount of protonated external itaconate. With this mechanism regulating gene expression in the host strain, a new dynamic pH homeostatic system can be developed.

Chapter 3

General discussion and outlook

3 General discussion and outlook

3.1 Optimization of the itaconate production in *U. maydis* by by-product reduction, filamentous growth prevention, and transporter upregulation using rational strain design

With the exciting results in hand, I want to set these into the context of the literature. While microbes perform interesting syntheses, the parameters required for an industrial viable production are highly challenging to achieve, indeed. One possibility to improve the production of a target metabolite is the rewiring of metabolic network by metabolic engineering. Rational strain engineering, if successful, allows flux rerouting into the biosynthesis pathway of choice by manipulating specific genes. Genes involved in product or precursor synthesis are generally overexpressed, while genes required for by-product formation are deleted [209,210]. Production parameters such as titer, productivity, and product to substrate yield can be maximized this way [210,211].

So far, a limited number of selection markers including hygromycin, carboxin, and geneticin hindered the integration of multiple mutations in a single *U. maydis* strain. The establishment of a new genome editing system in *U. maydis* based on CRISPR-Cas9 solved this problem [156]. It allows marker-free target gene disruption due to marker loss after each round of modification. This study showed that even the deletion of whole gene clusters is realizable with this system. Nevertheless, the novel technique also goes along with some challenges: numerous growth cycles for marker loss, mixed cultures consisting of wildtype and mutant cells even after several rounds of cell separation, and the occurrence of unintended side effects during the disruption of long genomic stretches – even without significant similarities between repair template and the affected region. The latter was observed for the deletion of genes directly flanking the target region or, regarding the deletion of whole gene clusters, for genes within the target region that were planned to be deleted, but still existed after genome editing. Due to the lack of a suitable positive control, correct deletions are harder to detect by PCR if unwanted off-target effects occur. In the event of detection issues, smaller repair templates – so called “microhomology regions”, and successfully proven in other fungi, such as *A. fumigatus* [212] – might be worth a try instead of the used 1000 bp repair template flanks. Alternatively, if possible, localization in the actual genomic locus with the design of a new repair sequence homologous to a slightly shifted region up- and downstream of the target. Also an optimized combination of different cloning techniques based on the experiences of this work likely improves the cloning success and reduces off-target effects. For example, the CRISPR-Cas system can be used for marker-free deletion of single genes, while the FLP/FRT method is applied for the deletion of larger genomic sequences. The results obtained in this work show that higher time requirements than expected from the literature might be necessary for a genome editing strategy, nonetheless, the CRISPR-Cas system has the great advantage of circumventing the problem of a limited number of selection markers available for *Ustilago* [156].

In this study, the deletion of 2-HP, MEL, UA, and TAG synthesis reduced the versatility of the *U. maydis* production spectrum extensively. The overexpression of

ria1, encoding for the transcriptional regulator of the itaconate biosynthesis gene cluster, upregulated the whole itaconate gene cluster. In addition, the overexpression of *ria1* extensively reduced malate production by 84 %. Due to the TCA cycle-mediated conversion of malate into the itaconate precursors citrate and *cis*-aconitate [74], malate can also be considered a precursor of itaconate being exchanged with mitochondrial *cis*-aconitate by the mitochondrial antiporter *mtt1*, which is also upregulated [78,80]. This leads to an increased transport of malate from the cytosol back into mitochondria likely decreasing malate secretion [78]. In this context, there is an interesting combinatory theory: It is assumed that an improved malate-to-mitochondrion transport only fortifies the TCA cycle, if the amount of acetyl-CoA, which malate is coupled to via oxaloacetate, is adequately high [213]. The disruption of lipid biosynthesis pathways might increase the availability of acetyl-CoA providing a synergistic effect of the elimination of the competing pathways and the upregulation of the ITA cluster likely giving a further strong “push” towards ITA production (Figure 30).

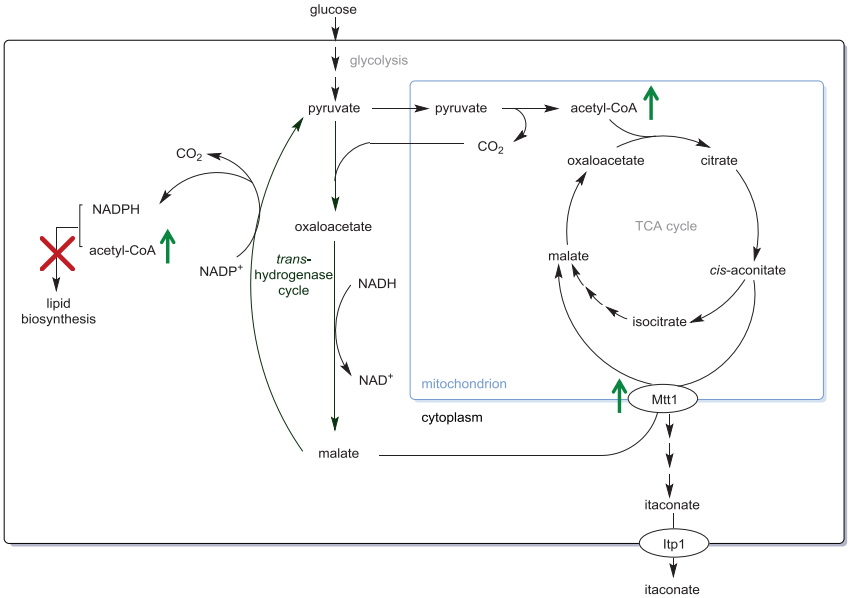

Figure 30: Hypothetical correlation between elimination of lipid synthesis pathways and upregulation of the ITA gene cluster by the overexpression of *ria1* (modified from [213]).

A combination of all the modifications mentioned above, together with filamentous growth prevention and integration of an *A. terreus mttA* copy, successfully increased the carbon flux towards itaconate and optimized its production. Compared to the published itaconate hyper-producing strain *U. maydis* MB215 Δ*cyp3* ΔP_{ria1}::P_{etef} [78], *U. maydis* MB215 Δ*cyp3* ΔMEL ΔUA Δ*dgat* ΔP_{ria1}::P_{etef} Δ*fuz7* ::P_{etef}*mttA*_K14 achieved a 95 % higher maximal titer, a 19 % higher overall productivity, a 42 % higher maximal rate, and a yield that could be more than doubled to a value of 0.64 ± 0.03 g_{ITA} g_{glu}, which is getting close to the theoretical maximum of 0.72. With

89 % of the theoretical yield and due to the fact that some glucose is also needed for microbial growth, the optimization potential of this parameter can be evaluated as almost exhausted [83].

Looking into the itaconate biosynthesis pathway identifies citrate as a precursor of itaconate. In comparison to glucose containing six oxygen atoms, citrate comprises seven. After itaconate production and carbon dioxide release, the overall stoichiometry is indeed closed, but the need of extra oxygen is reflected in an adequate and continuous aeration necessary for itaconate production [214]. 1.5 mol O_2 are consumed per mol itaconate produced from glucose [83]. It is known that even minutes of interrupted aeration damage the cells irreversible and dramatically reduce itaconate productivity [215]. In addition, two more processes fortify the continuous need of oxygen. Both processes are dependent on continuous ATP synthesis and therefore on the oxidative metabolism in the mitochondria: the maintenance of the internal pH by a plasma membrane ATPase and the transport of itaconate out of the cell against a concentration gradient [91]. The faster and more itaconate is produced, the higher the oxygen demand. To ensure aeration during cultivation in a bioreactor, an agitation rate of 1000 rpm was chosen. To evaluate the degree of shear stress the cells encounter, different factors determining shear sensitivity have to be considered, e.g., size and morphology of the cell or composition and thickness of the plasma membrane [216]. Regarding yeast-like growing *Ustilago* cells, shear-sensitivity is not an issue, as it is for filamentous fungi [83]. However, regarding the evolved strains featuring the lipid knockouts, ΔMEL ΔUA, and Δ*dgat*, it was clearly illustrated that they lost their increased fitness level resulting from the ALE process after lipid synthesis deletion. From the results, it is assumed that especially the missing TAG biosynthesis and therefore a majority of the readily metabolizable energy reserves and membrane building and maintaining elements significantly destabilizes the cells. This is particularly relevant for fermentations running under growth-limiting and stressful conditions for a long time. Any kind of additional stress, such as shear or osmotic pressure, would even intensify the destabilizing effect on the evolved cells that are consequently not able to utilize their whole itaconate production potential.

To counter this stress, one solution might be the reduction of oxygen sensitivity to be able to decrease the aeration rate and lower the shear stress. The expression of a hemoglobin gene of *Vitreoscilla* in *A. terreus* increased its itaconate production and improved the strain regeneration after disrupted aeration due to a decreased sensitivity to oxygen supply [85]. Another opportunity might be the cloning of different combinations of the three lipid knockouts to test if one deletion less still improves itaconate production, while maintains stress tolerance of the strain and therefore positively affects itaconate production.

The production of itaconate from glucose requires a high flux through glycolysis. During glycolysis, 2 mol of NADH are produced. A further mol NADH is generated during acetyl-CoA formation from pyruvate [214]. An increased itaconate production therefore goes along with an increased NADH/NAD^+ ratio and an indispensable need of NAD^+ regeneration. There are several different ways that mediate NADH depletion and NAD^+ regeneration. The mitochondrial electron transport chain is directly linked to ATP synthesis and therefore energy supply by generating a proton gradient during NADH to NAD^+ oxidation with oxygen as final electron acceptor [217,218]. Some fungal

mitochondrial membranes possess additional alternative components in their respiratory chains that are not linked to ATP synthesis. An external NADH dehydrogenase (Ndh-2) and an alternative oxidase (AOX) are the most prominent candidates. In combination, they reoxidized NADH by transferring electrons from cytosolic NADH to molecular oxygen as terminal electron acceptor. This alternative pathway is active during the production phase and regulates the intracellular redox balance without generating a proton motive force for ATP synthesis [218–222]. An overexpression of the mitochondrial and alternative electron transport chain might reduce the NADH level and support NAD^+ regeneration during both growth and production phase. This would exclude the NADH/NAD^+ conversion rate as bottleneck in itaconate production likely resulting in an enhanced itaconate production to fill the NADH sink.

Another approach to alter the redox cofactor status in *U. maydis* would be the heterologous expression of an NADH oxidase (NOX) under the control of an inducible promoter. The H_2O-forming NOX catalyzes the oxidation of NADH to NAD^+ using molecular oxygen as electron acceptor [223]. This alternative way of NAD^+ regeneration fosters itaconate and reduces malate production. It could be shown that a NOX overproduction in *L. lactis* lead to a metabolic shift characterized by a reduced lactate production with most of the pyruvate now converted to acetate, acetoin, or diacetyl [224]. A decrease of the intracellular NADH pool of *S. cerevisiae* by expression of a *L. lactis noxE* resulted in crucial metabolic flux changes from ethanol, glycerol, and succinate towards acetaldehyde, acetate, and acetoin production [225]. Due to its huge impact in the primary metabolism and redox balance of the microbial host, a suitable promoter has to be chosen to keep these effects under control and to establish the NOX as a powerful tool for metabolic modifications. Fine tuning has to be performed to be able to regulate the level and time slot of activity and to adapt these to the maximal NAD^+ regeneration rates of *U. maydis*.

The mentioned routes of maintaining cofactor balance have in common that they all rely on molecular oxygen as final electron acceptor. This underlies the consistently high need of oxygen supply during itaconate production in *U. maydis*. Under anaerobic or oxygen-limited conditions, NAD^+ regeneration has to occur on other ways catalyzed by dehydrogenases [226]. *S. cerevisiae*, e.g., uses NADH-coupled ethanol formation or the reduction of dihydroxyacetone phosphate to glycerol-3-phoshate which is converted to glycerol [227,228]. Also *Escherichia coli* produces ethanol from acetyl-CoA and in addition lactate from pyruvate [226,229]. *U. maydis* itself possesses a number of dehydrogenases suitable to catalyze appropriate reactions, such as UMAG_00123, a hypothetical protein related to L-lactate dehydrogenase, UMAG_00555, a putative glycerol-3-phosphate dehydrogenase, UMAG_05170, a putative formate dehydrogenase, and UMAG_05984, a putative glutamate dehydrogenase. However, all these mechanisms are based on the production of a further by-product going along with a reduced flux of substrate towards the itaconate biosynthesis pathway. It might be investigated if the effect of NAD^+ regeneration mediated this way on itaconate production is significant enough to deal with this loss of substrate. Another route also not based on the electron acceptor oxygen is the cytosolic oxaloacetate reduction to malate during the TCA cycle that is coupled to NADH-oxidation [230,231]. This reaction is catalyzed by cytosolic malate

dehydrogenases of which two *U. maydis* proteins are annotated encoded by the genes UMAG_00403 and UMAG_11161. Itaconate production drives the NAD^+-dependent glycolysis and TCA cycle leading to a high NADH/NAD^+ ratio. It consequently pushes malate to oxaloacetate conversion to remove NADH and regenerate NAD^+. This correlation reflects the outstanding role of malate formation during the process of itaconate production.

All these depicted prospects increase the rate of NAD^+ regeneration. Consequently, this "pushes" the flux into NADH-producing pathways, such as the itaconate production pathway, and away from NADH-depleting pathways, such as malate production from oxaloacetate, to balance the lowered NADH level. At its best, this increases itaconate production.

The reduction of the *U. maydis* by-product spectrum not only improved itaconate production itself, but is also supposed to simplify the general process performance, e.g. the downstream process as a crucial cost factor of microbial fermentations. A decreased general amount of by-products benefits itaconate recovery by improving the final product quality [83,232]. Especially, the elimination of glycolipid production positively affects product recovery and therefore optimized the downstream processing. Glycolipids are highly surface active biopolymers that tend to block surfaces rapidly. This complicated the usage of membranes for product recovery during downstream processing [232]. The deletion of MEL and UA biosynthesis likely leads to a significant increase in membrane permeability. This would also simplify and improve the performance of a continuous fermentation mode combined with a continuous product recovery via membrane-based filtration [232].

Strain optimization regarding by-product reduction therefore not only impacted the metabolic-regarding part of *U. maydis* in a positive way by increasing itaconate production, but also improved the application potential of this production host in terms of filtration performance during sample handling, continuous fermentation with simultaneous product recovery, or downstream processing.

3.2 Fitness improvement at acidic pH by Adaptive Laboratory Evolution

Simultaneously to the metabolic engineering approach, Adaptive Laboratory Evolution was used to increase pH and / or itaconate resistance in *U. maydis*. Acidic pH values are preferred in industrial organic acid production due to several advantages: A low pH supports the generation of auto-sterile conditions, reduces the amount of pH-controlling agents needed to balance the produced acids therefore minimizing the final volume of the culture broth, and it also allows a direct separation of itaconate from the culture broth via crystallization by cooling or evaporation-crystallization during the downstream process [83]. The conversion of the salt to the free acid [32] can be prevented this way. The downstream processing is a major relevant cost factor of microbial fermentation processes. By the avoidance of additional waste and separation steps, the last factors extremely simplify the downstream process, lower its costs and therefore increase the acid value. A critical disadvantage of low pH values, the fostered attraction of proteins by membranes [232], can be minimized significantly by deleted glycolipid production fortifying the filtration performance as described in section 3.1.

Besides the advantages going along with an acidic-pH-tolerant strain, it was assumed that an optimized resistance delays a stop in itaconate production resulting in an increased maximal itaconate titer. This hypothesis could not be demonstrated with the evolved strains. Indeed, these strains showed a higher fitness level than the wt reflected in high glucose uptake rates. However, the strains were not able to transfer this advantage onto their itaconate production.

Screening was performed by validating growth rate and final optical density of evolved single clones cultivated in minimal medium with a pH of 4 and in the presence of 40 g L^{-1} itaconate. The clones achieving the fastest growth rates or the highest densities were selected for itaconate production optimization using metabolic engineering. Screening for these two parameters with the intention of an optimized itaconate production hypothesizes a close relationship between growth on acidic pH and itaconate and its production. Thereby, it has to be considered that the optical density does not only reflect biomass accumulation, but also includes secondary growth. Interestingly, the strains achieving the highest final optical densities were the ones with the longest lag phases.

The selection parameters did not lead to the desired goal. Has there been another way to evaluate the evolved clones with regard to their potential in producing itaconate to use their proven improved fitness? An alternative approach might be to directly investigate the itaconate production of the clones. An endpoint determination of the itaconate titer of each clone would simplify handling and shorten the expenditure of time. One sample is obtained after 72 to 96 h, when glucose is (almost) depleted. With this procedure, it would directly be verified if the fitness positively influenced itaconate production.

Another possibility might be the choice of an *Ustilago* strain characterized by a naturally defined tolerance to acidic pH and integrate all knockouts turned out to positively effect itaconate production in the previous chapter 3.1. One candidate is *U. cynodontis*. In a screening of 68 Ustilaginaceae strains, *U. cynodontis* was identified as most promising itaconate producer with a lower pH limit for acid production compared to *U. maydis* [150]. In his work, H. Hosseinpour Tehrani verified this by determining a pH optimum of 3.6 for *U. cynodontis*' itaconate production [170]. With the knowledge about how to prevent the filamentous phenotype, the strong disadvantage of *U. cynodontis* observed during bioreactor cultivations could be overcome (H. Hosseinpour Tehrani, personal communication).

3.3 Conclusions & Outlook

To establish alternative production hosts to the filamentous fungus *A. terreus* for industrial itaconate production, this thesis focused on the basidiomycete *U. maydis* MB215. A combination of metabolic engineering and adaptive laboratory evolution was applied to make this organism competitive. To "push" the flux of substrate towards itaconate as main product, the manifold by-product spectrum of *U. maydis* was minimized by eliminating the production of 2-hydroxyparaconate, mannosylerythritol lipids, ustilagic acid, and triacylglycerols and reducing malate production. Preventing the formation of the filamentous phenotype and expressing the *A. terreus* mitochondrial tricarboxylate transporter *mttA* completed the rational strain design steps performed for optimizing the itaconate production performance.

With the engineered strain, itaconate production in terms of maximal titer, overall productivity, and product to substrate yield could be drastically enhanced compared to the hyper-producing strain published by Geiser *et al*. [78]. By ALE, the fitness of the cells could be enhanced resulting in high optical densities and glucose uptake rates. However, it was not possible to further improve the effects resulting from the metabolic engineering modifications by an increased fitness.

Some modifications not only had a positive influence on the microorganism performance regarding itaconate production, but also on the process handling in general. The guarantee of single-cell growth eliminated vessel wall growth and enhanced the reproducibility of experiments. The prevention of glycolipid production can facilitate effective membrane usage due to reduced blocking and therefore increased membrane permeability. This simplifies product recovery during fermentation or downstream processing.

In small scale, the final engineered strain showed its potential to achieve a yield value representing 89 % of the theoretical maximum. Considering the need of glucose for microbial production, the optimization potential of this parameter can be evaluated as almost exhausted. Further optimization strategies therefore should be focus on aspects, such as space-time yield, usage of cheap and sustainable substrates, and final titer [83]. A high final product concentration will reduce overall separation and concentrating costs [32]. A lowered itaconate production rate in the end of each fermentation reflects the effect of product toxicity. To avoid this and keep the productivity at a constantly high level during the whole production phase, a combination of continuous fermentation and simultaneous product removal might be a suitable choice. Due to the fact that the downstream process is a major cost factor, it is essentiell to optimize both, up- and downstream process, and to adapt them to each other.

Chapter 4

Materials and methods

4 Material and Methods

4.1 Strains, media, and culture conditions

All *U. maydis* MB215 strains generated and used in this work are listed in Table 20.

Table 20: Strains used within this study with description of mutation sites and reference.

strain name (iAMB strain collection no.)	description	reference
U. maydis MB215 (#2162)	wildtype strain	Prof. M. Bölker, Philipps University Marburg, Germany
U. maydis MB215 Δ*cyp3* $\Delta P_{ria1}::P_{etef}$ (#4175)	*U. maydis* MB215 with deletion of UMAG_05074 and overexpression of UMAG_05080	provided by H. Hosseinpour Tehrani
U. maydis MB215 Δ*cyp1* (#2340)	*U. maydis* MB215 with deletion of UMAG_06463	Prof. M. Bölker, Philipps University Marburg, Germany
U. maydis MB215 Δ*cyp1* Δ*emt1* (#2287)	*U. maydis* MB215 with deletion of UMAG_06463 and UMAG_03117	Prof. M. Bölker, Philipps University Marburg, Germany
U. maydis MB215 ΔUMAG_05079 :: P_{etef}*AT_mttA* (#3092)	*U. maydis* MB215 with the deletion of UMAG_05079 and the overexpression of a single copy of ATEG_09970 of *A. terreus*	M. Meier
U. maydis MB215 Δ*cyp3* (#3785)	*U. maydis* MB215 with deletion of UMAG_05074	this study
U. maydis MB215 Δ*emt1* (#4386)	*U. maydis* MB215 with deletion of UMAG_03117	this study
U. maydis MB215 ΔUA	*U. maydis* MB215 with deletion of UMAG_96458, UMAG_06459, UMAG_06460, UMAG_06461, UMAG_06462, UMAG_06463, UMAG_06464, UMAG_06465, UMAG_06466, UMAG_06467, UMAG_11813 and UMAG_12340	this study
U. maydis MB215 ΔMEL (#4385)	*U. maydis* MB215 with deletion of UMAG_03114, UMAG_03115, UMAG_03116, UMAG_03117, UMAG_10636	this study
U. maydis MB215 Δ*cyp3* ΔMEL (#4387)	*U. maydis* MB215 with deletion of UMAG_05074, UMAG_03117 and UMAG_10636	this study
U. maydis MB215 Δ*cyp3* ΔMEL ΔUA (#4388)	*U. maydis* MB215 with deletion of UMAG_05074, UMAG_03117, UMAG_10636, UMAG_96458, UMAG_06459, UMAG_06460, UMAG_06461, UMAG_06462, UMAG_06463, UMAG_06464, UMAG_06465, UMAG_06466, UMAG_06467, UMAG_11813 and UMAG_12340	this study
U. maydis MB215 Δ*cyp3* ΔMEL ΔUA Δ*dgat* (#4389)	*U. maydis* MB215 with deletion of UMAG_05074, UMAG_03117, UMAG_10636, UMAG_96458, UMAG_06459, UMAG_06460, UMAG_06461, UMAG_06462, UMAG_06463, UMAG_06464, UMAG_06465, UMAG_06466, UMAG_06467, UMAG_11813,	this study

strain name (iAMB strain collection no.)	description	reference
	UMAG_12340 and UMAG_03937	
U. maydis MB215 Δ*cyp3* ΔMEL ΔUA Δ*dgat* ΔP_{ria1}::P_{etef} (#4854)	*U. maydis* MB215 with deletion of UMAG_05074, UMAG_03117, UMAG_10636, UMAG_96458, UMAG_06459, UMAG_06460, UMAG_06461, UMAG_06462, UMAG_06463, UMAG_06464, UMAG_06465, UMAG_06466, UMAG_06467, UMAG_11813, UMAG_12340 and UMAG_03937, and with the overexpression of UMAG_05080	this study
U. maydis MB215 Δ*cyp3* ΔMEL ΔUA Δ*dgat* ΔP_{ria1}::P_{etef} Δ*fuz7* (#4855)	*U. maydis* MB215 with deletion of UMAG_05074, UMAG_03117, UMAG_10636, UMAG_96458, UMAG_06459, UMAG_06460, UMAG_06461, UMAG_06462, UMAG_06463, UMAG_06464, UMAG_06465, UMAG_06466, UMAG_06467, UMAG_11813, UMAG_12340, UMAG_03937 and UMAG_01514, and overexpression of UMAG_05080	this study
U. maydis MB215 Δ*cyp3* ΔMEL ΔUA Δ*dgat* ΔP_{ria1}::P_{etef} Δ*fuz7* ::P_{etef}*AT_mttA* _K3	*U. maydis* MB215 with deletion of UMAG_05074, UMAG_03117, UMAG_10636, UMAG_96458, UMAG_06459, UMAG_06460, UMAG_06461, UMAG_06462, UMAG_06463, UMAG_06464, UMAG_06465, UMAG_06466, UMAG_06467, UMAG_11813, UMAG_12340, UMAG_03937 and UMAG_01514, and overexpression of UMAG_05080 and ATEG_09970 of *A. terreus*	this study
U. maydis MB215 Δ*cyp3* ΔMEL ΔUA Δ*dgat* ΔP_{ria1}::P_{etef} Δ*fuz7* ::P_{etef}*AT_mttA* _K8	*U. maydis* MB215 with deletion of UMAG_05074, UMAG_03117, UMAG_10636, UMAG_96458, UMAG_06459, UMAG_06460, UMAG_06461, UMAG_06462, UMAG_06463, UMAG_06464, UMAG_06465, UMAG_06466, UMAG_06467, UMAG_11813, UMAG_12340, UMAG_03937 and UMAG_01514, and overexpression of UMAG_05080 and ATEG_09970 of *A. terreus*	this study
U. maydis MB215 Δ*cyp3* ΔMEL ΔUA Δ*dgat* ΔP_{ria1}::P_{etef} Δ*fuz7* ::P_{etef}*AT_mttA* _K9	*U. maydis* MB215 with deletion of UMAG_05074, UMAG_03117, UMAG_10636, UMAG_96458, UMAG_06459, UMAG_06460, UMAG_06461, UMAG_06462, UMAG_06463, UMAG_06464, UMAG_06465, UMAG_06466, UMAG_06467, UMAG_11813, UMAG_12340, UMAG_03937 and UMAG_01514, and overexpression of UMAG_05080 and ATEG_09970 of *A. terreus*	this study

strain name (iAMB strain collection no.)	description	reference
U. maydis MB215 Δ*cyp3* ΔMEL ΔUA Δ*dgat* ΔP_{ria1}::P_{etef} Δ*fuz7* ::P_{etef}*AT_mttA* _K10	*U. maydis* MB215 with deletion of UMAG_05074, UMAG_03117, UMAG_10636, UMAG_96458, UMAG_06459, UMAG_06460, UMAG_06461, UMAG_06462, UMAG_06463, UMAG_06464, UMAG_06465, UMAG_06466, UMAG_06467, UMAG_11813, UMAG_12340, UMAG_03937 and UMAG_01514, and overexpression of UMAG_05080 and ATEG_09970 of *A. terreus*	this study
U. maydis MB215 Δ*cyp3* ΔMEL ΔUA Δ*dgat* ΔP_{ria1}::P_{etef} Δ*fuz7* ::P_{etef}*AT_mttA*_K14 (#4856)	*U. maydis* MB215 with deletion of UMAG_05074, UMAG_03117, UMAG_10636, UMAG_96458, UMAG_06459, UMAG_06460, UMAG_06461, UMAG_06462, UMAG_06463, UMAG_06464, UMAG_06465, UMAG_06466, UMAG_06467, UMAG_11813, UMAG_12340, UMAG_03937 and UMAG_01514, and overexpression of UMAG_05080 and ATEG_09970 of *A. terreus*	this study
U. maydis MB215 G1.1_K4 (#4857)	*U. maydis* MB215 evolved on pH 4 and 50 g L^{-1} itaconate	this study
U. maydis MB215 G1.1_K23	*U. maydis* MB215 evolved on pH 4 and 50 g L^{-1} itaconate	this study
U. maydis MB215 G1.2_K2	*U. maydis* MB215 evolved on pH 4 and 60 g L^{-1} itaconate	this study
U. maydis MB215 G1.3_K2	*U. maydis* MB215 evolved on pH 4 and 40 g L^{-1} itaconate	this study
U. maydis MB215 G1.4_K2 (#4858)	*U. maydis* MB215 evolved on pH 4 and 50 g L^{-1} itaconate	this study
U. maydis MB215 G1.4_K21	*U. maydis* MB215 evolved on pH 4 and 60 g L^{-1} itaconate	this study
U. maydis MB215 G1.1_K4 Δ*cyp3* ΔP_{ria1}::P_{etef} (#4860)	*U. maydis* MB215 evolved on pH 4 and 50 g L^{-1} itaconate with deletion of UMAG_05074 and overexpression of UMAG_05080	this study
U. maydis MB215 G1.1_K23 Δ*cyp3* ΔP_{ria1}::P_{etef}	*U. maydis* MB215 evolved on pH 4 and 50 g L^{-1} itaconate with deletion of UMAG_05074 and overexpression of UMAG_05080	this study
U. maydis MB215 G1.3_K2 Δ*cyp3* ΔP_{ria1}::P_{etef}	*U. maydis* MB215 evolved on pH 4 and 40 g L^{-1} itaconate with deletion of UMAG_05074 and overexpression of UMAG_05080	this study
U. maydis MB215 G1.4_K2 Δ*cyp3* ΔP_{ria1}::P_{etef} (#4861)	*U. maydis* MB215 evolved on pH 4 and 50 g L^{-1} itaconate with deletion of UMAG_05074 and overexpression of UMAG_05080	this study
U. maydis MB215 G1.4_K21 Δ*cyp3* ΔP_{ria1}::P_{etef}	*U. maydis* MB215 evolved on pH 4 and 60 g L^{-1} itaconate with deletion of UMAG_05074 and overexpression of UMAG_05080	this study
U. maydis MB215 G1.1_K4 Δ*cyp3* ΔP_{ria1}::P_{etef} Δ*dgat* (#4862)	*U. maydis* MB215 evolved on pH 4 and 50 g L^{-1} itaconate with deletion of UMAG_05074, overexpression of UMAG_05080, deletion of UMAG_03937	this study

strain name (iAMB strain collection no.)	description	reference
U. maydis MB215 G1.4_K2 Δ*cyp3* ΔP_{ria1}::P_{etef} Δ*dgat* (#4863)	*U. maydis* MB215 evolved on pH 4 and 50 g L^{-1} itaconate with deletion of UMAG_05074, overexpression of UMAG_05080, deletion of UMAG_03937	this study
U. maydis MB215 G1.1_K4 Δ*cyp3* ΔP_{ria1}::P_{etef} Δ*dgat* ΔMEL (#4864)	*U. maydis* MB215 evolved on pH 4 and 50 g L^{-1} itaconate with deletion of UMAG_05074, overexpression of UMAG_05080, deletion of UMAG_03937, UMAG_03114, UMAG_03115, UMAG_03116, UMAG_03117, UMAG_10636	this study
U. maydis MB215 G1.4_K2 Δ*cyp3* ΔP_{ria1}::P_{etef} Δ*dgat* ΔMEL (#4865)	*U. maydis* MB215 evolved on pH 4 and 50 g L^{-1} itaconate with deletion of UMAG_05074, overexpression of UMAG_05080, deletion of UMAG_03937, UMAG_03114, UMAG_03115, UMAG_03116, UMAG_03117, UMAG_10636	this study
U. maydis MB215 G1.1_K4 Δ*cyp3* ΔP_{ria1}::P_{etef} Δ*dgat* ΔMEL ΔUA (#4866)	*U. maydis* MB215 evolved on pH 4 and 50 g L^{-1} itaconate with deletion of UMAG_05074, overexpression of UMAG_05080, deletion of UMAG_03937, UMAG_03114, UMAG_03115, UMAG_03116, UMAG_03117, UMAG_10636, UMAG_96458, UMAG_06459, UMAG_06460, UMAG_06461, UMAG_06462, UMAG_06463, UMAG_06464, UMAG_06465, UMAG_06466, UMAG_06467, UMAG_11813, UMAG_12340	this study
U. maydis MB215 G1.4_K2 Δ*cyp3* ΔP_{ria1}::P_{etef} Δ*dgat* ΔMEL ΔUA (#4867)	*U. maydis* MB215 evolved on pH 4 and 50 g L^{-1} itaconate with deletion of UMAG_05074, overexpression of UMAG_05080, deletion of UMAG_03937, UMAG_03114, UMAG_03115, UMAG_03116, UMAG_03117, UMAG_10636, UMAG_96458, UMAG_06459, UMAG_06460, UMAG_06461, UMAG_06462, UMAG_06463, UMAG_06464, UMAG_06465, UMAG_06466, UMAG_06467, UMAG_11813, UMAG_12340	this study
U. maydis MB215 G1.1_K4 Δ*cyp3* ΔP_{ria1}::P_{etef} Δ*dgat* ΔMEL ΔUA Δ*fuz7* (#4868)	*U. maydis* MB215 evolved on pH 4 and 50 g L^{-1} itaconate with deletion of UMAG_05074, overexpression of UMAG_05080, deletion of UMAG_03937, UMAG_03114, UMAG_03115, UMAG_03116, UMAG_03117, UMAG_10636, UMAG_96458, UMAG_06459, UMAG_06460, UMAG_06461, UMAG_06462, UMAG_06463, UMAG_06464, UMAG_06465, UMAG_06466, UMAG_06467, UMAG_11813, UMAG_12340, UMAG_01514	this study

strain name (iAMB strain collection no.)	description	reference
U. maydis MB215 G1.4_K2 Δ*cyp3* ΔP_{ria1}::P_{etef} Δ*dgat* ΔMEL ΔUA Δ*fuz7* (#4869)	*U. maydis* MB215 evolved on pH 4 and 50 g L^{-1} itaconate with deletion of UMAG_05074, overexpression of UMAG_05080, deletion of UMAG_03937, UMAG_03114, UMAG_03115, UMAG_03116, UMAG_03117, UMAG_10636, UMAG_96458, UMAG_06459, UMAG_06460, UMAG_06461, UMAG_06462, UMAG_06463, UMAG_06464, UMAG_06465, UMAG_06466, UMAG_06467, UMAG_11813, UMAG_12340, UMAG_01514	this study

U. maydis was grown at 30 °C in liquid YEPS medium consisting of 1 % (w/v) yeast extract, 1 % (w/v) peptone, and 1 % (w/v) sucrose and additionally 2 % (w/v) agar for solid medium. For itaconate production experiments, *U. maydis* strains were cultivated in either System Duetz® 24 well plates with a filling volume of 1.5 mL at 30 °C and 300 rpm (shaking diameter = 50 mm, relative air humidity = 80 %) [233] or in 500 mL Erlenmeyer flasks with a filling volume of 50 mL at 30 °C and 200 rpm (shaking diameter = 25 mm, relative air humidity = 80 %). Precultures were performed in the same medium as the main culture which was inoculated to a final OD_{600} of 0.5.

As screeening medium, modified Tabuchi medium (MTM) was used containing 50 g L^{-1} or 100 g L^{-1} glucose, 0.8 g L^{-1} NH_4Cl, 0.2 g L^{-1} $MgSO_4x7H_2O$, 0.01 g L^{-1} $FeSO_4x7H_2O$, 0.5 g L^{-1} KH_2PO_4, 1 mL L^{-1} vitamin solution, and 1 mL L^{-1} trace element solution. The vitamin solution contained 0.05 g D-biotin, 1 g D-calcium panthotenate, 1 g nicotinic acid, 25 g myo-inositol, 1 g thiamine hydrocholoride, 1 g pyridoxol hydrochloride, and 0.2 g paraaminobenzoic acid per liter. The trace element solution contained 1.5 g EDTA, 0.45 g $ZnSo_4x7H_2O$, 0.10 g $MnCl_2x4H_2O$, 0.03 g $CoCl_2x6H_2O$, 0.03 g $CuSO_4x5H_2O$, 0.04 g $Na_2MoO_4x2H_2O$, 0.45 g $CaCl_2x2H_2O$, 0.3 g $FeSO_4x7H_2O$, 0.10 g H_3BO_3, and 0.01 g KI per liter. As buffer, 100 mM 2-(N-morpholino) ethanesulfonic acid (MES), adjusted to a pH of 6.5 with NaOH, or different concentrations of $CaCO_3$ were used [150].

For glycolipid extraction, strains were incubated for 72 h at 30 °C in YNB medium (1.7 g L^{-1} Yeast Nitrogen Base, 5 % glucose) [143].

Fed-batch fermentations were performed in 1.3 L New Brunswick BioFlo® 115 bioreactors (Eppendorf, Germany) with a working volume of 0.5 L. The MTM contained 200 g L^{-1} glucose, 4 g L^{-1} NH_4Cl, 0.2 g L^{-1} $MgSO_4x7H_2O$, 0.01 g L^{-1} $FeSO_4x7H_2O$, 0.5 g L^{-1} KH_2PO_4, 1 mL L^{-1} vitamin solution, 1 mL L^{-1} trace element solution, and 1 g L^{-1} yeast extract. During cultivation, the pH was automatically kept constant at 6.5 with10 M NaOH. The addition of antifoam 204 (Sigma Life Science, USA) avoided foam formation. The stirring rate was adjusted to 1000 rpm, the aeration rate to 1 L min^{-1} (2 vvm) and the temperatur to 30 °C. It was inoculated to a final OD_{600} of 0.75 from a 48 h preculture.

For ALE, *U. maydis* MB215 was grown in MTM buffered with 100 mM potassium hydrogen pthalate at pH 4.0 and a stepwise increase of the itaconate concentration starting with a concentration of 0 g L^{-1} and ending up with up to 60 g L^{-1} itaconate.

100 mL Erlenmeyer flasks with a working volume of 10 mL were used. Inoculation of fresh MTM with an increased itaconate concentration was performed every 2 – 4 days with 0.5 mL of the preculture.

4.2 Cloning procedures

4.2.1 Plasmids and primers

Table 21: Plasmids used within this study with description of construct composition and reference.

plasmid name (iAMB strain collection no.)	description	reference
pJET1.2/blunt	Ori ColE1; AmpR	Thermo Scientific, Germany
pJET1.2-*ura*-sgRNA (#3669)	pJET1.2 with sgRNA of *ura* for CRISPR/Cas9 modifications	provided by H. Hosseinpour Tehrani
pMS8-Cas9 (#3595)	U6 promoter; constitutive *otef* promoter; codon-optimized *cas9* from *Streptococcus pyogenes*; ip^R; ARS; ampR;	Prof. R. Kahmann, Philipps University Marburg, Germany
pFLPexpC	*Pcrg1* promoter; synthetic *FLP recombinase* gene; cbxR; ARS; AmpR	Prof. M. Feldbrügge, Heinrich-Heine University Düsseldorf, Germany
pStorI-1rh wt	FRTwt-HygR-FRTwt cassette; GentR	Prof. M. Feldbrügge, Heinrich-Heine University Düsseldorf, Germany
pUMa1523	FRTm1-HygR-FRTm1 cassette; GentR	Dr. K. Schipper, Heinrich-Heine University Düsseldorf, Germany
pJET1.2-*cyp3*-donor template (#4930)	pJET1.2 with 5'- and 3'-UTR flank of UMAG_05074 as deletion construct	this study
pJET1.2-*cyp3*-sgRNA (#3783)	pJET1.2 with sgRNA of UMAG_05074 for CRISPR/Cas9 modifications	this study
pMS8-*cyp3*-sgRNA (#3784)	pMS8-Cas9 with sgRNA of UMAG_05074 for CRISPR/Cas9 modifications	this study
pJET1.2-MEL cluster-donor template (#4931)	pJET1.2 with 5'-UTR flank of UMAG_03114 and 3'-UTR flank of UMAG_10636 as deletion construct	this study
pJET1.2-*emt1*-donor template (#4934)	pJET1.2 with ampR; 5'- and 3'-UTR flank of UMAG_03117	this study
pJET1.2-*emt1*-sgRNA (#4932)	pJET1.2 with sgRNA of UMAG_03117 for CRISPR/Cas9 modifications	this study
pMS8-*emt1*-sgRNA (#4933)	pMS8-Cas9 with sgRNA of UMAG_03117 for CRISPR/Cas9 modifications	this study
pJET1.2-UA cluster-donor template (#4938)	pJET1.2 with 5'-UTR flank of UMAG_96458 and 3'-UTR flank of UMAG_12340 as deletion construct	this study
pJET1.2-*cyp1*-donor template (#4937)	pJET1.2 with 5'- and 3'-UTR flank of UMAG_06463 as deletion construct	this study
pJET1.2-*cyp1*-sgRNA (#4935)	pJET1.2 with sgRNA of UMAG_06463 for CRISPR/Cas9 modifications	this study
pMS8-*cyp1*-sgRNA (#4936)	pMS8-Cas9 with sgRNA of UMAG_06463 for CRISPR/Cas9 modifications	this study
pJET1.2-*dgat* 5'-UTR flank - FRTwt-HygR-FRTwt-dgat 3'-UTR flank (#4939)	pJET1.2 with 5'- and 3'-UTR flank of UMAG_03937 as deletion construct; HygR; FRT wt recombination sites for HygR recycling	this study

plasmid name (iAMB strain collection no.)	description	reference
pJET1.2-*fuz7* 5'-UTR flank - FRTm1-HygR-FRTm1-fuz7 3'-UTR flank (#4940)	pJET1.2 with 5'- and 3'-UTR flank of UMAG_01514 as deletion construct; HygR; FRT m1 recombination sites for HygR recycling	this study
pJET1.2-UMAG_02068 5'-UTR flank -FRTm1-HygR-FRTm1- UMAG_02068 3'-UTR flank	pJET1.2 with 5'- and 3'-UTR flank of UMAG_02068 as deletion construct; HygR; FRT m1 recombination sites for HygR recycling	this study
pJET1.2-UMAG_03806 5'-UTR flank -FRTm1-HygR-FRTm1- UMAG_03806 3'-UTR flank	pJET1.2 with 5'- and 3'-UTR flank of UMAG_03806 as deletion construct; HygR; FRT m1 recombination sites for HygR recycling	this study
pMS8-Um_P_{oma}-sgRNA (#4019)	pMS8-Cas9 with sgRNA of P_{oma} promoter for CRISPR/Cas9 modifications	provided by H. Hosseinpour Tehrani
pJET1.2-Um_P_{etef} - donor template (#4072)	pJET1.2 with cDNA of P_{etef} promoter as deletion construct	provided by H. Hosseinpour Tehrani
P_{etef} -Cbx-*AT_mttA* (#3010)	constitutive P_{etef} promoter, cDNA of *A. terreus* ATEG_09970 (mttA), cbxR, ampR	provided by E. Geiser

Table 22: Primers used within this study with information about sequence and application.

primer	sequence & description
JB-1_fwd	AGATGGCGTTGCCAGAATCGGTTTTAGAGCTAGAA Amplification of pJET1.2-*ura*-sgRNA to change *ura*-sgRNA by *cyp3*-sgRNA
JB-2_fwd	ctcgagtttttcagcaagatGTAGACGAAAGCCACCTG Amplification of 5'-UTR flank for *cyp3* donor template construction
JB-3_rev	catcggtgtcGATGCTCCCAAACGCCTC Amplification of 5'-UTR flank for *cyp3* donor template construction
JB-4_fwd	tgggagcatcGACACCGATGCAGCCGCA Amplification of 3'-UTR flank for *cyp3* donor template construction
JB-5_rev	aggagatcttctagaaagatTCGGCTTCCACCCGCTTG Amplification of 3'-UTR flank for *cyp3* donor template construction
JB-6_fwd	CCACCTGCGTGTACAGCTTG Amplification of *cyp3* donor template
JB-7_rev	CAAGTCGTGAGTCGGACAAG Amplification of *cyp3* donor template
JB-8_fwd	CAAAATTCCATTCTACAACGAGAT Amplification of *cyp3*-sgRNA for insertion into pMS8-Cas9
JB-9_fwd	CTTCAAGGCCACCACAAC Verification of *cyp3* deletion
JB-64_rev	TGCTGCCATGGTGCTACTCC Verification of *cyp3* deletion
JB-11_fwd	TCAGCTCGTACGCCGTCGCTGTTTTAGAGCTAGAA Amplification of pJET1.2-*ura*-sgRNA to change *ura*-sgRNA by *emt1*-sgRNA
JB-12_fwd	CAAAATTCCATTCTACAACGTCAG Amplification of *emt1*-sgRNA for insertion into pMS8-Cas9
JB-13_fwd	ctcgagtttttcagcaagatGACGAGGCTTAGCTAGTC Amplification of 5'-UTR flank for *emt1* donor template construction
JB-14_rev	taacaccatcCCTCGACACTCACGACTC Amplification of 5'-UTR flank for *emt1* donor template construction
JB-15_fwd	agtgtcgaggGATGGTGTTAGGTTCCGAG Amplification of 3'-UTR flank for *emt1* donor template construction
JB-16_rev	aggagatcttctagaaagatCTGTGGCACGTCTCTGAT Amplification of 3'-UTR flank for *emt1* donor template construction
JB-17_fwd	CTAGCCTGAGAAGCTCTATC Amplification of *emt1* donor template
JB-18_rev	GTGAATGGTTCATGGATGGC Amplification of *emt1* donor template

primer	sequence & description
JB-19_fwd	GACGAGGAGGTGTGGATTTC Verification of *emt1* deletion
JB-20_rev	GAGTACCAGATTCGCCAGCT Verification of *emt1* deletion
JB-21_fwd	ctcgagtttttcagcaagatCGCATTTGCTCACATGTATCGC Amplification of 5'-UTR flank of *mat1* for MEL gene cluster donor template construction
JB-22_rev	cagcaatgggCAGGCCAAGCTATGGCCG Amplification of 5'-UTR flank of *mat1* for MEL gene cluster donor template construction
JB-23_fwd	gcttggcctgCCCATTGCTGTCACTCTC Amplification of 3'-UTR flank of *mac2* for MEL gene cluster donor template construction
JB-24_rev	aggagatcttctagaaagatGACTCCCAACTGTGGGCA Amplification of 3'-UTR flank of *mac2* for MEL gene cluster donor template construction
JB-25_fwd	GTTGCAGTTCCAAGCTAACG Amplification of MEL cluster donor template
JB-26_rev	CGATTGCGGTGAAGGGATGC Amplification of MEL cluster donor template
JB-28_rev	GTCAGTCGTGAGTGTTAAGG Verification of MEL gene cluster deletion
JB-29_fwd	TCACGGTTCCCTCTGTTATC Verification of MEL gene cluster deletion
JB-41_fwd	ACGCGTCGTCAGTGTAAATG Verification of MEL gene cluster deletion
JB-42_rev	ACCCGTCCAGCACAGTATCCA Verification of MEL gene cluster deletion
JB-65_fwd	GCCCACCACTCACCACTTTC Verification of MEL cluster deletion
JB-66_rev	ACACCACCGATAGTCCATTG Verification of MEL cluster deletion
JB-31_fwd	TCTGCATGTACGAGAAAAGCGTTTTAGAGCTAGAA Amplification of pJET1.2-*ura*-sgRNA to change *ura*-sgRNA by *cyp1*-sgRNA
JB-38_fwd	CAAAATTCCATTCTACAACGTCTG Amplification of *cyp1*-sgRNA for insertion into pMS8-Cas9
JB-43_fwd	ctcgagtttttcagcaagatGATTCCATCCGAAGCTGC Amplification of 5'-UTR flank of *rua1* for UA gene cluster donor template construction
JB-44_rev	caattttcacGACGGAAGATGAGAATCG Amplification of 5'-UTR flank of *rua1* for UA gene cluster donor template construction
JB-45_fwd	atcttccgtcGTGAAAATTGGGGCCAATGAC Amplification of 3'-UTR flank of *ahd1* for MEL gene cluster donor template construction
JB-46_rev	aggagatcttctagaaagatCGATTGCCTTTGCCGTGC Amplification of 3'-UTR flank of *ahd1* for MEL gene cluster donor template construction
JB-47_fwd	GCTTCTCGGCTGACGACAAC Amplification of UA cluster donor template
JB-48_rev	GCCATTTCGCCTGTGTACTC Amplification of UA cluster donor template
JB-50_rev	GCCATTTCGCCTGTGTACTC Verification of UA cluster deletion
JB-51_rev	TGAGGGCAATTGTTGTCCTG Verification of UA cluster deletion
JB-67_fwd	GAGCCAGTCAGTCAACAATC Verification of UA gene cluster deletion
JB-53_fwd	ctcgagtttttcagcaagatGTTGATGCCGGTGTGGTTG Amplification of 5'-UTR flank for generation of *dga*t deletion construct
JB-56_rev	aggagatcttctagaaagatCGAACAACACAGTCAAGATGTC Amplification of 3'-UTR flank for generation of *dgat* deletion construct

primer	sequence & description
JB-84_rev	acttctggccGGCTCGTCTGAAGGGTCG Amplification of 5'-UTR flank for generation of *dgat* deletion construct
JB-85_fwd	cagacgagccGGCCAGAAGTTCCTATTC Amplification of FRT_wt-HygR-FRT_wt cassette for generation of *dgat* deletion construct
JB-86_rev	gcacatatcgGGCCAGAAGTTCCTATAC Amplification of FRT_wt-HygR-FRT_wt cassette for generation of *dgat* deletion construct
JB-87_fwd	acttctggccCGATATGTGCGGGTGCAG Amplification of 3'-UTR flank for generation of *dgat* deletion construct
JB-58_fwd	CGCTTGCTGCCAGCTGATTG Amplification of *dgat* deletion construct
JB-59_rev	AGCATACCGCCACCCTCTTG Amplification of *dgat* deletion construct
JB-60_fwd	TCTCTACCTTTGCCGATCTG Verification of *dgat* deletion
JB-61_rev	GTGCAGGTGGTTTGGATTTG Verification of *dgat* deletion
JB-68_fwd	GAAGTGGCTGAGTCGTGTAG Verification of *dgat* deletion
JB-69_rev	ACAGACTGCCAGTCACATTC Verification of *dgat* deletion
JB-89_fwd	ctcgagtttttcagcaagatCCGATCGCTGTTAGGACAC Amplification of 5'-UTR flank for generation of *fuz7* deletion construct
JB-90_rev	acttctggccCGTGAAACGTTGCAAAACAG Amplification of 5'-UTR flank for generation of *fuz7* deletion construct
JB-91_fwd	acgtttcacgGGCCAGAAGTTCCTATTC Amplification of FRT_m1-HygR-FRT_m1 cassette for generation of *fuz7* deletion construct
JB-92_rev	tctcagtcggCCCGGGAAGTTCCTATAC Amplification of FRT_m1-HygR-FRT_m1 cassette for generation of *fuz7* deletion construct
JB-93_fwd	acttcccgggCCGACTGAGAGATTATGGTC Amplification of 3'-UTR flank for generation of *fuz7* deletion construct
JB-94_rev	aggagatcttctagaaagatAATCGGAACCGTGTACCTG Amplification of 3'-UTR flank for generation of *fuz7* deletion construct
JB-101_fwd	ctcgagtttttcagcaagatGGACGTTGGACGGCAGCG Amplification of 5'-UTR flank for generation of UMAG_02068 deletion construct
JB-102_rev	acttctggccACGCGTCGTTGAATGCGC Amplification of 5'-UTR flank for generation of UMAG_02068 deletion construct
JB-103_fwd	aacgacgcgtGGCCAGAAGTTCCTATTC Amplification of FRT_m1-HygR-FRT_m1 cassette for generation of UMAG_02068 deletion construct
JB-104_rev	cacgtataacCCCGGGAAGTTCCTATAC Amplification of FRT_m1-HygR-FRT_m1 cassette for generation of UMAG_02068 deletion construct
JB-105_fwd	acttcccgggGTTATACGTGTACAATGAATTGTAATATG Amplification of 3'-UTR flank for generation of UMAG_02068 deletion construct
JB-106_rev	aggagatcttctagaaagatGATCTGTGACGATCGACTATTG Amplification of 3'-UTR flank for generation of UMAG_02068 deletion construct
JB-107_fwd	CAGCGGCTGTTGCTTCTCAC Amplification of UMAG_02068 deletion construct
JB-108_rev	ATTTCCTGTGGCTGCTGTTG Amplification of UMAG_02068 deletion construct
JB-109_fwd	ctcgagtttttcagcaagatCGGCGAGCAATATGCAATG Amplification of 5'-UTR flank for generation of UMAG_03806 deletion construct
JB-110_rev	acttctggccCGACTGAGTAAGGAGGGAC Amplification of 5'-UTR flank for generation of UMAG_03806 deletion construct
JB-111_fwd	tactcagtcgGGCCAGAAGTTCCTATTC Amplification of FRT_m1-HygR-FRT_m1 cassette for generation of UMAG_03806 deletion construct

primer	sequence & description
JB-112_rev	ttggaggtcgCCCGGGAAGTTCCTATAC Amplification of FRT_m1-HygR-FRT_m1 cassette for generation of UMAG_03806 deletion construct
JB-113_fwd	acttcccgggCGACCTCCAAGCCTCAAATC Amplification of 3'-UTR flank for generation of UMAG_03806 deletion construct
JB-114_rev	aggagatcttctagaaagatGCGACGGATATATAGGCG Amplification of 3'-UTR flank for generation of UMAG_03806 deletion construct
JB-115_fwd	ATGCAATGCGGATCGACAAG Amplification of UMAG_03806 deletion construct
JB-116_rev	ATATAGGCGCTTGTTGGCTG Amplification of UMAG_03806 deletion construct
JB-117_fwd	GCGAGCCAGTCTTACGATAC Verification of UMAG_02068 deletion
JB-118_rev	TGGCGAGCTGACTTGCTTAG Verification of UMAG_02068 deletion
JB-119_fwd	TTCGCTTGCTTCAACTAGGG Verification of UMAG_03806 deletion
JB-120_rev	GGCAGCCAACCATATACAAG Verification of UMAG_03806 deletion
JB-126_fwd	ATGGCTTCTCAATCGCAC Amplification of reference gene UMAG_02592 during qRT-PCR
JB-127_rev	CCTGGTGTTGAGGATGAG Amplification of reference gene UMAG_02592 during qRT-PCR
JB-128_fwd	ACATCGTCAAGGCTATCG Amplification of reference gene UMAG_03726 during qRT-PCR
JB-129_rev	AAAGAACACCGGACTTGG Amplification of reference gene UMAG_03726 during qRT-PCR
JB-132_fwd	AACACGTTCAACTGCGTCAA Amplification of *mttA* during qRT-PCR
JB-133_rev	GAACATGATGGCCGAGGTG Amplification of *mttA* during qRT-PCR
HT-4a_rev	ACAGACGTCGCGGTGAGTTC Verification of FRT-HygR-cassette based insertions
HT-8a_rev	GTCGAGCTCGGTACGGGT Amplification of target sgRNA from pJET1.2 backbone for insertion into pMS8-Cas9
HT-9_fwd	CCTTGCAATTCGCGCACACC Verification of target-sgRNA insertion into pMS8-Cas9
HT-10_rev	GCTCGGTACGGGTACTAATG Verification of target-sgRNA insertion into pMS8-Cas9
HT-12_rev	CGTTGTAGAATGGAATTTTG Amplification of pJET1.2-*ura*-sgRNA to change *ura*-sgRNA by target-sgRNA
HT-125_fwd	ATGTCGAGGCCAACTGTG Amplification of *pETEF* promoter upstream of *ria1*
HT-127_rev	TCGAGCCAAATCAATGCG Amplification of *pETEF* promoter upstream of *ria1*
HT-153_fwd	GACAGCGCCCTTTATTGG Verification of *pOMA* to *pETEF* promoter exchange upstream of *ria1*
HT-159_fwd	GCCCAACTGATTAGCTGTGCCCCCTCGC Verification of pJET1.2-Um_*pETEF*-F-donor template upstream of *ria1*
HT-186_rev	AGTTGGGTTCGCTCGATG Verification of *pOMA* to *pETEF* promoter exchange upstream of *ria1*
HT-202_fwd	TCCTGCGTCAGTCGTCCAAC Verification of *pETEF-mttA* integration
HT-203_fwd	GTCCGAGGGCAAAGGAATAG Verification of *fuz7* deletion
HT-210_fwd	TCGCTGTTAGGACACAACTG Amplification of *fuz7* deletion construct
HT-210a_fwd	TCGGTGTGCGGCGATTTCTG Verification of *fuz7* deletion

primer	sequence & description
HT-211_rev	CCGTGTACCTGGCTGTGTAG Amplification of *fuz7* deletion construct
HT-220_rev	GATTCTGTGGGACAAGAAGC Verification of *fuz7* deletion
pJET1.2_fwd	CGACTCACTATAGGGAGAGCGGC Amplification of constructs cloned into pJET1.2-vector
pJET1.2_rev	AAGAACATCGATTTTCCATGGCAG Amplification of constructs cloned into pJET1.2-vector
Tnos_rev	CAAGACCGGCAACAGGATTC Verification of *pETEF-mttA* integration

4.2.2 Generation of *U. maydis* protoplasts and transformation

Protoplast transformation was performed according to Tsukuda *et al*. [234]. For the generation of *U. maydis* protoplasts, a preculture was grown in 100 mL Erlenmeyer flasks with a filling volume of 10 mL for 24 h at 30 °C shaking at 200 rpm. 50 mL of the main culture were inoculated in a 500 mL Erlenmeyer flask to a final OD_{600} of 0.2. Reaching an OD_{600} of 0.8, the culture was centrifuged (10 min, 4 °C, 4,000 rpm) and the pellet was resuspended in 25 mL SCS. SCS was a mixture of two solutions. Solution I consisted of 2 mM sodium citrate and 1 M D-sorbitol and was adjusted to a pH of 5.8 with solution II containing 2 mM citric acid and 1 M D-sorbitol. The solved pellet was centrifuged (10 min, 4 °C, 4,000 rpm) and resuspended in 2 mL SCS/20 mg mL^{-1} *Trichoderma harzianum* Lysing Enzyme (Sigma) to induce protoplast formation. The process was controlled by microscopy and stopped with the addition of 10 mL SCS when 80 % of the cells had formed protoplasts. The cells were centrifuged (10 min, 4 °C, 2,300 rpm) and washed three times with 10 mL SCS. The protoplasts were resuspended in 500 µL STC and stored in 50 µL aliquots at -80 °C. The STC solution contained 100 mM calcium chloride, 1 M D-sorbitol, and 10 mM Tris-HCl (pH 7.5).

For transformation of foreign DNA into *U. maydis* protoplasts, protoplasts were thawed on ice, before 500 – 1,500 ng DNA were added and the cells were incubated on ice for 10 min. 500 µl 40 % PEG 4000 (Roth, Germany)/STC solution were added followed by a 10 min incubation time on ice. The cells were plated on REG agar plates. REG agar plates consisted of a bottom and a top layer (1 M D-sorbitol in YEPS medium, 1,5 % agar). To the bottom layer, 4 µg mL^{-1} carboxin (Sigma) or 400 µg mL^{-1} Hygromycin B (Roth, Germany) were added.

4.2.3 Generation of deletion and overexpression constructs

For genome editing using CRISPR/Cas9, two plasmids were designed for each deletion: pMS8-target-sgRNA and pJET1.2-donor template. To get the pMS8-target-sgRNA, pJET1.2-ura-sgRNA was amplified with a forward primer specific for each deletion, namely JB-1 for *cyp3*, JB-11 for *emt1*/MEL cluster, JB-31 for *cyp1*/UA cluster deletion, and HT-12 to change *ura* sgRNA with the new target sgRNA resulting in pJET1.2-target-sgRNA. To insert the target sgRNAs into pMS8-Cas9, the backbone vector was Acc65I-linearised and the target sgRNAs were amplified with the primer pairs JB-8/HT-8a for *cyp3*, JB-12/HT-8a for *emt1*, JB-38/HT-8a for *cyp1* sgRNA, before Gibson cloning was performed to get the final pMS8-target-

sgRNA vectors. pMS8-Um_P_{oma}-sgRNA included the sgRNA for the native *ria1* promoter. Donor template constructs were generated consisting of a 1,000 bp long 5'-UTR and 3'-UTR flank enclosing the region going to be deleted. The flanks were amplified with the following primer pairs: JB-2/JB-3 and JB-4/JB-5 for *cyp3*, JB-13/JB-14 and JB-15/JB-16 for *emt1*, JB-21/JB-22 and JB-23/JB-24 for MEL cluster, JB-43/JB-44 and JB-45/JB-46 for UA cluster donor template. The amplified flanks were inserted into pJET1.2/blunt by Gibson cloning. For *ria1* promoter exchange to overexpress *ria1*, the plasmid pJET1.2-Um_P_{etef}-donor template carried the corresponding donor template.

For FRT/FLP based genome editing, deletion constructs consisting of 5'-UTR, 3'-UTR target flank and FRT-HygR-FRT cassette had to be designed. The three fragments were amplified with the following primer pairs: JB-53/JB-84, JB-87/JB-56 and JB-85/JB-86 for *dgat*, JB-89/JB-90, JB-93/JB-94 and JB-91/JB-92 for *fuz7*, JB-101/JB-102, JB-105/JB-106 and JB-103/JB-104 for UMAG_02068, JB-109/JB-110, JB-113/JB-114 and JB-111/JB-112 for UMAG_03806 donor template. To generate the final constructs, all fragments corresponding to one mutation event were inserted into pJET1.2/blunt by Gibson cloning. For transformation into *U. maydis*, the donor templates were amplified from the pJET vectors using JB-6/JB-7 for *cyp3*, JB-17/JB-18 for *emt1*, JB-25/JB-26 for MEL cluster, JB-47/JB-48 for UA cluster, JB-58/JB-59 for *dgat*, HT-210/HT-211 for *fuz7*, JB-107/JB-108 for UMAG_02068, and JB-115/JB-116 for UMAG_03806 deletion. To integrate an overexpressed form of *mttA*, the plasmid P_{etef} -Cbx-*AT_mttA* was used.

4.2.4 Rapid extraction of *U. maydis* genomic DNA

To isolate genomic DNA from *U. maydis* strains, 2 mL of culture broth were centrifuged (1 min, 13,000 rpm) and resuspended in 500 µl lysis buffer. The lysis buffer consisted of 10 mM Tris-HCl (pH 8.0), 100 mM NaCl, 1 mM EDTA, 1 % /w/v) SDS, and 2 % (w/v) Triton X-100. Glass beads and 500 µl 50 % (v/v) phenol/chloroform were added and the whole mixture was shaken for 15 – 20 min using the IKA® Vibrax VXR basic (IKA, Germany). After centrifugation (10 min, 13,000 rpm), the upper aqueous phase was transferred into a new Eppendorf tube and mixed with 1 mL 100 % cold ethanol, before it was centrifuged again (10 min, 13,000 rpm). The pellet was resuspended in 500 µl 70 % cold ethanol and centrifuged (5 min, 13,000 rpm). The pellet was dried at 65 °C for 15 min, before it was solved in 50 µl 10 mg mL^{-1} RNase A (Roth, Germany)/TE buffer (10 mM Tris-HCl (pH 8.0), 1 mM EDTA) and stored at 4 °C.

4.2.5 Isolation of high-quality genomic DNA from *U. maydis*

To isolate high-quality genomic DNA from *U. maydis* strains, 2 mL of culture broth were centrifuged (1 min, 13,000 rpm), resuspended in 500 µl H_2O, centrifuged again (1 min, 13,000 rpm) and resuspended in 400 µl lysis buffer and 400 µl phenol-chloroform-isoamyl alcohol (24:24:1, v/v). Glass beads were added, before the mixture was shaken for 15 – 20 min using the IKA® Vibrax VXR basic (IKA, Germany). After the addition of 200 µl TE buffer and centrifugation (2 min, 12,000 rpm), the aqueous phase was transferred into a new Eppendorf tube, mixed with 1 mL 100 % cold ethanol and centrifuged (2 min, 12,000 rpm). The pellet was

solved in 400 µl TE buffer and 5 µl 10 mg mL^{-1} RNase A/TE buffer, before it was incubated for 1 h at 37 °C. 500 µl phenol-chloroform-isoamyl alcohol (24:24:1, v/v) were added followed by strong shaking for 20 s at the IKA® Vibrax VXR basic and centrifugation (10 min, 12,000 rpm). The aquatic phase was transferred into a new Eppendorf tube and 500 µl chloroform-isoamyl alcohol (24:1, v/v) were added. These last three steps were repeated two more time, before the pellet was solved in 2.5-fold volume of cold 0.3 M ammonium acetate ethanol. The sample was centrifuged (2 min, 12,000 rpm), the pellet was dried, resuspended in 50 µl H_2O or TE buffer and stored at 4 °C.

DNA concentration and purity were quantified by the NanoDrop™ One Microvolume UV-Vis Spectrophotometer (Thermo Scientific, Germany).

4.2.6 Quantitative PCR (qPCR)

qPCR was applied to determine the copy number of *mttA* integrated into the *U. maydis* genome using Luna® Universal qPCR Master Mix (NEB, Germany). Primers were designed using "GenScript Real-Time PCR (TaqMan) Primer Design" tool (Gen Script, New Jersey, USA). Primer sequences are given in Table 22. As reference genes, UMAG_02592 and UMAG_03726 were amplified with the primer pairs JB-126/JB-127 and JB-128/JB-129. JB-132/JB-133 specifically bound within the *mttA* sequence. Amplification curves were taken by Bio-Rad CFX Connect™ Real-Time PCR Detection system and data were analyzed by using Bio-Rad CFX Manager™ 3.1 software (Bio-Rad Laboratories, Hercules, USA) and ΔCt method according to Pfaffl [173].

4.3 Analytical methods

All itaconate production experiments were performed in triplicates. For lipid analysis by FAMES, sextuples were extracted. In diagrams and tables, the arithmetic mean of the replicates is shown, while error bars and ± values indicate the standard deviation from the mean.

Cell densities were determined in an Ultrospec 10 Cell Density Meter by measuring the absorbance at a wavelength of 600 nm. When $CaCO_3$ was used as buffer, the culture broth was diluted 1:1 with 4 M HCl, before OD_{600} and HPLC measurements were performed [235].

To investigate growth in terms of growth rates and cell densities, a Growth Profiler GP960 (EnzyScreen, Heemstede, The Netherlands) for microtiterplates was used. Strains were cultivated in polystyrene grey square 24-deepwell microplates (17 x 17 x 40 mm, CR1424d, EnzyScreen, Heemstede, The Netherlands) with transparent bottom and a filling volume of 1.5 mL (30 °C, 224 rpm). A picture was taken every 20 min. With the EnzyScreen image analyzing software, growth curves could be generated from the green values measured.

To analyze substrate and product concentrations in the supernatants, samples were filtered with Rotilabo® Syringe Filters (CA membrane, 0.2 µm, Ø 15 mm) or – when the samples were previously treated with HCl – with Acrodisc® Syringe Filters (GHP membrane, 0.2 µm, Ø 13 mm) and diluted 1:10 with distilled water. Glucose, malate, (S)-2-hydroxyparaconate, erythritol, and itaconate concentrations in the supernatants were quantified by HPLC with a DIONEX UltiMate 3000 High

Performance Liquid Chromatography System (Thermo Scientific, Germany) with an ISERA Metab-AAC column 300 x 7.8 mm column (ISERA, Germany) kept at 40 °C As eluent, 5 mM H_2SO_4 with a constant flow rate of 0.6 mL min^{-1} was used. For detection, a SHODEX RI 101 detector (Showa Denko Europe GmbH, Germany) and a DIONEX UltiMate 3000 Variable Wavelength Detector at 210 nm were used. Ammonium concentrations were calculated by a colorimetric method according to Willis [236].

Extracellular glycolipids were detected by thin-layer chromatography (TLC). 300 µl culture broth (cultivation for 72 h in YNB medium + 5 % glucose, System Duetz®) were mixed with 600 µl ethyl acetate for 20 min. After centrifugation (5 min, 14,000 g), the ethyl acetate phase was dried overnight at room temperature (RT). The pellet was resuspended in 50 µl methanol, whereof 6 µl were dropped on a TLC Silica gel 60 aluminum sheet (20 x 20 cm, Merck KGaA, Darmstadt, Germany) and dried for 5 min at RT. As running buffer, a mixture of chloroform, methanol and H_2O (71:28:1, v/v) was used. The plate was dried for 10 min at RT, before glycolipids were visualized by staining with a mixture of acetic acid, *p*-anisaldehyde and sulfuric acid (97:1:2, v/v) and heating at 120 °C for 3-5 min [150].

For fatty acid methyl esters (FAMES) analysis, lipid extracts were obtained from 9 mL culture broth after 72 h of cultivation in MTM (50 g L^{-1} glucose, pH 6.5 buffered with 100 mM MES, System Duetz®). Lipid composition was analyzed by lipid hydrolysis, esterification to fatty acid methyl esters using methanolic H_2SO_4 as transmethylating reagent, and hexane extraction. GC-FID separation was performed in a Shimadzu GC-MS QP 2010 using an OPTIMA® 225 column (30 m, 0.25 mm, 0.25 µm; Macherey-Nagel, Germany).

For genome re-sequencing, genomic DNA was isolated by phenol-chloroform-isoamyl alcohol extraction (section 4.2.5). Whole-genome sequencing was performed by GATC Biotech AG (Konstanz, Germany) using Genome Sequencer Illumina HiSeq 2500 technology (sequence mode: 2x150 bp read length) and the HiSeq Control Software v2.0.12.0. Variance analysis in terms of SNP and InDel detection was conducted by mapping the re-sequencing data onto the *U. maydis* 521 reference genome (Refseq assembly GCF_000328475.2) [151]. Mapping and variant calling results were visualized with Integrative Genomics Viewer (IGV) software [237].

References

5 References

1. Roser M, Ortiz-Ospina E. World population growth. *World Population Growth*. https://ourworldindata.org/world-population-growth. Published 2013. Accessed December 19, 2018.
2. Kremer M. Population growth and technological change: one million B.C. to 1990. *Q J Econ*. 1993;108(3):681-716.
3. Godfray HCJ, Beddington JR, Crute IR, et al. Food security: The challenge of feeding 9 billion people. *Science*. 2010;327(5967):812-818.
4. Baulcombe, D., Crute, I., Davies, B., Dunwell, J., Gale , M., Jones, J., Pretty, J., Sutherland, W. and Toulmin C. *Reaping the Benefits: Science and the Sustainable Intensification of Global Agriculture*. The Royal Society. London, UK; 2009.
5. World Bank. *World Development Report 2008: Agriculture for Development*. Washington, DC; 2008.
6. International Energy Agency. *World Outlook Energy 2015*. OECD Publishing. Paris; 2015.
7. Demirbaş A. Biomass resource facilities and biomass conversion processing for fuels and chemicals. *Energy Convers Manag*. 2001;42(11):1357-1378.
8. Klass DL. Biomass for renewable energy and fuels. *Encycl Energy*. 2004;1:193-212.
9. Saha BC, Kennedy GJ, Qureshi N, Bowman MJ. Production of itaconic acid from pentose sugars by *Aspergillus terreus*. *Biotechnol Prog*. 2017;33(4):1059-1067.
10. Rodhe H. A comparison of the contribution of various gases to the greenhouse effect. *Science*. 1990;248(4960):1217-1219.
11. EPA. What is acid rain?https://www.epa.gov/acidrain/what-acid-rain. Accessed January 4, 2019.
12. Klass DL. *Biomass for Renewable Energy, Fuels, and Chemicals*. San Diego, California, USA: Academic Press; 1998.
13. Ragauskas AJ, Williams CK, Davison BH, et al. The path forward for biofuels and biomaterials. *Science*. 2006;311(5760):484-489.
14. Van Wyk JPH. Biotechnology and the utilization of biowaste as a resource for bioproduct development. *Trends Biotechnol*. 2001;19(5):172-177.
15. RIVM - Dutch National Institute for Public Health and the Environment. Biobased economy.https://www.rivm.nl/en/biobased-economy. Published 2014. Accessed December 20, 2018.
16. Chum HL, Overend RP. Biomass and renewable fuels. *Fuel Process Technol*. 2001;71(1-3):187-195.
17. Stout BA, Butler JL, Gavett EE. Energy use and management in US agriculture. In: Springer, Berlin, Heidelberg; 1984:169-189.
18. Zörb C, Lewandowski I, Kindervater R, Göttert U, Patzelt D. Biobased resources and value chains. In: *Bioeconomy*. Cham: Springer International Publishing; 2018:75-95.
19. Cuff DJ, Young WJ. *The United States Energy Atlas*. New York: Free Press; 1980.
20. FAOSTAT (2014) Food and agriculture organization of the United States - Statistics Division.http://www.fao.org/. Accessed January 4, 2019.
21. Lee RA, Lavoie J-M. From first- to third-generation biofuels: Challenges of producing a commodity from a biomass of increasing complexity. *Anim Front*. 2013;3(2):6-11.
22. Sharif Hossain A, Salleh A, Nasrulhaq Boyce A, Chowdhury P, Naqiuddin M. Biodiesel fuel production from algae as renewable energy. *Am J Biochem Biotechnol*. 2008;4(3):250-254.
23. Mitchel D. *A Note on Rising Food Prices*. The World Bank; 2008.
24. Stephen JD, Mabee WE, Saddler JN. Will second-generation ethanol be able to compete with first-generation ethanol? Opportunities for cost reduction. *Biofuels, Bioprod Biorefining*. 2012;6(2):159-176.
25. Brennan L, Owende P. Biofuels from microalgae - A review of technologies for production, processing, and extractions of biofuels and co-products. *Renew Sustain Energy Rev*. 2010;14(2):557-577.
26. Griffiths MJ, Harrison STL. Lipid productivity as a key characteristic for choosing algal species for biodiesel production. *J Appl Phycol*. 2009;21(5):493-507.
27. Sheehan J, Dunahay T, Benemann J, Roessler P. *A Look Back at the U.S. Department of Energy's Aquatic Species Program: Biodiesel from Algae Close-out Report*.; 1978.
28. Chisti Y. Biodiesel from microalgae beats bioethanol. *Trends Biotechnol*. 2008;26(3):126-131.
29. Tsukahara K SS. Liquid fuel production using microalgae. *J Japan Pet Inst*. 2005;48(5):251-259.
30. Fachagentur Nachwachsende Rohstoffe e.V. *Bioenergy in Germany Facts and Figures 2017*.;

2017.
31. Wagner S, Graf N, Böchzelt H, Schnitzer H. Nachwachsende Rohstoffe für die chemische Industrie.http://www.nachhaltigwirtschaften.at. Published 2005. Accessed December 27, 2018.
32. Werpy T, Petersen G, Aden A, et al. Top value added chemicals from biomass. Volume 1 - results of screening for potential candidates from sugars and synthesis gas. *US-DoE*. 2004.
33. Okabe M, Lies D, Kanamasa S, Park EY. Biotechnological production of itaconic acid and its biosynthesis in *Aspergillus terreus*. *Appl Microbiol Biotechnol*. 2009;84(4):597-606.
34. Willke T, Vorlop KD. Biotechnological production of itaconic acid. *Appl Microbiol Biotechnol*. 2001;56(3-4):289-295.
35. Baup S. Ueber eine neue Pyrogen-Citronensäure, und über Benennung der Pyrogen-Säuren überhaupt. *Ann der Pharm*. 1836;19(1):29-38.
36. Kinoshita K. Über die Produktion von Itaconsaure und Mannit durch einen neuen Schimmelpilz, *Aspergillus itaconicus*. *Acta Phytochim*. 1932;5:271-287.
37. Satoh K, Lee D-H, Nagai K, Kamigaito M. Precision synthesis of bio-based acrylic thermoplastic elastomer by RAFT polymerization of itaconic acid derivatives. *Macromol Rapid Commun*. 2014;35(2):161-167.
38. Steiger MG, Blumhoff ML, Mattanovich D, Sauer M. Biochemistry of microbial itaconic acid production. *Front Microbiol*. 2013;4:23.
39. Klement T, Milker S, Jager G, Grande PM, Dominguez de Maria P, Buchs J. Biomass pretreatment affects *Ustilago maydis* in producing itaconic acid. *Microb Cell Fact*. 2012;11:43.
40. Geilen FMA, Engendahl B, Harwardt A, Marquardt W, Klankermayer J, Leitner W. Selective and flexible transformation of biomass-derived platform chemicals by a multifunctional catalytic system. *Angew Chemie Int Ed*. 2010;49(32):5510-5514.
41. Global Industry Analysis. The global itaconic acid market.https://www.strategyr.com/MarketResearch/Itaconic_Acid_IA_Market_Trends.asp. Published 2016. Accessed January 4, 2019.
42. Ahmed El-Imam A, Du C. Fermentative itaconic acid production. *J Biodiversity, Bioprospecting Dev*. 2014;1(1):1-8.
43. Scopus. Scopus.https://www.elsevier.com/solutions/scopus. Published 2017. Accessed April 16, 2019.
44. Cunha da Cruz J, Machado de Castro A, Camporese Sérvulo EF. World market and biotechnological production of itaconic acid. *3 Biotech*. 2018;8(138).
45. De Carvalho JC, Magalhães AI, Soccol CR. Biobased itaconic acid market and research trends - is it really a promising chemical? *Chim Oggi - Chem Today*. 2018;36(4):56-58.
46. Verma V, Iqbal S. Itaconic acid market size, share, price - Report 2024.https://www.gminsights.com/industry-analysis/itaconic-acid-market. Published 2016. Accessed December 28, 2018.
47. Weastra. *WP 8.1. Determination of Market Potential for Selected Platform Chemicals*.; 2012.
48. Shriner RL, Ford SG, Roll LJ. Itaconic anhydride and itaconic acid. *Org Synth*. 1931;11:70.
49. Kane JH, Finlay AC, Philip F. Amann. Production of itaconic acid. Patent: US 2385283. 1945.
50. Bafana R, Pandey RA. New approaches for itaconic acid production: bottlenecks and possible remedies. *Crit Rev Biotechnol*. 2017;38(1):68-82.
51. Pichler H, Obenaus F, Franz G. *Erdöl Kohle Erdgas Petrochemie*. Industrieverlag von Hernhaussen, Hamburg; 1967.
52. Berg RG, Hetzel DS. Preparation of citraconic anhydride. Patent: US 4100179. 1978.
53. Tate BE. Itaconic acid and derivatives. In: *Kirk-Othmer Encyclopedia of Chemical Technology*. 3rd ed. Colorado, USA: John Wiley & Sons, Inc.; 1981:865-873.
54. Calam CT, Oxford AE, Raistrick H. Studies in the biochemistry of microorganisms: Itaconic acid, a metabolic product of a strain of *Aspergillus terreus* Thom. *Biochem J*. 1939;33(9):1488-1495.
55. Lockwood LB, Moyer AJ. Method for the production of itaconic acid. Patent: US 2462981. 1949.
56. Lockwood LB, Reeves MD. Some factors affecting the production of itaconic acid by *Aspergillus terreus*. *Arch Biochem*. 1945;6(3):455-469.
57. Pfeifer VF, Vojnovich C, Heger EN. Itaconic acid by fermentation with *Aspergillus terreus*. *Ind Eng Chem*. 1952;44(12):2975-2980.
58. Da Cruz JC, Camporese Sérvulo EF, De Castro AM. Microbial production of itaconic acid. In: *Microbial Production of Food Ingredients and Additives*. ; 2017:291-316.
59. Haskins RH, Thorn JA, Boothroyd B. Biochemistry of the Ustilaginales: XI. Metabolic products of *Ustilago zeae* in submerged culture. *Can J Microbiol*. 1955;1(9):749-756.
60. Tabuchi T, Sugisawa T, Ishidori T, Nakahara T, Sugiyama J. Itaconic acid fermentation by a yeast belonging to the genus *Candida*. *Agric Biol Chem*. 1981;45(2):475-479.
61. Kawamura D, Furuhashi M, Saito O, Matsui H. Production of itaconic acid by fermentation.

Patent: JP 56137893. 1981.
62. Levinson WE, Kurtzman CP, Kuo TM. Production of itaconic acid by *Pseudozyma antarctica* NRRL Y-7808 under nitrogen-limited growth conditions. *Enzyme Microb Technol*. 2006;39(4):824-827.
63. Sugimoto M, Sakagami H, Yokote Y, et al. Non-targeted metabolite profiling in activated macrophage secretion. *Metabolomics*. 2012;8(4):624-633.
64. Krull S, Hevekerl A, Kuenz A, Prüße U. Process development of itaconic acid production by a natural wild type strain of *Aspergillus terreus* to reach industrially relevant final titers. *Appl Microbiol Biotechnol*. 2017;101(10):4063-4072.
65. Kuenz A, Gallenmüller Y, Willke T, Vorlop K-D. Microbial production of itaconic acid: developing a stable platform for high product concentrations. *Appl Microbiol Biotechnol*. 2012;96(5):1209-1216.
66. Hevekerl A, Kuenz A, Vorlop K-D. Influence of the pH on the itaconic acid production with *Aspergillus terreus*. *Appl Microbiol Biotechnol*. 2014;98(24):10005-10012.
67. Robert C. Nubel, Wantagh Ratajak, Edwin J. Ratajak. Process for producing itaconic acid. Patent: US 3044941. 1960.
68. Kautola H, Vahvaselkä M, Linko Y-Y, Linko P. Itaconic acid production by immobilized *Aspergillus terreus* from xylose and glucose. *Biotechnol Lett*. 1985;7(3):167-172.
69. Karaffa L, Díaz R, Papp B, Fekete E, Sándor E, Kubicek CP. A deficiency of manganese ions in the presence of high sugar concentrations is the critical parameter for achieving high yields of itaconic acid by *Aspergillus terreus*. *Appl Microbiol Biotechnol*. 2015;99(19):7937-7944.
70. Reddy CSK, Singh RP. Enhanced production of itaconic acid from corn starch and market refuse fruits by genetically manipulated *Aspergillus terreus* SKR10. *Bioresour Technol*. 2002;85(1):69-71.
71. Dwiarti L, Otsuka M, Miura S, Technology MY-B, 2007 U. Itaconic acid production using sago starch hydrolysate by *Aspergillus terreus* TN484-M1. *Bioresour Technol*. 2007;98(17):3329-3337.
72. Nikolay V, Almudena M, Gilberto M, Antonia G, Vanessa M, Maria V. Solubilization of animal bonechar by a filamentous fungus employed in solid state fermentation. *Ecol Eng*. 2013;58:165-169.
73. Ying-Chieh Tsai, Min-Chang Huang, Shuen-Fuh Lin, Yuan-Chi Su. Method for the production of itaconic acid using *Aspergillus terreus* solid state fermentation. Patent: US 6171831B1. 2001.
74. Blumhoff ML, Steiger MG, Mattanovich D, Sauer M. Targeting enzymes to the right compartment: Metabolic engineering for itaconic acid production by *Aspergillus niger*. *Metab Eng*. 2013;19:26-32.
75. Harder B-J, Bettenbrock K, Klamt S. Model-based metabolic engineering enables high yield itaconic acid production by *Escherichia coli*. *Metab Eng*. 2016;38:29-37.
76. Araki T, Yamazaki Y, Suzuki N. Production of itaconic acid by *Helicobasidium mompa* TANAKA. *Japanese J Phytopathol*. 1957;22(2):83-87.
77. Maassen N, Panakova M, Wierckx N, et al. Influence of carbon and nitrogen concentration on itaconic acid production by the smut fungus *Ustilago maydis*. *Eng Life Sci*. 2014;14(2):129-134.
78. Geiser E, Przybilla SK, Engel M, et al. Genetic and biochemical insights into the itaconate pathway of *Ustilago maydis* enable enhanced production. *Metab Eng*. 2016;38:427-435.
79. Blazeck J, Hill A, Jamoussi M, Pan A, Miller J, Alper HS. Metabolic engineering of *Yarrowia lipolytica* for itaconic acid production. *Metab Eng*. 2015;32:66-73.
80. Jaklitsch WM, Kubicek CP, Scrutton MC. The subcellular organization of itaconate biosynthesis in *Aspergillus terreus*. *J Gen Microbiol*. 1991;137(3):533-539.
81. Li A, van Luijk N, ter Beek M, Caspers M, Punt P, van der Werf M. A clone-based transcriptomics approach for the identification of genes relevant for itaconic acid production in *Aspergillus*. *Fungal Genet Biol*. 2011;48(6):602-611.
82. Huang X, Lu X, Li Y, Li X, Li JJ. Improving itaconic acid production through genetic engineering of an industrial *Aspergillus terreus* strain. *Microb Cell Fact*. 2014;13(119).
83. Klement T, Büchs J. Itaconic acid - a biotechnological process in change. *Bioresour Technol*. 2013;135:422-431.
84. Tevž G, Benčina M, Legiša M. Enhancing itaconic acid production by *Aspergillus terreus*. *Appl Microbiol Biotechnol*. 2010;87(5):1657-1664.
85. Lin Y-H, Li Y-F, Huang M-C, Tsai Y-C. Intracellular expression of *Vitreoscilla* hemoglobin in *Aspergillus terreus* to alleviate the effect of a short break in aeration during culture. *Biotechnol Lett*. 2004;26(13):1067-1072.
86. Li A, Pfelzer N, Zuijderwijk R, Brickwedde A, van Zeijl C, Punt P. Reduced by-product formation and modified oxygen availability improve itaconic acid production in *Aspergillus niger*. *Appl Microbiol Biotechnol*. 2013;97(9):3901-3911.

87. Huang X, Chen M, Lu X, Li Y, Li X, Li J-J. Direct production of itaconic acid from liquefied corn starch by genetically engineered *Aspergillus terreus*. *Microb Cell Fact*. 2014;13(108).
88. Grislis J, Zamalh V, Kaulins P, Lukso V, Stankevich P. Itaconic acid. Patent: SU 507633. 1976.
89. Kobayashi T. Production of itaconic acid from wood waste. *Process Biochem*. 1978;13(5):15-22.
90. Geiser E. Itaconic acid production by *Ustilago maydis*. Dissertation. RWTH Aachen University. Institute of Applied Microbiology. 2015.
91. Gyamerah MH. Oxygen requirement and energy relations of itaconic acid fermentation by *Aspergillus terreus* NRRL 1960. *Appl Microbiol Biotechnol*. 1995;44(1-2):20-26.
92. Yahiro K, Takahama T, Park YS, Okabe M. Breeding of *Aspergillus terreus* mutant TN-484 for itaconic acid production with high yield. *J Ferment Bioeng*. 1995;79(5):506-508.
93. Zambanini T, Hosseinpour Tehrani H, Geiser E, et al. Efficient itaconic acid production from glycerol with *Ustilago vetiveriae* TZ1. *Biotechnol Biofuels*. 2017;10(131):1-15.
94. Wasewar KL, Shende D, Keshav A. Reactive extraction of itaconic acid using tri-n-butyl phosphate and aliquat 336 in sunflower oil as a non-toxic diluent. *J Chem Technol Biotechnol*. 2011;86(2):319-323.
95. Kuenz A. Itaconsäureherstellung aus nachwachsenden Rohstoffen als Ersatz fur petrochemisch hergestellte Acrylsäure. Dissertation. Technische Universität Braunschweig. 2008.
96. de Hoog GS. Risk assessment of fungi reported from humans and animals. *Mycoses*. 1996;39(11-12):407-417.
97. Edite Bezerra da Rocha M, Freire F da CO, Erlan Feitosa Maia F, Izabel Florindo Guedes M, Rondina D. Mycotoxins and their effects on human and animal health. *Food Control*. 2014;36(1):159-165.
98. Paulino BN, Pessôa MG, Molina G, et al. Biotechnological production of value-added compounds by ustilaginomycetous yeasts. *Appl Microbiol Biotechnol*. 2017;101(21):7789-7809.
99. Feldbrügge M, Kellner R, Schipper K. The biotechnological use and potential of plant pathogenic smut fungi. *Appl Microbiol Biotechnol*. 2013;97(8):3253-3265.
100. Jeya M, Lee KM, Tiwari MK, et al. Isolation of a novel high erythritol-producing *Pseudozyma tsukubaensis* and scale-up of erythritol fermentation to industrial level. *Appl Microbiol Biotechnol*. 2009;83(2):225-231.
101. Guevarra ED, Tabuchi T. Accumulation of itaconic, 2-hydroxyparaconic, itatartaric, and malic acids by strains of the genus *Ustilago*. *Agric Biol Chem*. 1990;54(9):2353-2358.
102. Chang M-H, Kim H-J, Jahng K-Y, Hong S-C. The isolation and characterization of *Pseudozyma* sp. JCC 207, a novel producer of squalene. *Appl Microbiol Biotechnol*. 2008;78(6):963-972.
103. Oliveira JV de C, Dos Santos RAC, Borges TA, Riaño-Pachón DM, Goldman GH. Draft genome sequence of *Pseudozyma brasiliensis* sp. nov. strain GHG001, a high producer of endo-1,4-xylanase isolated from an insect pest of sugarcane. *Genome Announc*. 2013;1(6):1-2.
104. Kaupert Neto AA, Borin GP, Goldman GH, Damásio AR de L, Oliveira JV de C. Insights into the plant polysaccharide degradation potential of the xylanolytic yeast *Pseudozyma brasiliensis*. Ah Kang H, ed. *FEMS Yeast Res*. 2016;16(2):1-12.
105. Morita T, Ogura Y, Takashima M, et al. Isolation of *Pseudozyma churashimaensis* sp. nov., a novel ustilaginomycetous yeast species as a producer of glycolipid biosurfactants, mannosylerythritol lipids. *J Biosci Bioeng*. 2011;112(2):137-144.
106. Cavalcante Fai AE, Resende Simiqueli AP, de Andrade CJ, Ghiselli G, Pastore GM. Optimized production of biosurfactant from *Pseudozyma tsukubaensis* using cassava wastewater and consecutive production of galactooligosaccharides: An integrated process. *Biocatal Agric Biotechnol*. 2015;4(4):535-542.
107. Kirk PM, Cannon PF, Minter DW, Stalpers JA. *Ainsworth and Bisby's Dictionary of the Fungi*. 10th ed. CABI; 2008.
108. Wang Q-M, Begerow D, Groenewald M, et al. Multigene phylogeny and taxonomic revision of yeasts and related fungi in the Ustilaginomycotina. *Stud Mycol*. 2015;81:55-83.
109. Bakkeren G, Kämper J, Schirawski J. Sex in smut fungi: Structure, function and evolution of mating-type complexes. *Fungal Genet Biol*. 2008;45:S15-S21.
110. Matei A, Doehlemann G. Cell biology of corn smut disease - *Ustilago maydis* as a model for biotrophic interactions. *Curr Opin Microbiol*. 2016;34:60-66.
111. Teun Boekhout, Fonseca Á, Sampaio JP, Bandoni RJ, Jack W.Fell, Kyung J.Kwon-Chung. Discussion of teleomorphic and anamorphic basidiomycetous yeasts. *The Yeasts*. 2011:1339-1372.
112. Begerow D, Schäfer AM, Kellner R, et al. 11 Ustilaginomycotina 0 Ustilaginomycotina. In: *Systematics and Evolution*. Berlin, Heidelberg: Springer Berlin Heidelberg; 2014:295-329.
113. Nasr S, Soudi MR, Shahzadeh Fazeli SA, Nguyen HDT, Lutz M, Piątek M. Expanding

evolutionary diversity in the Ustilaginomycotina: Fereydouniaceae fam. nov. and *Fereydounia* gen. nov., the first urocystidalean yeast lineage. *Mycol Prog*. 2014;13(1012):1217-1226.
114. Bauer R, Begerow D, Oberwinkler E, Piepenbring M, Berbee ML. Ustilaginomycetes. In: *Systematics and Evolution*. Berlin, Heidelberg: Springer Berlin Heidelberg; 2001:57-83.
115. León-Ramírez CG, Alejandro Sánchez-Arreguín J, Ruiz-Herrera J. *Ustilago maydis*, a delicacy of the aztec cuisine and a model for research. *Nat Resour*. 2014;5:256-267.
116. Abbas HK, Shier WT, Plasencia J, et al. Mycotoxin contamination in corn smut (*Ustilago maydis*) galls in the field and in the commercial food products. *Food Control*. 2017;71:57-63.
117. Jasso-Robles FI, Jiménez-Bremont JF, Becerra-Flora A, et al. Inhibition of polyamine oxidase activity affects tumor development during the maize-*Ustilago maydis* interaction. *Plant Physiol Biochem*. 2016;102:115-124.
118. Abbas HK. *Aflatoxin and Food Safety*. Boca Raton, FL, US: CRC Taylor & Francis; 2005.
119. Banuett F, Herskowitz I. Identification of Fuz7, a *Ustilago maydis* MEK / MAPKK homolog required steps in the fungal life cycle. *Genes Dev*. 1994;8:1367-1378.
120. Brefort T, Doehlemann G, Mendoza-Mendoza A, Reissmann S, Djamei A, Kahmann R. *Ustilago maydis* as a pathogen. *Annu Rev Phytopathol*. 2009;47(1):423-445.
121. Shurtleff MC. Compendium of corn diseases (2nd ed.). *Dis Compend Ser*. 1980.
122. Abbas HK, Zablotowicz RM, Shier WT, et al. Aflatoxin and fumonisin in corn (*Zea mays*) infected by common smut *Ustilago maydis*. *Plant Dis*. 2015;99(9):1236-1240.
123. Kubicek CP, Punt PJ, Visser J. Production of organic acids by filamentous fungi. In: *The Mycota: Industrial Applications*. ; 2010:215-234.
124. Pérez-Martín J, Castillo-Lluva S, Sgarlata C, et al. Pathocycles: *Ustilago maydis* as a model to study the relationships between cell cycle and virulence in pathogenic fungi. *Mol Genet Genomics*. 2006;276(3):211-229.
125. Geiser E, Przybilla SK, Friedrich A, et al. *Ustilago maydis* produces itaconic acid via the unusual intermediate trans-aconitate. *Microb Biotechnol*. 2016;9(1):116-126.
126. Boothroyd B, Thorn JA, Haskins RH. Biochemistry of the Ustilaginales: XII. Characterization of extracellular glycolipids produced by *Ustilago* sp. *Can J Biochem Physiol*. 1956;34(1):10-14.
127. Bölker M, Basse CW, Schirawski J. *Ustilago maydis* secondary metabolism - from genomics to biochemistry. *Fungal Genet Biol*. 2008;45:S88-S93.
128. Aguilar LR, Pardo JP, Lomelí MM, Bocardo OIL, Juárez Oropeza MA, Guerra Sánchez G. Lipid droplets accumulation and other biochemical changes induced in the fungal pathogen *Ustilago maydis* under nitrogen-starvation. *Arch Microbiol*. 2017;199(8):1195-1209.
129. Moon HJ, Jeya M, Kim IW, Lee JK. Biotechnological production of erythritol and its applications. *Appl Microbiol Biotechnol*. 2010;86(4):1017-1025.
130. Hewald S, Linne U, Scherer M, Marahiel MA, Kämper J, Bölker M. Identification of a gene cluster for biosynthesis of mannosylerythritol lipids in the basidiomycetous fungus *Ustilago maydis*. *Appl Environ Microbiol*. 2006;72(8):5469-5477.
131. Teichmann B, Liu L, Schink KO, Bölker M. Activation of the ustilagic acid biosynthesis gene cluster in *Ustilago maydis* by the C2H2 zinc finger transcription factor Rua1. *Appl Environ Microbiol*. 2010;76(8):2633-2640.
132. Guo Y, Cordes KR, Farese R V, Walther TC. Lipid droplets at a glance. *J Cell Sci*. 2009;122(6):749-752.
133. Ron EZ, Rosenberg E. Natural roles of biosurfactants. *Environ Microbiol*. 2001;3(4):229-236.
134. Zavala-Moreno A, Arreguin-Espinosa R, Pardo JP, Romero-Aguilar L, Guerra-Sánchez G. Nitrogen source affects glycolipid production and lipid accumulation in the phytopathogen fungus *Ustilago maydis*. *Adv Microbiol*. 2014;4(13):934-944.
135. Hewald S, Josephs K, Bölker M. Genetic analysis of biosurfactant production in *Ustilago maydis*. *Appl Environ Microbiol*. 2005;71(6):3033-3040.
136. Kurz M, Eder C, Isert D, et al. Ustilipids, acylated β-D-mannopyranosyl D-erythritols from *Ustilago maydis* and *Geotrichum candidum*. *J Antibiot (Tokyo)*. 2003;56(2):91-101.
137. Fluhartyf AL, O'Brien JS. A mannose-and erythritol-containing glycolipid from *Ustilago maydis*. *Biochemistry*. 1969;8(6):2627-2632.
138. Gorin PAJ, Haskins R, Spencer JFT. Biochemistry of the Ustilaginales: XIII. Observations on the structure and biosynthesis of 4-O-β-D-mannopyranosyl-D-erythritol. *Can J Biochem Physiol*. 1960;38(2):165-169.
139. Kitamoto D, Akiba S, Hioki C, Tabuchi T. Extracellular accumulation of mannosylerythritol lipids by a strain of *Candida antarctica*. *Agric Biol Chem*. 1990;54(1):31-36.
140. Haskins RH. Biochemistry of the Ustilaginales: I. Preliminary cultural studies of *Ustilago zeae*. *Can J Res*. 1950;28(2):213-223.
141. Haskins RH, Thorn JA. Biochemistry of the Ustilaginales: VII. Antibiotic activity of ustilagic acid. *Can J Bot*. 1951;29(6):585-592.
142. Lemieux RU, Charanduk R. Biochemistry of the Ustilaginales: VI: The acyl groups of ustilagic

acid. *Can J Chem*. 1951;29(9):759-766.
143. Teichmann B, Linne U, Hewald S, Marahiel MA, Bölker M. A biosynthetic gene cluster for a secreted cellobiose lipid with antifungal activity from *Ustilago maydis*. *Mol Microbiol*. 2007;66(2):525-533.
144. Teichmann B, Labbé C, Lefebvre F, Bölker M, Linne U, Bélanger RR. Identification of a biosynthesis gene cluster for flocculosin a cellobiose lipid produced by the biocontrol agent *Pseudozyma flocculosa*. *Mol Microbiol*. 2011;79(6):1483-1495.
145. Liu Y, Zhang C, Shen X, et al. Microorganism lipid droplets and biofuel development. *BMB Rep*. 2013;46(12):575-581.
146. Beopoulos A, Chardot T, Nicaud J-M. *Yarrowia lipolytica*: A model and a tool to understand the mechanisms implicated in lipid accumulation. *Biochimie*. 2009;91(6):692-696.
147. Levine B, Klionsky DJ. Development by self-digestion: Molecular mechanisms and biological functions of autophagy. *Dev Cell*. 2004;6(4):463-477.
148. Hsieh H-J, Su C-H, Chien L-J. Accumulation of lipid production in *Chlorella minutissima* by triacylglycerol biosynthesis-related genes cloned from *Saccharomyces cerevisiae* and *Yarrowia lipolytica*. *J Microbiol*. 2012;50(3):526-534.
149. Harris CA, Haas JT, Streeper RS, et al. DGAT enzymes are required for triacylglycerol synthesis and lipid droplets in adipocytes. *J Lipid Res*. 2011;52(4):657-667.
150. Geiser E, Wiebach V, Wierckx N, Blank LM. Prospecting the biodiversity of the fungal family Ustilaginaceae for the production of value-added chemicals. *Fungal Biol Biotechnol*. 2014;1:2.
151. Kämper J, Kahmann R, Bölker M, et al. Insights from the genome of the biotrophic fungal plant pathogen *Ustilago maydis*. *Nature*. 2006;444:97-101.
152. Geiser E, Ludwig F, Zambanini T, Wierckx N, Blank LM. Draft genome sequences of itaconate-producing Ustilaginaceae. *Genome Announc*. 2016;4(6):e01291-16.
153. Geiser E, Hosseinpour Tehrani H, Meyer S, Blank LM, Wierckx N. Evolutionary freedom in the regulation of the conserved itaconate cluster by Ria1 in related Ustilaginaceae. *Fungal Biol Biotechnol*. 2018;5:14.
154. Zambanini T, Hartmann SK, Schmitz LM, et al. Promoters from the itaconate cluster of *Ustilago maydis* are induced by nitrogen depletion. *Fungal Biol Biotechnol*. 2017;4:11.
155. Hartmann SK, Stockdreher Y, Wandrey G, et al. Online *in vivo* monitoring of cytosolic NAD redox dynamics in *Ustilago maydis*. *Biochim Biophys Acta - Bioenerg*. 2018;1859(10):1015-1024.
156. Schuster M, Schweizer G, Reissmann S, Kahmann R. Genome editing in *Ustilago maydis* using the CRISPR-Cas system. *Fungal Genet Biol*. 2016;89:3-9.
157. Khrunyk Y, Münch K, Schipper K, Lupas AN, Kahmann R. The use of FLP-mediated recombination for the functional analysis of an effector gene family in the biotrophic smut fungus *Ustilago maydis*. *New Phytol*. 2010;187:957-968.
158. Terfrüchte M, Joehnk B, Fajardo-Somera R, et al. Establishing a versatile Golden Gate cloning system for genetic engineering in fungi. *Fungal Genet Biol*. 2014;62:1-10.
159. Lung S-C, Weselake RJ. Diacylglycerol acyltransferase: a key mediator of plant triacylglycerol synthesis. *Lipids*. 2006;41(12):1073-1088.
160. Yen C-LE, Stone SJ, Koliwad S, Harris C, Farese R V. Thematic review series: Glycerolipids. DGAT enzymes and triacylglycerol biosynthesis. *J Lipid Res*. 2008;49(11):2283-2301.
161. Liu Q, Siloto RMP, Snyder CL, Weselake RJ. Functional and topological analysis of yeast acyl-CoA:diacylglycerol acyltransferase 2, an endoplasmic reticulum enzyme essential for triacylglycerol biosynthesis. *J Biol Chem*. 2011;286(15):13115-13126.
162. Huang CB, Alimova Y, Myers TM, Ebersole JL. Short- and medium-chain fatty acids exhibit antimicrobial activity for oral microorganisms. *Arch Oral Biol*. 2011;56(7):650-654.
163. Zambanini T, Sarikaya E, Kleineberg W, et al. Efficient malic acid production from glycerol with *Ustilago trichophora* TZ1. *Biotechnol Biofuels*. 2016;9:67.
164. Zambanini T, Kleineberg W, Sarikaya E, et al. Enhanced malic acid production from glycerol with high-cell density *Ustilago trichophora* TZ1 cultivations. *Biotechnol Biofuels*. 2016;9:135.
165. Kuenz A, Krull S. Biotechnological production of itaconic acid - things you have to know. *Appl Microbiol Biotechnol*. 2018;102(9):3901-3914.
166. Christensen JJ. Corn smut caused by *Ustilago maydis*. *Monogr Am Phytopathol Soc*. 1963;2.
167. Klose J, De Sá MM, Kronstad JW. Lipid-induced filamentous growth in *Ustilago maydis*. *Mol Microbiol*. 2004;52(3):823-835.
168. Lovely C Ben, Aulakh KB, Perlin MH. Role of Hsl7 in morphology and pathogenicity and its interaction with other signaling components in the plant pathogen *Ustilago maydis*. *Eukaryot Cell*. 2011;10(7):869-883.
169. Lovely C Ben, Perlin MH. Cla4, but not Rac1, regulates the filamentous response of *Ustilago maydis* to low ammonium conditions. *Commun Integr Biol*. 2011;4(6):670-673.
170. Hosseinpour Tehrani H. Engineering the morphology and metabolism in *Ustilago* to expand the

process window for itaconic acid production. Dissertation. RWTH Aachen University. Institute of Applied Microbiology. 2019.
171. Steiger MG, Punt PJ, Ram AFJ, Mattanovich D, Sauer M. Characterizing MttA as a mitochondrial *cis*-aconitic acid transporter by metabolic engineering. *Metab Eng*. 2016;35:95-104.
172. Hosseinpour Tehrani H, Geiser E, Engel M, et al. The interplay between transport and metabolism in fungal itaconic acid production. *Fungal Genet Biol*. 2019;125:45-52.
173. Pfaffl MW. A new mathematical model for relative quantification in real-time RT-PCR. *Nucleic Acids Res*. 2001;29(9):2002-2007.
174. Ruiz-Herrera J, Leon CG, Guevara-Olvera L, Carabez-Trejo A. Yeast-mycelial dimorphism of haploid and diploid strains of *Ustilago maydis*. *Microbiology*. 1995;141(3):695-703.
175. Guevarra ED, Tabuchi T. Production of 2-hydroxyparaconic and itatartaric acids by *Ustilago cynodontis* and simple recovery process of the acids. *Agric Biol Chem*. 1990;54(9):2359-2365.
176. Cervantes-Montelongo JA, Aréchiga-Carvajal ET, Ruiz-Herrera J. Adaptation of *Ustilago maydis* to extreme pH values: A transcriptomic analysis. *J Basic Microbiol*. 2016;56(11):1222-1233.
177. Peñalva MA, Arst HN. Regulation of gene expression by ambient pH in filamentous fungi and yeasts. *Microbiol Mol Biol Rev*. 2002;66(3):426-446.
178. Peñalva MA, Arst, Jr. HN. Recent advances in the characterization of ambient pH regulation of gene expression in filamentous fungi and yeasts. *Annu Rev Microbiol*. 2004;58(1):425-451.
179. Franco-Frías E, Ruiz-Herrera J, Aré Chiga-Carvajal ET. Transcriptomic analysis of the role of Rim101/PacC in the adaptation of *Ustilago maydis* to an alkaline environment. *Microbiology*. 2014;160:1985-1998.
180. Fonseca-García C, León-Ramírez CG, Ruiz-Herrera J. The regulation of different metabolic pathways through the Pal/Rim pathway in *Ustilago maydis*. *FEMS Yeast Res*. 2012;12(5):547-556.
181. Aréchiga-Carvajal ET, Ruiz-Herrera J. The *RIM101/pacC* homologue from the basidiomycete *Ustilago maydis* is functional in multiple pH-sensitive phenomena. *Society*. 2005;4(6):999-1008.
182. Arst HN, Peñalva MA. pH regulation in *Aspergillus* and parallels with higher eukaryotic regulatory systems. *Trends Genet*. 2003;19(4):224-231.
183. Sauer U. Evolutionary engineering of industrially important microbial phenotypes. In: Nielsen J, Eggeling L, Dynesen J, et al., eds. *Advances in Biochemical Engineering/Biotechnology*. Vol 73. Springer Science & Business Media; 2001:129-169.
184. Choi S, Song CW, Shin JH, Lee SY. Biorefineries for the production of top building block chemicals and their derivatives. *Metab Eng*. 2015;28:223-239.
185. Marrs B, Delagrave S, Murphy D. Novel approaches for discovering industrial enzymes. *Curr Opin Microbiol*. 1999;2(3):241-245.
186. Bailey CR, Penfold HA, Arst HN. *Cis*-dominant regulatory mutations affecting the expression of GABA permease in *Aspergillus nidulans*. *MGG Mol Gen Genet*. 1979;169(1):79-83.
187. Caddick MX, Brownlee AG, Arst HN. Regulation of gene expression by pH of the growth medium in *Aspergillus nidulans*. *MGG Mol Gen Genet*. 1986;203(2):346-353.
188. Espeso EA, Arst HN. On the mechanism by which alkaline pH prevents expression of an acid-expressed gene. *Mol Cell Biol*. 2000;20(10):3355-3363.
189. Caddick MX, Arst HN. Structural genes for phosphatases in *Aspergillus nidulans*. *Genet Res*. 1986;47(2):83-91.
190. Pérez-Gonzalez JA, De Graaff LH, Visser J, Ramón D. Molecular cloning and expression in *Saccharomyces cerevisiae* of two *Aspergillus nidulans* xylanase genes. *Appl Environ Microbiol*. 1996;62(6):2179-2182.
191. MacCabe AP, Orejas M, Pérez-González JA, Ramón D. Opposite patterns of expression of two *Aspergillus nidulans* xylanase genes with respect to ambient pH. *J Bacteriol*. 1998;180(5):1331-1333.
192. Caddick MX, Brownlee AG, Arst HN. Phosphatase regulation in *Aspergillus nidulans*: Responses to nutritional starvation. *Genet Res*. 1986;47(2):93-102.
193. Brown DW, Yu JH, Kelkar HS, et al. Twenty-five coregulated transcripts define a sterigmatocystin gene cluster in *Aspergillus nidulans*. *Proc Natl Acad Sci U S A*. 1996;93(4):1418-1422.
194. Gielkens M, Gonzalez-Candelas L, Sanchez-Torres P, van de Vondervoort P, de Graaff L, Visser J. The *abfB* gene encoding the major α-L-arabinofuranosidase of *Aspergillus nidulans*: nucleotide sequence, regulation and construction of a disrupted strain. *Microbiology*. 1999;145(3):735-741.
195. Booth IR. Regulation of cytoplasmic pH in bacteria. *Microbiol Rev*. 1985;49(4):359-378.
196. Matsumoto M, Ohishi H, Benno Y. H+-ATPase activity in *Bifidobacterium* with special reference

to acid tolerance. *Int J Food Microbiol*. 2004;93(1):109-113.
197. Yokota A, Amachi S, Ishii S, Tomita F. Acid sensitivity of a mutant of *Lactococcus lactis* subsp. *lactis* C2 with reduced membrane-bound ATPase activity. *Biosci Biotechnol Biochem*. 2009;59(10):2004-2007.
198. Guern J, Felle H, Mathieu Y, Kurkdjian A. Regulation of intracellular pH in plant cells. *Int Rev Cytol*. 1991;127:111-173.
199. O'Sullivan E, Condon S. Relationship between acid tolerance, cytoplasmic pH, and ATP and H+-ATPase levels in chemostat cultures of *Lactococcus lactis*. *Appl Environ Microbiol*. 1999;65(6):2287-2293.
200. Cervantes-Chávez JA, Ortiz-Castellanos L, Tejeda-Sartorius M, Gold S, Ruiz-Herrera J. Functional analysis of the pH responsive pathway Pal/Rim in the phytopathogenic basidiomycete *Ustilago maydis*. *Fungal Genet Biol*. 2010;47(5):446-457.
201. Eichhorn H, Lessing F, Winterberg B, et al. A ferroxidation/permeation iron uptake system is required for virulence in *Ustilago maydis*. *Plant Cell*. 2006;18(11):3332-3345.
202. Banks GR, Shelton PA, Kanuga N, Holden DW, Spanos A. The *Ustilago maydis nar 1* gene encoding nitrate reductase activity: sequence and transcriptional regulation. *Gene*. 1993;131(1):69-78.
203. Kobilka BK. G protein coupled receptor structure and activation. *Biochim Biophys Acta - Biomembr*. 2007;1768(4):794-807.
204. Böhmer M, Colby T, Böhmer C, Bräutigam A, Schmidt J, Bölker M. Proteomic analysis of dimorphic transition in the phytopathogenic fungus *Ustilago maydis*. *Proteomics*. 2007;7(5):675-685.
205. Rodríguez-Kessler M, Baeza-Montañez L, García-Pedrajas MD, et al. Isolation of *UmRrm75*, a gene involved in dimorphism and virulence of *Ustilago maydis*. *Microbiol Res*. 2012;167(5):270-282.
206. Regenfelder E, Spellig T, Hartmann A, Lauenstein S, Bölker M, Kahmann R. G proteins in *Ustilago maydis*: transmission of multiple signals? *EMBO J*. 1997;16(8):1934-1942.
207. Matsushika A, Negi K, Suzuki T, Goshima T, Hoshino T. Identification and characterization of a novel *Issatchenkia orientalis* GPI-anchored protein, IoGas1, required for resistance to low pH and salt stress. Yang S, ed. *PLoS One*. 2016;11(9):1-25.
208. Yin X, Shin H-D, Li J, Du G, Liu L, Chen J. Pgas, a low-pH-induced promoter, as a tool for dynamic control of gene expression for metabolic engineering of *Aspergillus niger*. *Appl Environ Microbiol*. 2017;83(6):1-14.
209. Yadav D, Tanveer A, Malviya N, Yadav S. Overview and principles of bioengineering: The drivers of omics technologies. *Omi Technol Bio-Engineering*. 2018:3-23.
210. Stephanopoulos G. Metabolic fluxes and metabolic engineering. *Metab Eng*. 1999;1(1):1-11.
211. Keasling JD. Manufacturing molecules through metabolic engineering. *Science*. 2010;330(6009):1355-1358.
212. Al Abdallah Q, Souza ACO, Martin-Vicente A, Ge W, Fortwendel JR. Whole-genome sequencing reveals highly specific gene targeting by in vitro assembled Cas9-ribonucleoprotein complexes in *Aspergillus fumigatus*. *Fungal Biol Biotechnol*. 2018;5(11):1-8.
213. Wynn JP, Hamid AA, Li Y, Ratledge C. Biochemical events leading to the diversion of carbon into storage lipids in the oleaginous fungi *Mucor circinelloides* and *Mortierella alpina*. *Microbiology*. 2001;147(10):2857-2864.
214. Karaffa L, Kubicek CP. Citric acid and itaconic acid accumulation: variations of the same story? *Appl Microbiol Biotechnol*. 2019;103(7):2889-2902.
215. Welter K. Biotechnische Produktion von Itaconsäure aus nachwachsenden Rohstoffen mit immobilisierten Zellen. Dissertation. Technical University Braunschweig. 2000.
216. Ramírez OT, Mutharasan R. The role of the plasma membrane fluidity on the shear sensitivity of hybridomas grown under hydrodynamic stress. *Biotechnol Bioeng*. 1990;36(9):911-920.
217. Joseph-Horne T, Wood PM, Heppner C, Hollomon DW. Involvement of the alternative oxidase in cellular energy production in the wheat 'take all' fungus, *Gaeumannomyces graminis* var *tritici*. *Pestic Sci*. 1999;55(3):367-370.
218. Joseph-Horne T, Hollomon DW, Wood PM. Fungal respiration: a fusion of standard and alternative components. *Biochim Biophys Acta - Bioenerg*. 2001;1504(2-3):179-195.
219. Joseph-Horne T, Hollomon DW. Functional diversity within the mitochondrial electron transport chain of plant pathogenic fungi. *Pest Manag Sci*. 2000;56(1):24-30.
220. Vries S, Grivell LA. Purification and characterization of a rotenone-insensitive NADH: Q6 oxidoreductase from mitochondria of *Saccharomyces cerevisiae*. *Eur J Biochem*. 1988;176(2):377-384.
221. Rasmusson AG, Soole KL, Elthon TE. Alternative NAD(P)H dehydrogenases of plant mitochondria. *Annu Rev Plant Biol*. 2004;55:23-39.
222. Buchanan BB, Gruissem W, Jones RL. *Biochemistry and Molecular Biology of Plants*.

Rockville, MD: American Society of Plant Physiologists; 2002.
223. Kim JW, Seo SO, Zhang GC, Jin YS, Seo JH. Expression of *Lactococcus lactis* NADH oxidase increases 2,3-butanediol production in Pdc-deficient *Saccharomyces cerevisiae*. *Bioresour Technol*. 2015;191:512-519.
224. Lopez de Felipe F, Kleerebezem M, de Vos WM, Hugenholtz J. Cofactor engineering: a novel approach to metabolic engineering in *Lactococcus lactis* by controlled expression of NADH oxidase. *J Bacteriol*. 1998;180(15):3804-3808.
225. Heux S, Cachon R, Dequin S. Cofactor engineering in *Saccharomyces cerevisiae*: Expression of a H2O-forming NADH oxidase and impact on redox metabolism. *Metab Eng*. 2006;8(4):303-314.
226. Blank LM, Ebert BE, Bühler B, Schmid A. Metabolic capacity estimation of *Escherichia coli* as a platform for redox biocatalysis: constraint-based modeling and experimental verification. *Biotechnol Bioeng*. 2008;100(6):1050-1065.
227. Albertyn J, Hohmann S, Thevelein JM, Prior BA. GPD1, which encodes glycerol-3-phosphate dehydrogenase, is essential for growth under osmotic stress in *Saccharomyces cerevisiae*, and its expression is regulated by the high-osmolarity glycerol response pathway. *Mol Cell Biol*. 1994;14(6):4135-4144.
228. Jain VK, Divol B, Prior BA, Bauer FF. Effect of alternative NAD+-regenerating pathways on the formation of primary and secondary aroma compounds in a *Saccharomyces cerevisiae* glycerol-defective mutant. *Appl Microbiol Biotechnol*. 2012;93(1):131-141.
229. Wang Q, Ou MS, Kim Y, Ingram LO, Shanmugam KT. Metabolic flux control at the pyruvate node in an anaerobic *Escherichia coli* strain with an active pyruvate dehydrogenase. *Appl Environ Microbiol*. 2010;76(7):2107-2114.
230. Brown SH, Bashkirova L, Berka R, et al. Metabolic engineering of *Aspergillus oryzae* NRRL 3488 for increased production of L-malic acid. *Appl Microbiol Biotechnol*. 2013;97(20):8903-8912.
231. Zelle RM, de Hulster E, van Winden WA, et al. Malic acid production by *Saccharomyces cerevisiae*: engineering of pyruvate carboxylation, oxaloacetate reduction, and malate export. *Appl Environ Microbiol*. 2008;74(9):2766-2777.
232. Carstensen F, Klement T, Büchs J, Melin T, Wessling M. Continuous production and recovery of itaconic acid in a membrane bioreactor. *Bioresour Technol*. 2013;137:179-187.
233. Duetz WA, Rüedi L, Hermann R, O'Connor K, Büchs J, Witholt B. Methods for intense aeration, growth, storage, and replication of bacterial strains in microtiter plates. *Appl Environ Microbiol*. 2000;66(6):2641-2646.
234. Tsukuda T, Carleton S, Fotheringham S, Holloman WK. Isolation and characterization of an autonomously replicating sequence from *Ustilago maydis*. *Mol Cell Biol*. 1988;8(9):3703-3709.
235. Zambanini T, Buescher JM, Meurer G, Wierckx N, Blank LM. Malic acid production from glycerol with *Ustilago trichophora*. *Chemie Ing Tech*. 2016;88(9):1245-1245.
236. Willis RB, Montgomery ME, Allen PR. *Improved Method for Manual, Colorimetric Determination of Total Kjeldahl Nitrogen Using Salicylate*. Vol 44.; 1996.
237. Thorvaldsdottir H, Robinson JT, Mesirov JP. Integrative Genomics Viewer (IGV): high-performance genomics data visualization and exploration. *Brief Bioinform*. 2013;14(2):178-192.
238. Hosseinpour Tehrani H, Tharmasothirajan A, Track E, Blank LM, Wierckx N. Engineering the morphology and metabolism of pH tolerant *Ustilago cynodontis* for efficient itaconic acid production. *Metab Eng*. 2019;54:293-300.
239. Robert Specht, Aurich Andreas, Eva Kreyß, Barth Gerold, Christian Bodinus. Verfahren zur biotechnologischen Herstellung von Itaconsäure. Patent: DE 102008011854B4. 2014.
240. Zambanini T, Hosseinpour Tehrani H, Geiser E, et al. Metabolic engineering of *Ustilago trichophora* TZ1 for improved malic acid production. *Metab Eng Commun*. 2017;4:12-21.
241. Goldberg I, Rokem JS, Pines O. Organic acids: old metabolites, new themes. *J Chem Technol Biotechnol*. 2006;81(10):1601-1611.
242. Zeikus JG, Jain MK, Elankovan P. Biotechnology of succinic acid production and markets for derived industrial products. *Appl Microbiol Biotechnol*. 1999;51(5):545-552.
243. Müller C. Optimization of itaconic acid and erythritol production in *Ustilago maydis*. Master's thesis. RWTH Aachen University. Institute of Applied Microbiology. 2018.
244. Hirata Y, Igarashi K, Ezaki S, Atomi H, Imanaka T. High-level production of erythritol by strain 618A-01 isolated from pollen. *J Biosci Bioeng*. 1999;87(5):630-635.
245. Röper H, Goossens J. Erythritol, a new raw material for food and non-food applications. *Starch - Stärke*. 1993;45(11):400-405.
246. Wisselink H., Weusthuis R., Eggink G, Hugenholtz J, Grobben G. Mannitol production by lactic acid bacteria: a review. *Int Dairy J*. 2002;12(2-3):151-161.
247. Ghoreishi SM, Shahrestani RG. Innovative strategies for engineering mannitol production. *Trends Food Sci Technol*. 2009;20(6-7):263-270.

248. Spoeckner S, Wray V, Nimtz M, Lang S. Glycolipids of the smut fungus *Ustilago maydis* from cultivation on renewable resources. *Appl Microbiol Biotechnol*. 1999;51(1):33-39.
249. Alimadadi N, Soudi MR, Talebpour Z. Efficient production of tri-acetylated mono-acylated mannosylerythritol lipids by *Sporisorium* sp. aff. *sorghi* SAM20. *J Appl Microbiol*. 2018;124(2):457-468.
250. Kitamoto D, Ikegami T, Suzuki GT, et al. Microbial conversion of n-alkanes into glycolipid biosurfactants, mannosylerythritol lipids, by *Pseudozyma* (*Candida antarctica*). *Biotechnol Lett*. 2001;23(20):1709-1714.
251. Morita T, Konishi M, Fukuoka T, Imura T, Kitamoto D. Discovery of *Pseudozyma rugulosa* NBRC 10877 as a novel producer of the glycolipid biosurfactants, mannosylerythritol lipids, based on rDNA sequence. *Appl Microbiol Biotechnol*. 2006;73(2):305-313.
252. Kitamoto D, Isoda H, Nakahara T. Functions and potential applications of glycolipid biosurfactants - from energy-saving materials to gene delivery carriers. *J Biosci Bioeng*. 2002;94(3):187-201.
253. Morita T, Koike H, Koyama Y, et al. Genome sequence of the basidiomycetous yeast *Pseudozyma antarctica* T-34, a producer of the glycolipid biosurfactants mannosylerythritol lipids. *Genome Announc*. 2013;1(2).
254. Roxburgh JM, Spencer JFT, Sallans HR. Factors affecting the production of ustilagic acid by *Ustilago Zeae*. *Agric Food Chem*. 1954;2(22):1121-1124.
255. Takakuwa N, Nagahama S, Matsumura H, Kinoshita M, Ohnishi M. Efficient conversion of crude glycerol into triacylglycerol by the yeast *Pseudozyma* sp . TYC- 2187 for biodiesel production. *J Oleo Sci*. 2013;62(8):605-612.
256. Ageitos JM, Vallejo JA, Veiga-Crespo P, Villa TG. Oily yeasts as oleaginous cell factories. *Appl Microbiol Biotechnol*. 2011;90(4):1219-1227.

Curriculum vitae

6 Curriculum vitae

Personal Data

Name	Johanna Loevenich (née Becker)
Born	January 23rd, 1990 in Pinneberg, Germany
Nationality	German
Mobile	+491726159387
Email	johanna.becker@rwth-aachen.de

Education

2016-2019	Ph.D. student at the Institute of Applied Microbiology, RWTH Aachen University, Aachen, Germany
2014-2016	Master of Science in Molecular and Applied Biotechnology at the RWTH Aachen University, Aachen, Germany Master thesis "Identification of new parasitophorous vacuole proteins in the human malaria parasite *Plasmodium falciparum*" at the Bernhard-Nocht-Institute for Tropical Medicine, Hamburg, Germany
2011-2014	Bachelor of Science in Biology at the RWTH Aachen University, Aachen, Germany Bachelor thesis "Expression and function of phospholipases in the blood stages of *Plasmodium falciparum*" at the Institute of Molecular Biotechnology, RWTH Aachen University, Aachen, Germany
2010-2011	Bachelor of Science in Biochemistry at the Ruhr-University Bochum, Bochum, Germany
2009	Abitur at the Johann-Rist-Gymnasium, Wedel, Germany

Work Experience

2016-2019	Research assistant and doctoral candidate at the Institute of Applied Microbiology, RWTH Aachen University, Aachen, Germany

Publications

Khosh-Naucke, M., Becker, J., Mesén-Ramírez, P., Kiani, P., Birnbaum, J., Fröhlke, U., Jonscher, E., Schlüter, H., Spielmann, T.: Identification of novel parasitophorous vacuole proteins in *P. falciparum* parasites using BioID. *Int J Med Microbiol*. 2018;308(1):13-24 (https://doi.org/10.1016/j.ijmm.2017.07.007)

Poster Presentations

Becker, J.; Blank, L.M.; Wierckx, N. – Generation of an *Ustilago maydis* MB215 strain for enhanced itaconic acid production. 12th VAAM Symposium "Molecular Biology of Fungi", 28th – 30th September 2017, Jena, Germany